SOLUTE INTERACTIONS IN NITRIDED IRON ALLOYS

A dissertation submitted for the degree of

Doctor of Philosophy

of the University of Newcastle upon Tyne

by

Steven Henderson

Department of Metallurgy and Engineering Materials

University of Newcastle upon Tyne

September 1976

PREFACE

This dissertation describes original work which has not been submitted for a degree at any other University.

The investigations were carried out in the Crystallography Laboratory of the Department of Metallurgy and Engineering Materials at the University of Newcastle upon Tyne during the period October 1971 to September 1974 under the supervision of Professor K.H. Jack.

The thesis describes the study of mixed solute-atom clustering in nitrided iron-titanium, iron-molybdenum and iron-molybdenum-titanium alloys and is part of a wider investigation at Newcastle on the effect of substitutional alloying elements on the behaviour of nitrogen in iron.

ACKNOWLEDGEMENTS

I wish to thank Professor K.H. Jack for advice, encouragement and general supervision of work.

I also wish to express gratitude to:

The Wolfson Foundation for the award of a maintenance grant;

Many colleagues for stimulating discussion, and particularly Dr. A. Hendry, Dr. J.H. Driver and Dr. D.P. Thompson for instruction and advice on many technical aspects of the work;

Mrs. Rule for typing the script.

I wish to thank my parents for their support, encouragement and understanding.

S. Henderson.

August, 1976.

ABSTRACT

Using the gas-metal equilibration method of constant activity ageing, high densities of fine, homogeneous nitride precipitates or substitutional-interstitial solute-atom clusters are produced in low alloy steels in the temperature range 350-750°C under appropriate nitriding conditions.

In Fe-Ti alloys, hardness and lattice parameter measurements, together with electron microscopy, show the formation of very fine disc-shaped zones. The tweed contrast of electron micrographs and the diffuse electron and X-ray scattering effects observed are attributed to the partial ordering of the zones which consist of equatomic Ti-N monolayer plates on matrix cube planes. Excess nitrogen equivalent to twice the nitrogen content of the "TiN" plate is accommodated as part of the cluster but is removed by ageing in hydrogen. A model is suggested for the zone structure which accounts for its limiting compositions "Fe_4TiN_3" and "Fe_2TiN" and for the occurrence of nitrogen in two different chemical environments with different stabilities. The "TiN" zone stoichiometry and morphology is stable even at high temperatures and overageing of the structure, accompanied by softening, takes several hours at 800°C. The strengthening which occurs in Fe-Ti alloys nitrided at intermediate temperatures is due to a particle shear mechanism.

For Fe-Mo alloys nitrided under similar conditions the microstructures are much coarser. Tweed contrast is not observed but other electron and X-ray diffraction

effects are similar to those for Fe-Ti alloys.

Zones containing both titanium and molybdenum are formed in nitrided Fe-Mo-Ti alloys nitrided under similar conditions and the properties are determined mainly by the titanium present in the alloy; the most pronounced effect of the molybdenum is observed in the nitriding kinetics. A model proposed for the Mo-Ti-N zone structure accounts for the difference between the observed properties and those expected from a simple summation of the separate Mo-N and Ti-N interactions.

CONTENTS

Chapter I

INTRODUCTION

I.1. General Introduction

Age-hardening in aluminium alloys involves the homogeneous formation of solute-atom clusters within the solvent lattice (Guinier-Preston zones) although it is generally classified under the heading of "precipitation hardening".

For homogeneous precipitation in face-centred cubic alloys such as aluminium-copper, a solute solubility is required which decreases rapidly with decreasing temperature to give a high degree of supersaturation (see Figure I.1). Guinier-Preston (G.P.) zones are metastable with respect to the equilibrium precipitate and so have a higher solubility. At the low temperatures where the necessary supersaturation can be achieved, the solute-atom diffusivity is too small to allow clustering unless there is an abnormally high quenched-in vacancy concentration. Because these conditions can not usually be achieved in body-centred cubic alloys, Guinier-Preston zones have not been observed in substitutional body-centred cubic iron alloys except at relatively high alloying-element concentrations. Interstitial solutes such as nitrogen have high diffusivities in iron even at room temperature and recent work on the quench-ageing of nitrogen-ferrite shows that at high supersaturations and low ageing temperatures ($\sim 20^{\circ}C$) homogeneous precipitation of α''-$Fe_{16}N_2$ is preceded by

Fig.I.1.

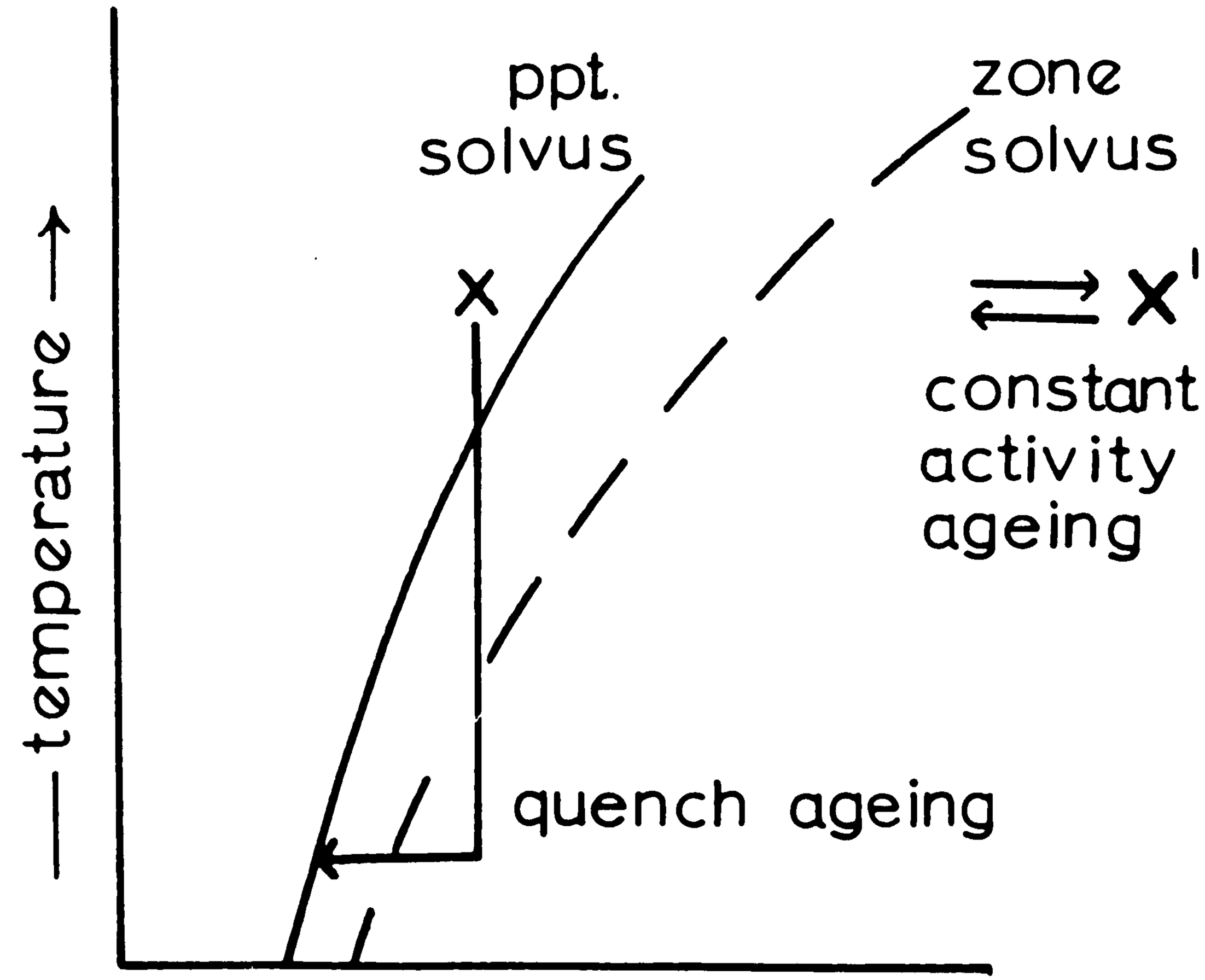

Conditions for Homogeneous
Precipitation and G.P Zone Formation

interstitial-atom clustering i.e. by Guinier-Preston zone formation.

One disadvantage of quench-ageing is that the supersaturation of nitrogen - the driving force for precipitation - rapidly decreases as the solid solution is depleted during the precipitation process. This may be overcome by equilibrating the ferrite at an elevated temperature in appropriate ammonia:hydrogen gas mixtures so as to maintain a constant high activity of nitrogen in solid solution. Using this technique of constant activity ageing, mixed substitutional-interstitial solute-atom clusters were produced in Fe-3^{a}/oMo equilibrated in an ammonia:hydrogen gas mixture in the temperature range 400-650^{o}C (Speirs, 1969). This observation demonstrated the existence of a new method of metal strengthening by mixed substitutional-interstitial zone formation (Speirs et al, 1970). Subsequent research at Newcastle showed the occurrence of mixed clustering in many other ferritic and austenitic Fe-X-N alloys where X represents the substitutional alloying element (Jack, 1974). The scope of the research has recently been widened to include Fe-X-C systems and also non-ferrous alloys such as Ag-Mg-O and Ag-Al-O. A schematic representation of the ternary systems investigated is shown in Figure I.2.

The present work started with the intention of examining the mutual effects of two substitutional solutes together in a nitrogen ferrite. Molybdenum and titanium were chosen because of their different affinities for nitrogen and because some work had already been carried out on the appropriate ternary systems. Although much was already known from previous investigations about the effects of molybdenum in ternary nitrogen ferrites, less was known about titanium, and so the Fe-Ti-N system was investigated

Fig. I.2.

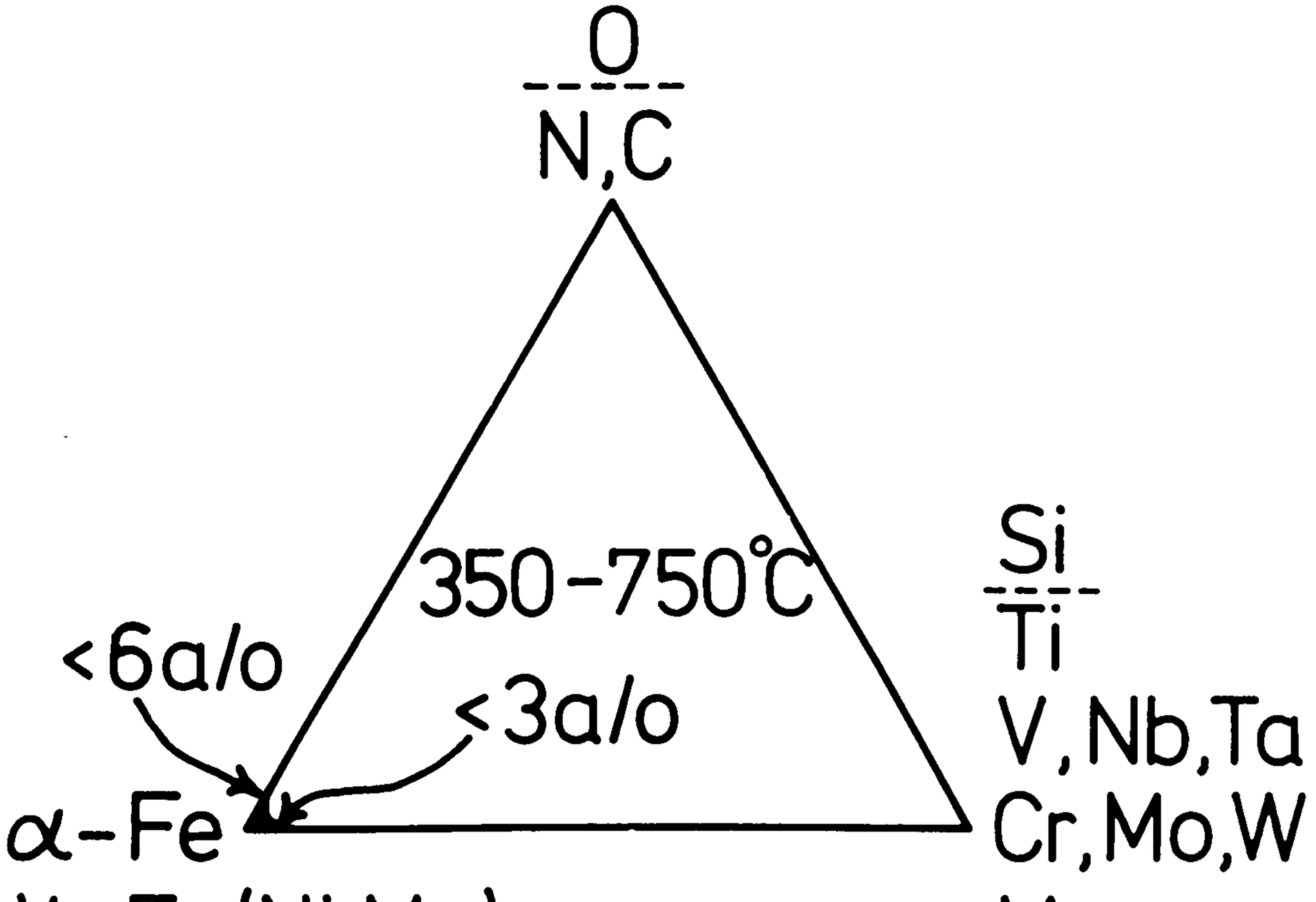

Ternary Systems Studied at Newcastle
Showing Substitutional-Interstitial
Solute Interactions

to provide the basis for the study of the Fe-Mo-Ti-N quaternary system. Some work was also carried out on the Fe-Mo-N system to supplement previous results. The main subject of the present thesis is the investigation of the Fe-Ti-N system and to a lesser extent the Fe-Mo-Ti-N and Fe-Mo-N systems.

I.2. Constant Activity Ageing

The high nitrogen supersaturations that can be maintained in solid solution even at high temperatures by constant activity ageing in ammonia:hydrogen gas mixtures allow the isothermal formation of mixed substitutional-interstitial clusters. During constant activity ageing an Fe-X alloy is equilibrated at constant temperature in the range 350°-750°C with a gas mixture in which the ammonia:hydrogen ratio is maintained constant so as to produce any required nitrogen potential - in some cases equivalent to many thousands of atmospheres of molecular nitrogen - at the specimen surface. In this temperature range the diffusivity of interstitial atoms in iron is several orders of magnitude greater than that of any substitutional solute. Thus, nitrogen can diffuse throughout an iron alloy specimen in the same time that the substitutional solute atoms have moved only a few atomic distances. By maintaining a constant nitrogen potential at the surface of a specimen any nitrogen removed from solution is immediately replenished from the gas and precipitation or clustering can occur until all the substitutional solute has been consumed. This can give higher densities of zones than by any other technique.

With this gas equilibration method the activity of

of the interstitial solute can be maintained constant at any desired value. Apart from using very high activities to produce mixed substitutional-interstitial solute-atom clusters, the method is useful in the selective precipitation of particular nitrides (Unthank et al, 1972). Constant activity ageing can also be applied to the controlled introduction of carbon and oxygen into metals by equilibration in appropriate gas mixtures.

Chapter II

PREVIOUS WORK

II.1. The Iron-Nitrogen Phase Diagram

Figure II.1 shows the iron-nitrogen phase diagram. There are five major phases formed with increasing nitrogen potential: α -nitrogen-ferrite, γ -nitrogen-austenite, γ'-Fe_4N, ε -$Fe_{3-2}N$ and ζ -Fe_2N. There are two additional phases α' -nitrogen-martensite obtained by quenching γ, and α''-$Fe_{16}N_2$ formed during tempering nitrogen-martensite and ageing nitrogen-ferrite. Nitrogen austenite can exist down to 590°C at which temperature it contains 9.4a/o nitrogen. The maximum solubility of nitrogen in ferrite is about 0.4a/o at 590°C.

γ'-Fe_4N has a face-centred cubic arrangement of iron atoms like austenite but the nitrogen atoms are fully ordered and occupy one quarter of the available octahedral interstices (see Figure II.2).

Body-centred tetragonal α''-$Fe_{16}N_2$ can be regarded as a fully-ordered supersaturated solid solution of nitrogen in body-centred cubic iron, i.e. a fully-ordered martensite. Alternatively, it is a distorted "Fe_4N" in which alternate nitrogen atoms are missing and which fits with the ferrite matrix with a Bain orientation relationship, (Jack, 1951a). α''-$Fe_{16}N_2$ is therefore intermediate both in structure and in composition between b.c.c.N-ferrite and f.c.c. γ'-Fe_4N.

Fig.II.1.

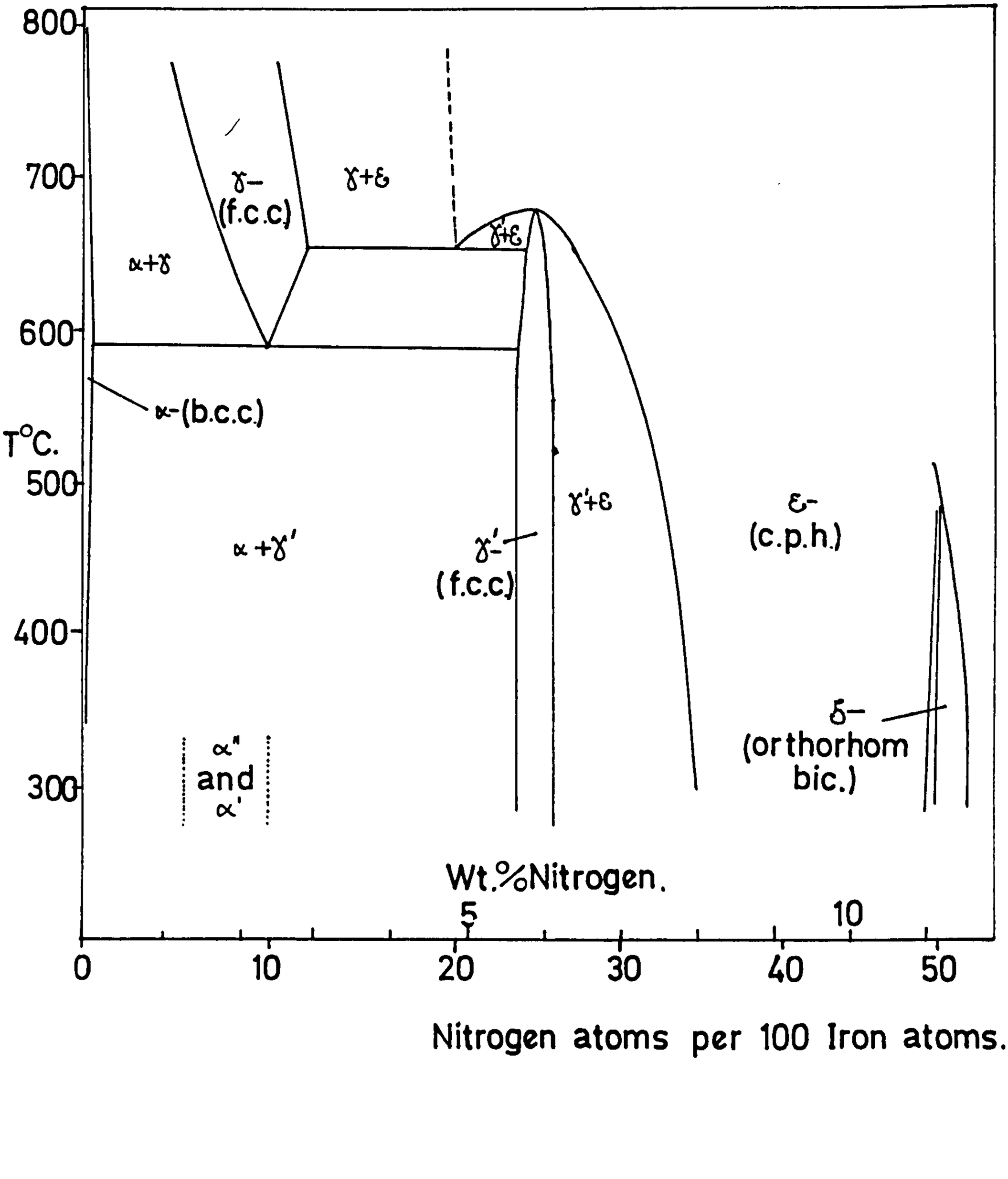

THE IRON-NITROGEN PHASE DIAGRAM.[After Jack, 1951].

Fig. II.2.

γ

nitrogen austenite

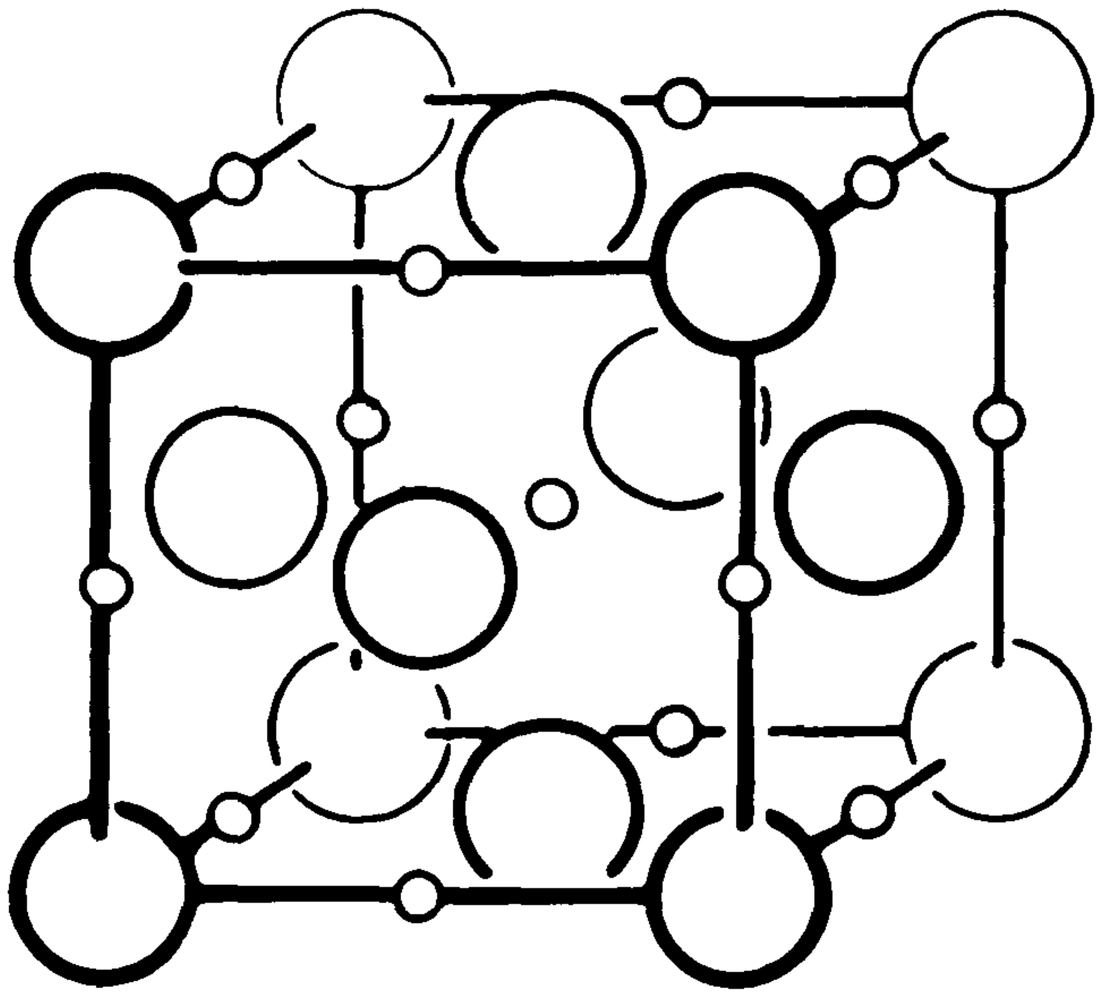

γ′

Fe_4N

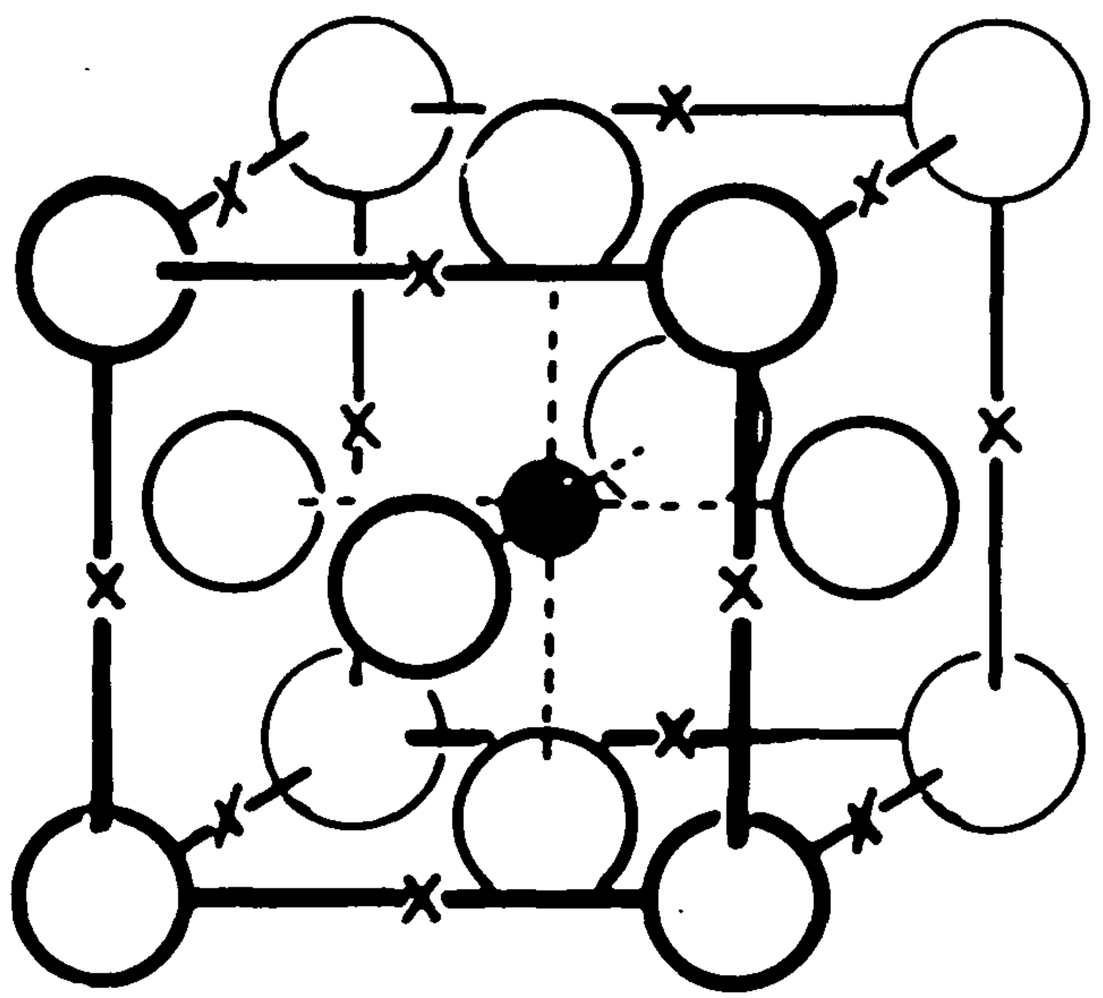

○ Fe atoms

× unoccupied interstices

o octahedral interstices 1 in 10 randomly filled

● N atom

The dilation of ferrite lattice by nitrogen in solution has been determined by Wriedt & Zwell (1962) as 0.008Å/a/oN. A value of 0.007Å/a/oN can be derived from the work of Jack (1951a,b).

II.2. The Quench-Ageing of Nitrogen-Ferrite

On cooling nitrogen ferrite to room temperature nitrogen is precipitated in a two-stage process (Dijkstra, 1949). Although from the phase diagram γ'-Fe_4N might be expected to precipitate (see Figure II.2) the initial precipitate is α''-$Fe_{16}N_2$ which forms as thin plates parallel to three cube planes in ferrite. α''-$Fe_{16}N_2$ is also produced by low-temperature tempering of nitrogen martensite (Jack, 1951a). Its structure (see Figure II.3) is that of fully ordered tetragonal martensite, that is, a b.c.c. arrangement of iron atoms anisotropically expanded in the c dimension because one in twenty-four octahedral interstices are occupied in an ordered manner. There is a consequent small contraction of the lattice in a directions (see Figure II.4). The structure is in fact ferrite with a nitrogen superlattice which causes some tetragonal strain. The α'' structure fits perfectly coherently with the ferrite matrix in "a" directions but there is a misfit in the c dimension. Therefore α''-$Fe_{16}N_2$ grows as plates, thin in the c direction, by diffusion, clustering and ordering of nitrogen atoms; no major movement of iron atoms is involved.

At high supersaturations and low temperatures ($\sim$20°C) precipitation of α''-$Fe_{16}N_2$ is homogeneous and occurs via Guinier-Preston zone formation (Roberts, 1970). As the temperature is increased and supersaturation decreases

Fig. II.3.

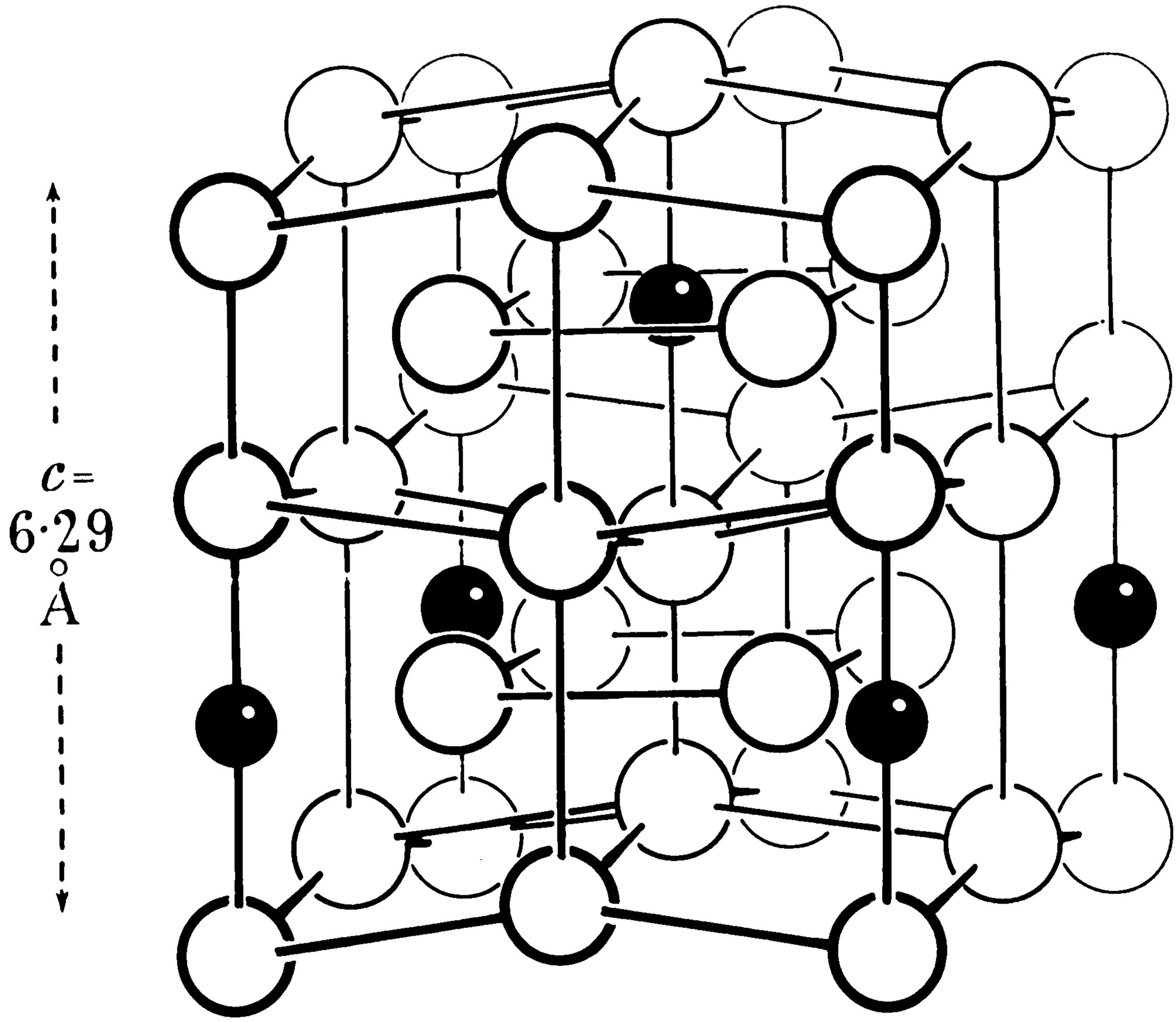

IRON ATOM

NITROGEN ATOM

Fig.II.4.

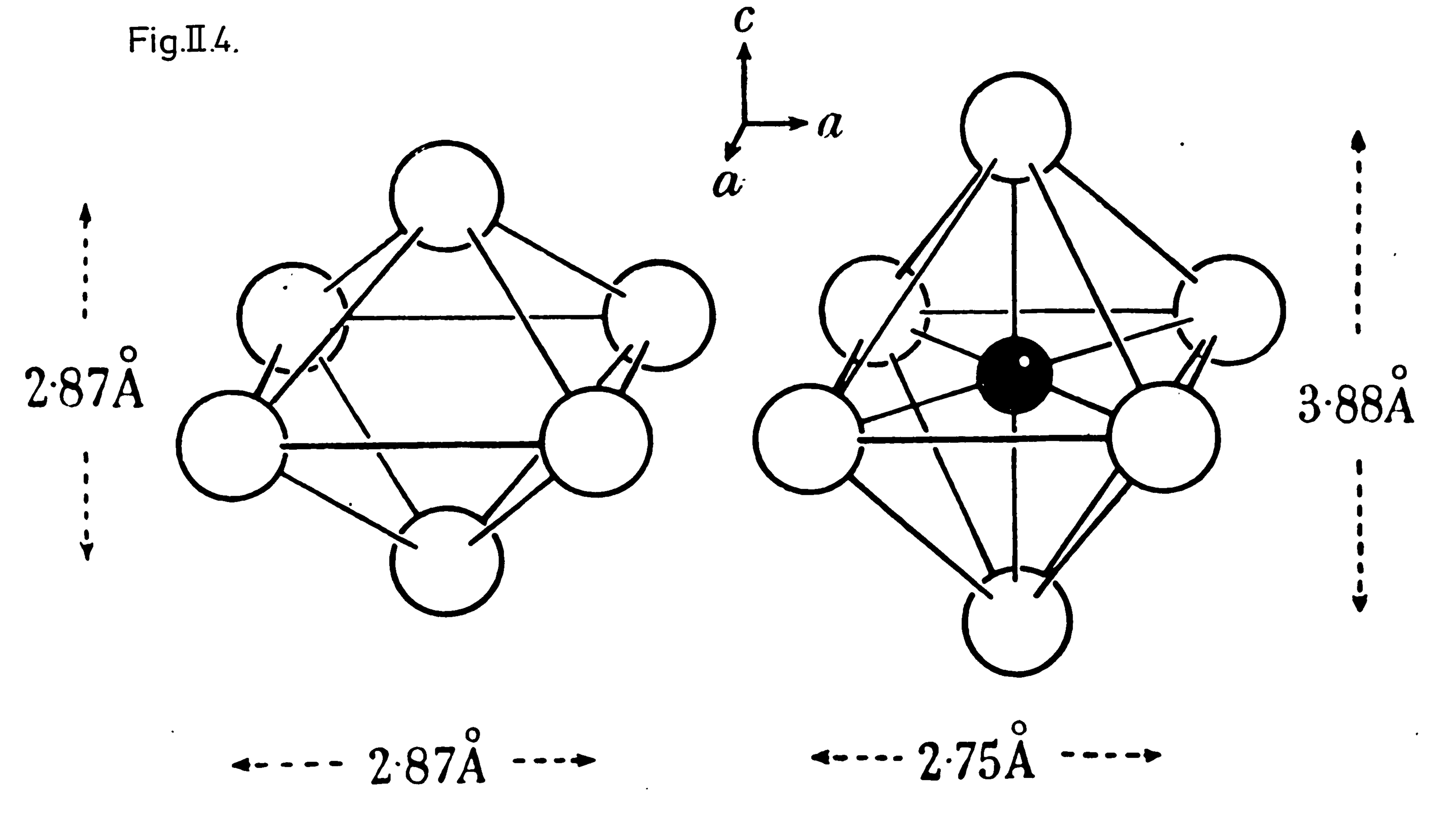

precipitation becomes heterogeneous (see Figure II.5).

γ'-Fe_4N precipitates at the expense of α''-$Fe_{16}N_2$ after long ageing times above about 170°C. However it also occurs as a grain boundary precipitate during the early stages of ageing at these temperatures (Roberts, 1970).

γ'-Fe_4N grows as plates such that $(112)_{\gamma'}$ is parallel to the plate surface (Mehl, Barrett & Jerabek, 1934; Booker, Norbury & Sutton, 1957).

II.3. Fe-X-N Systems

(i) Introduction

The substitutional-interstitial solute interactions occurring in nitrogen ferrites can be classified as taking place in three distinct ranges of temperature: high, medium, and low defined by the relative mobilities of the substitutional and interstitial solutes. At high temperatures substitutional solutes such as Ti, V, Cr, Mn, Nb, Mo, Ta and W move readily through ferrite matrix to precipitate alloy nitrides by reaction with nitrogen. At low temperatures where these solutes are unable to move they still affect the precipitation of iron nitrides because they change the activity coefficients of interstitial elements (Pipkin, 1968; Speirs, 1969; Mortimer et al, 1972). At intermediate temperatures, where substitutional solute atoms move over only short distances in the same time that nitrogen moves over large ones, mixed solute-atom clustering is observed (Speirs et al, 1970). The clustered non-random solid solution is a pre-precipitation stage in a continuous series of transformations and is accompanied by a very high specific strengthening. Prolonged overageing shows that

Fig. II. 5.

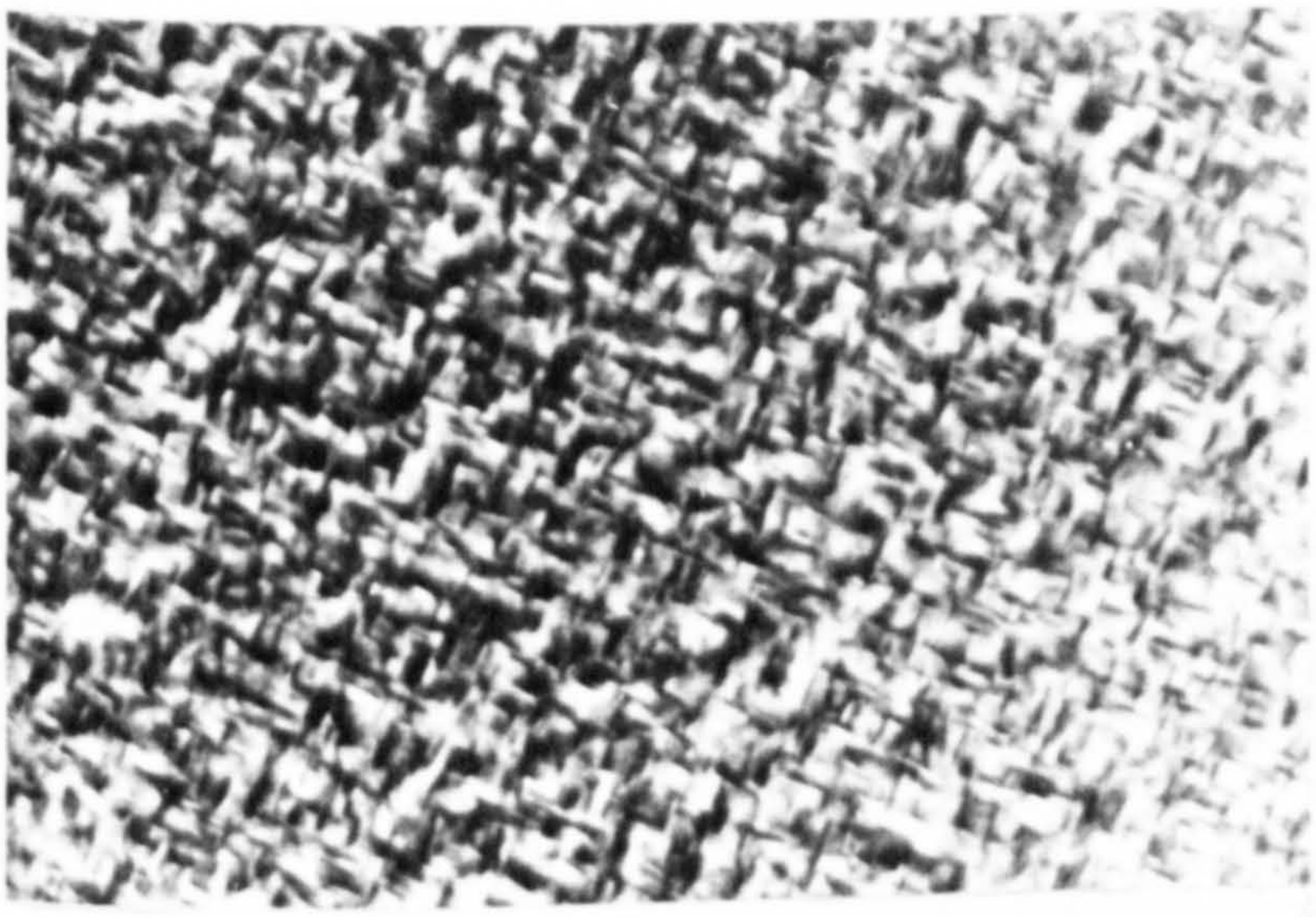

0·072%N. Aged 16h. 21°C.

Homogeneous only

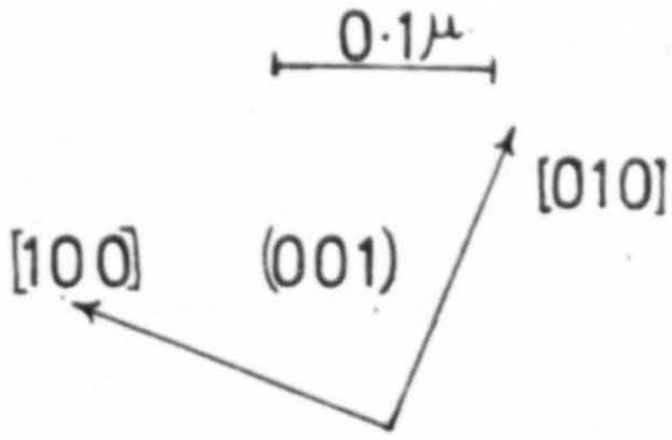

0·072%N. Aged 1h. 55°C.

Homogeneous +

Heterogeneous

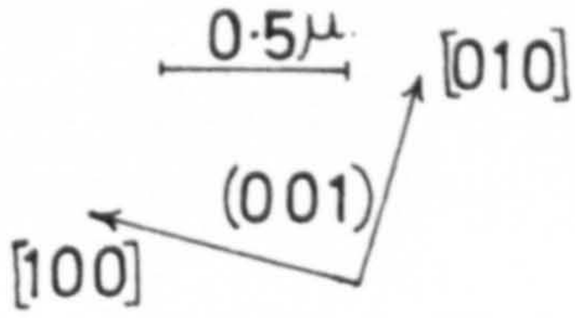

0·009%N. Aged 23h. 45°C.

Heterogeneous only

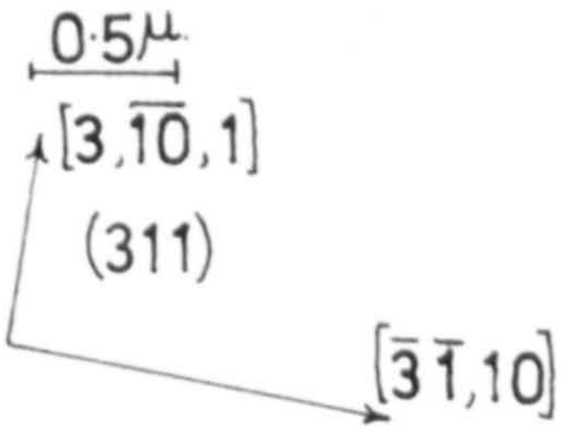

Eig PRECIPITATION MODES IN IRON-NITROGEN ALLOYS.

clustering is the first of a sequence of homogeneous precipitation stages analogous to those observed in the classical work on aluminium-copper alloys (Speirs et al, 1970).

During quench-ageing of Fe-X-N alloys the concentration of nitrogen and hence the driving force for the reaction decreases as the precipitation or clustering reaction proceeds and this can lead to a range of conditions under which different phases are stable at different stages of the treatment. Constant activity ageing eliminates this complication. Precipitation or clustering takes place at a rate controlled by the slowly diffusing substitutional solute whilst the nitrogen activity is maintained throughout the specimen by the rapidly diffusing nitrogen.

(ii) Zone formation in Fe-X-N system

Using constant activity ageing Speirs (1969) produced mixed substitutional-interstitial clusters i.e. Guinier-Preston zones in Fe-3^{a}/oMo nitrided at 590^{o}C in $6NH_3:94H_2$. High hardnesses and electron microstructures almost identical to those of Al-4^{w}/oCu aged at 160^{o}C for 5 hours were reported. Similar results are obtained for Fe-V, Fe-Mn, Fe-Nb and Fe-Ti alloys (Speirs et al, 1970); microstructures are also similar to those preceding the formation of α''-$Fe_{16}N_2$ in aged nitrogen ferrite; see Figure II.5.

Since the G.P. zones observed in these alloys are very small and only a few atom layers thick it might be argued that they are in fact very small coherent precipitates. However, the evidence that they are true G.P. zones formed by solute-atom clustering is based on the following

observations:

(a) the abnormal N/x ratios in the alloys are higher than can be accounted for by equilibrium nitride precipitates (Jack, K.H., 1975);

(b) very high nitrogen potentials are required to form the zones compared with those necessary to precipitate the equilibrium nitride;

(c) a zone solvus which is different from the solvus for the equilibrium nitride is observed (Roberts, 1970; Stephenson, 1973);

(d) continuous streaking of matrix reflections with no maxima characteristic of the precipitate structure occurs on electron diffraction patterns of nitrided Fe-X alloys;

(e) the electron microstructures observed are similar to those for classical G.P. zones (e.g. in Al-4^{w}/oCu;

(f) there is a similarity with the initial stages of quench-ageing of nitrogen-ferrite at room temperature where transformation occurs by diffusion and ordering of nitrogen atoms without major movement of iron atoms;

(g) the interstitial content of clusters in nitrided Fe-3a/oMo can be continuously changed and reduced to zero by ageing in hydrogen at 580°C to leave Mo atom clusters on {100} matrix planes; these Mo clusters can not be produced in Fe-3a/oMo without the introduction of nitrogen nor can they be obtained by decomposition of the equilibrium nitride precipitate (Driver, Unthank & Jack, 1972).

Further direct evidence is provided from measurement of the unit cell dimensions of these alloys. Krawitz & Sinclair (1975) show that the unit cell dimensions of a solid solution are essentially invariant with respect to the distribution and arrangement of its solute atoms. A matrix containing G.P. zones is a solid solution in which

non-random local atomic arrangements exist but its unit cell dimensions are the same as for a random solid solution having the same solute concentration. The unit-cell dimensions change to those of the solvent when precipitation occurs. The unit-cell dimensions of constant activity nitrided Fe-Mo and Fe-V alloys are in close agreement with those expected for iron containing the same amount of solute in random solution (Pope, Jones & Jack, 1975) but electron microscopy, field ion microscopy and electron diffraction patterns indicate that the solute-atom distribution can not be random. The solute atoms must therefore be clustered in a non-random solid solution.

(iii) Conditions for zone formation

The general conditions for zone formation in Fe-X-N alloys can be summarised as:

(a) the nitrogen potential must exceed that of the zone solvus;

(b) there must be a strong interaction between the substitutional solute and nitrogen and the most effective solutes are those which decrease the activity coefficient f_N^X of nitrogen in iron (see Figure II.6), that is, they increase the solubility of nitrogen prior to precipitation;

(c) the substitutional solute must have a high affinity for nitrogen (see Figure II.7);

(d) the temperature should be high enough for movement of substitutional atoms over short distances but not so high as to allow large-scale metal atom movement and thus the ready nucleation and growth of the equilibrium alloy nitride.

Fig. II.6.

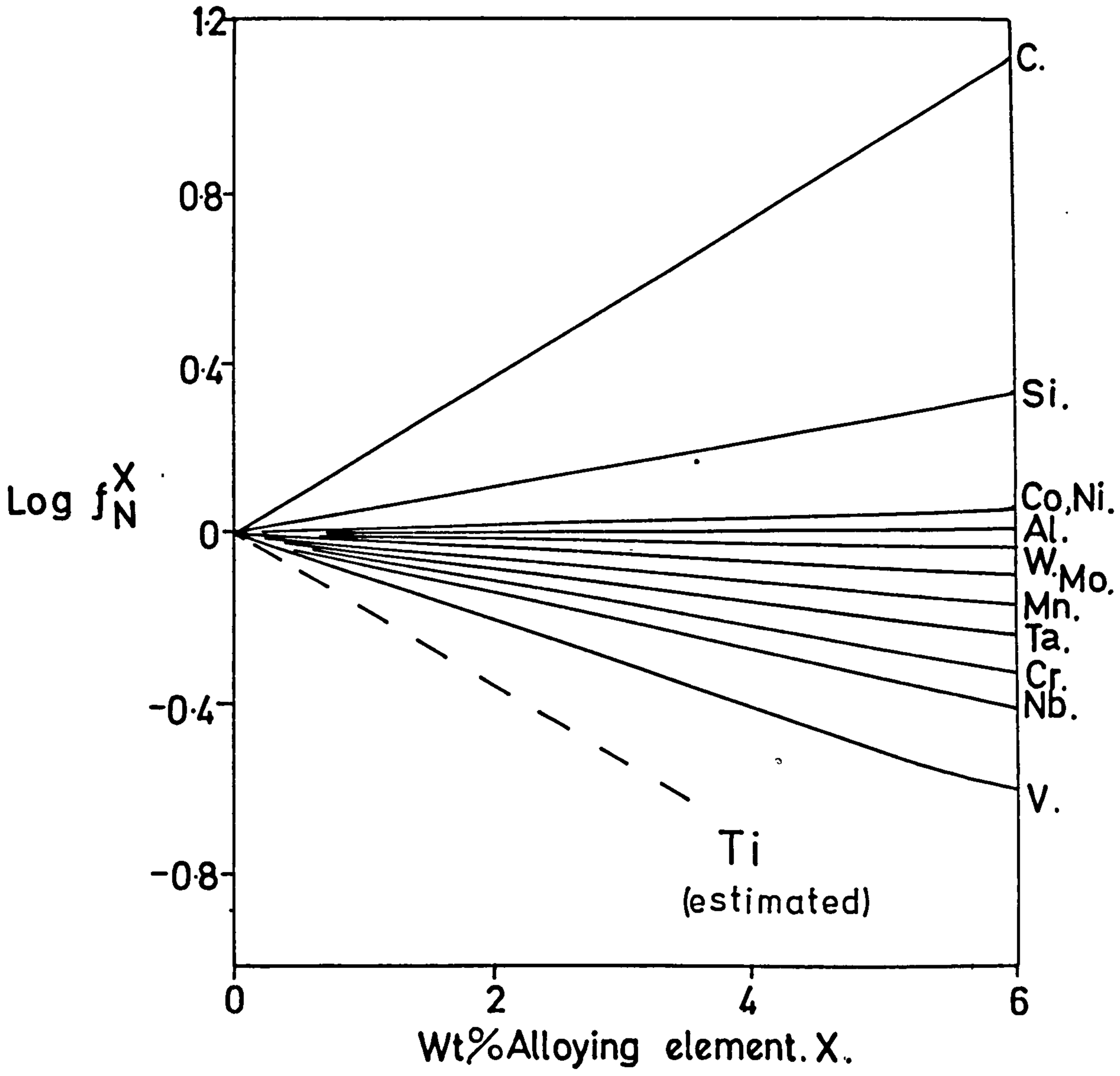

THE EFFECT OF ALLOYING ELEMENTS ON THE ACTIVITY COEFFICIENT OF NITROGEN IN IRON AT 1600°C.

[from Schenck et.al.(1958) & Pehlke and Elliott (1960).]

Fig. II.7.

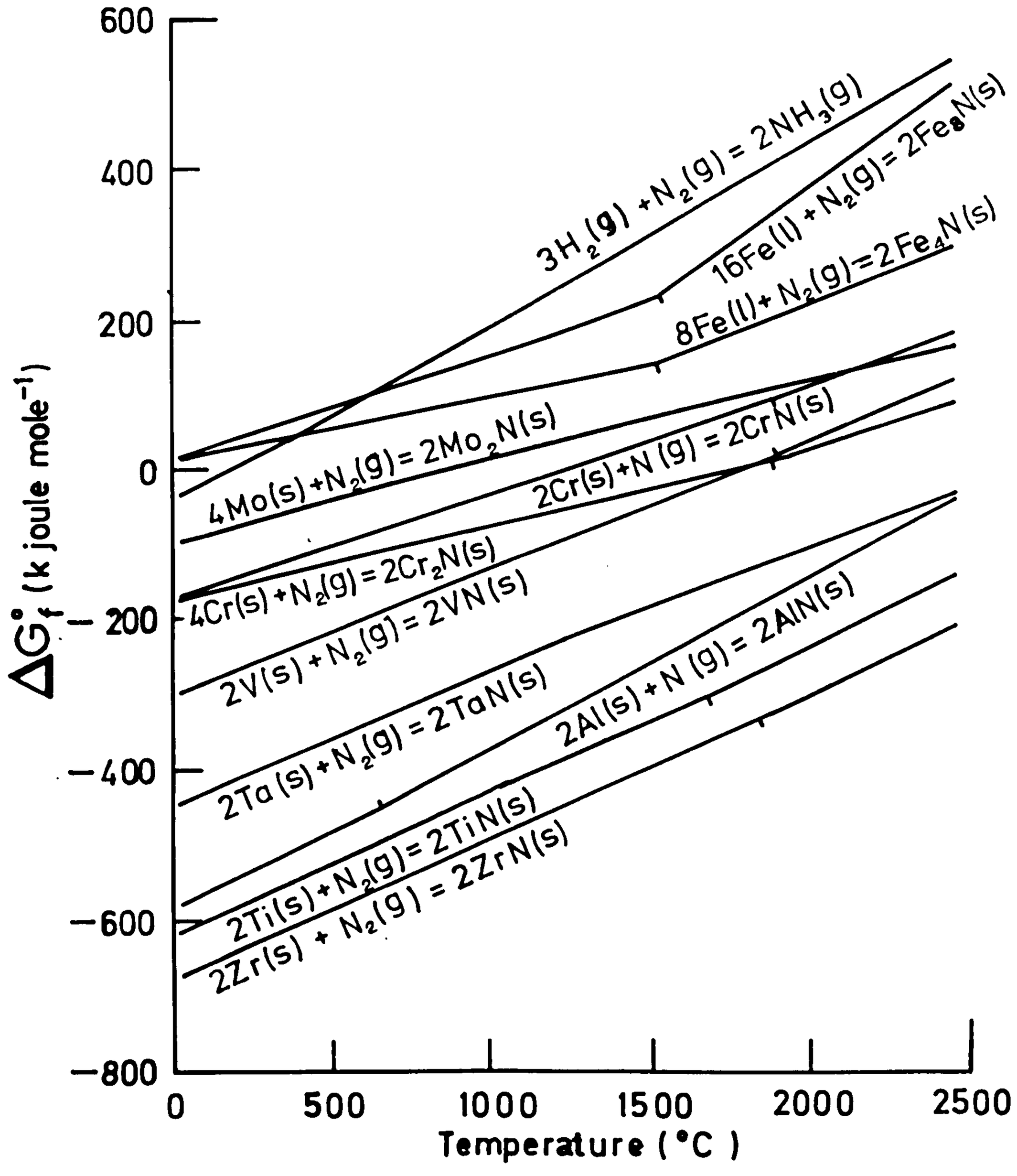

The reference states are pure phases which are stable at one atmosphere pressure and the designated temperature

The Standard Free Energies of Formation of some Nitrides

(iv) The precipitation sequence in nitrided Fe-X alloys

G.P. zones formed in Fe-X-N alloys age in a similar manner to those formed in Al-4^{w}/oCu alloys and the precipitation sequence is similar to the stages of homogeneous precipitation which occur in pure Fe-N alloys on quench-ageing at 0-200^{o}C. On nitriding b.c.c. Fe-X alloys, homogeneous precipitation occurs by continuous clustering and subsequent ordering within the clusters of both interstitial and substitutional solutes. The precipitation sequence can be represented as:

$$\underset{\text{I}}{\text{zones}} \xrightarrow{(1)} \underset{\text{IIa}}{\alpha''\text{-type intermediate}} \xrightarrow{(2)} \underset{\text{IIb}}{\gamma'\text{-type intermediate}} \xrightarrow{(3)} \underset{\text{III}}{\text{equilibrium precipitate}}$$

The designations α'' and γ' are not meant to imply rigid structure types but suggest respectively distorted b.c.c. and f.c.c. metal-atom arrangements accommodating nitrogen with or without ordering of either the substitutional or the interstitial solute atoms. Each particular system is different in detail. In Fe-Mo-N each of the above stages is fairly clearly recognised; in Fe-W-N, transformation (1) is rapid compared with (3). Thus, stage I is not observed (Stephenson, 1973) and stage II is the first to be recognised.

(v) The nitriding kinetics of Fe-X alloys

The nitriding of Fe-Ti, Fe-V and high-chromium Fe-Cr alloys occurs by the formation of a hard, sharply defined subscale which advances progressively into the bulk of the material. The kinetics of subscale advance are consistent with the internal nitriding equation (Hepworth, Smith &

Turkdogan, 1966).

$$\chi^2 = \cdot \frac{2}{r} \cdot \frac{[N]}{[X]} \cdot Dt \quad \ldots\ldots \quad \text{II.1.}$$

where χ = the subscale depth at time t

r = $^{N}/_{X}$ atom ratio in the "compound" formed

D = the diffusivity of nitrogen in iron at the reaction temperature

[N] = a/o nitrogen concentration at the surface

[X] = a/o of alloying element X

Departure from this behaviour occurs in Fe-Mo alloys (Jack et al, 1971) and at low substitutional solute concentrations in Fe-V (Pope, 1972) and Fe-Cr alloys (Mortimer, 1971).

There is a critical substitutional-interstitial activity product ($a_X . a_N$) and a critical nucleus size, both of which must be exceeded for precipitation or solute-atom clustering to occur (Hayes, 1973). The precipitation or clustering process therefore depends on the flux of the substitutional element as well as the flux of nitrogen. Therefore, in low substitutional content alloys, at high temperatures or where the substitutional solute has a low affinity for nitrogen, high nitrogen activities are required for the nucleation of clusters or precipitates.

In Fe-3a/oMo alloys, Jack et al (1971) observed a gradual build up in hardness across the whole specimen during nitriding at 570°C until a peak hardness is reached. The hardness profiles across partially nitrided specimens were slightly dish shaped. This type of hardening occurs if the effective nitrogen activity across the thickness of the specimen is uniform and may be achieved by the reduction

of the rate of the surface reaction so that the flux of nitrogen atoms is slow compared with the diffusion of nitrogen in the solid. Hayes (1973) shows that this behaviour is probably due to a thin oxide layer on the surface of the specimen and that with careful specimen preparation and pretreatment in pure hydrogen at the nitriding temperature, nitriding occurs by subscale advance. The subscale is not sharply defined but this is attributed to the relatively low affinity of molybdenum for nitrogen (see Figure II.7); the rate of subscale advance under these conditions is closely approximated by the internal nitriding equation (equation II.1).

II.4. The Iron-Titanium-Nitrogen System

The nitriding kinetics of Fe-Ti alloys containing 0.35-2.3^{a}/$_{o}$Ti are consistent with the internal nitriding equation II.1; see Jack et al, 1971 ; Chen, 1965.

The high hardness increments observed in the subscale of nitrided alloys are proportional to the square root of the titanium contents of the alloys (Kirkwood, Atasoy & Keown, 1974; Jack et al, 1971). This is similar to the chemical strengthening mechanism observed for age-hardened Al-Cu and Cu-Be alloys (Brown & Ham, 1971).

The nitrided alloys are very resistant to over-ageing and for an Fe-1.93^{a}/$_{o}$Ti alloy nitrided at 500^{o}C Kirkwood et al (1974) show on annealing for 24 hours at successively higher temperatures that softening does not occur below about 800^{o}C.

No clear microstructure has so far been resolved by electron microscopy for as-nitrided Fe-Ti alloys apart from the random dot contrast observed by Phillips & Seybolt (1968). Selected area electron diffraction shows matrix spot streaking along $\langle 100 \rangle$ directions (Speirs et al, 1970) indicating the presence of thin planar discontinuities on $\{100\}$ matrix planes. Kirkwood et al (1974) interpret this effect as being due to small coherent plate-like TiN precipitates. TiN precipitate spots are observed on electron diffraction patterns of Fe-1.83a/oTi nitrided at 600°C and aged in hydrogen for more than half an hour. Plate-like TiN precipitates with a Bain matrix orientation relationship can also be resolved on $\{100\}$ matrix planes and after prolonged ageing at 850°C the TiN precipitates become incoherent and appear as rectangular plates (Chen, 1965).

From diffractometer traces of nitrided Fe-Ti alloys Kirkwood et al (1974) have noted positive dilation of the ferrite lattice and asymmetry near the base of the $\{200\}$ Bragg peak. For alloys nitrided under certain conditions this splits into two peaks; a sharp Bragg peak of high intensity and a low intensity diffuse peak at higher Bragg angles. The latter was attributed to a tetragonal distortion of the ferrite lattice adjacent to the precipitate/zone plates. However, they also noted that for this interpretation to hold true, domains of precipitate plates parallel to each other would be expected in order to reinforce the tetragonality of the region. There is no evidence for this in the observed microstructures for the alloys aged at high temperatures. These results will be discussed in relation to the results of the present work in Chapter VII.

II.5. The Iron-Molybdenum System

The solubility of molybdenum in α-iron is about $4^{a}/o$ at $650^{\circ}C$ (Baen & Duwez, 1951; Hansen, 1958).

Irregularly shaped molybdenum-atom clusters have been observed in iron-molybdenum alloys (4-$6^{a}/o$Mo) aged at $550^{\circ}C$ (Ericsson & Cohen, 1971; Ericsson, Mourikis & Cohen, 1971). Hornbogen (1961) observed molybdenum discs on $\{100\}$ matrix planes on dislocation loops, formed from quenched-in vacancies in Fe-$20^{a}/o$Mo quenched from 1300-$1450^{\circ}C$ and aged at $500^{\circ}C$. Higgins & Wilkes (1972) also detected very fine scale clustering of molybdenum atoms in similarly aged Fe-$12^{a}/o$Mo. Thus in the Fe-Mo system substitutional and vacancy-modified substitutional solute-atom pre-precipitate clusters can be formed in alloys quenched from high temperatures and containing more than $4^{a}/o$Mo.

II.6. The Iron-Molybdenum-Nitrogen System

The effect of molybdenum on the solubility of nitrogen in iron-molybdenum alloys can be summarised as: at $500^{\circ}C$;

$$\log f_N^{Mo} = (-0.21 \pm 0.04)^{w}/oMo \quad \ldots\ldots \quad II.2$$

and for Fe-$1.01^{w}/o$Mo in the temperature range 400-$500^{\circ}C$;

$$\log f_N^{Mo} = -\frac{260}{T} + 0.13 \quad \ldots\ldots \quad II.3$$

where f_N^{Mo} is the ratio of the solubility of nitrogen in pure iron to that in iron-molybdenum alloys at the same

nitrogen potential (Pipkin et al, 1971). These equations hold true for iron-molybdenum alloys containing less than $2.16^{w}/_{o}Mo$ in solution and in which G.P. zones have not been formed.

The formation of mixed substitutional-interstitial clusters in nitrided iron-molybdenum alloys is accompanied by large hardness increments and Hayes (1972) has determined the zone solvus for Fe-$2.9^{a}/_{o}Mo$ and Fe-$1.7^{a}/_{o}Mo$ alloys from hardness measurements (see Figure II.8).

Electron diffraction patterns of Fe-$2.9^{a}/_{o}Mo$ nitrided at $580^{\circ}C$ in $7NH_3:93H_2$ are streaked at matrix spots along $\langle 100 \rangle$ directions and the bright field electron microstructure consists of a dense array of thin plate-like zones lying on $\{100\}$ matrix planes. From field-ion microscopy observations Driver & Papazian (1973) confirm that these are coherent disc-shaped clusters and not Mo_2N precipitates. Their evidence suggests that the Mo atoms exist randomly in the clusters but that the nitrogen atoms are partially or completely ordered in a similar manner to the nitrogen atoms in α''-$Fe_{16}N_2$ giving a zone composition $Fe_{10}Mo_6N_2$.

On ageing in hydrogen at $580^{\circ}C$ the nitrogen content of this alloy falls continuously (from $2.5^{a}/_{o}N$) until after 200 hours almost no nitrogen remains (see Figure II.9). In this condition the hardness of the alloy is 310VMH as compared to an annealed hardness of 150VMH and an as-nitrided hardness of 780VMH (Driver, Unthank & Jack, 1972). Electron microscopy shows that Mo zones about 500Å diameter and about 20Å thick are still present and electron diffraction patterns still show the same continuous streaking in $\langle 100 \rangle$ directions. This behaviour contrasts sharply with that reported by Brenner & Goodman (1971)

Fig. II.8.

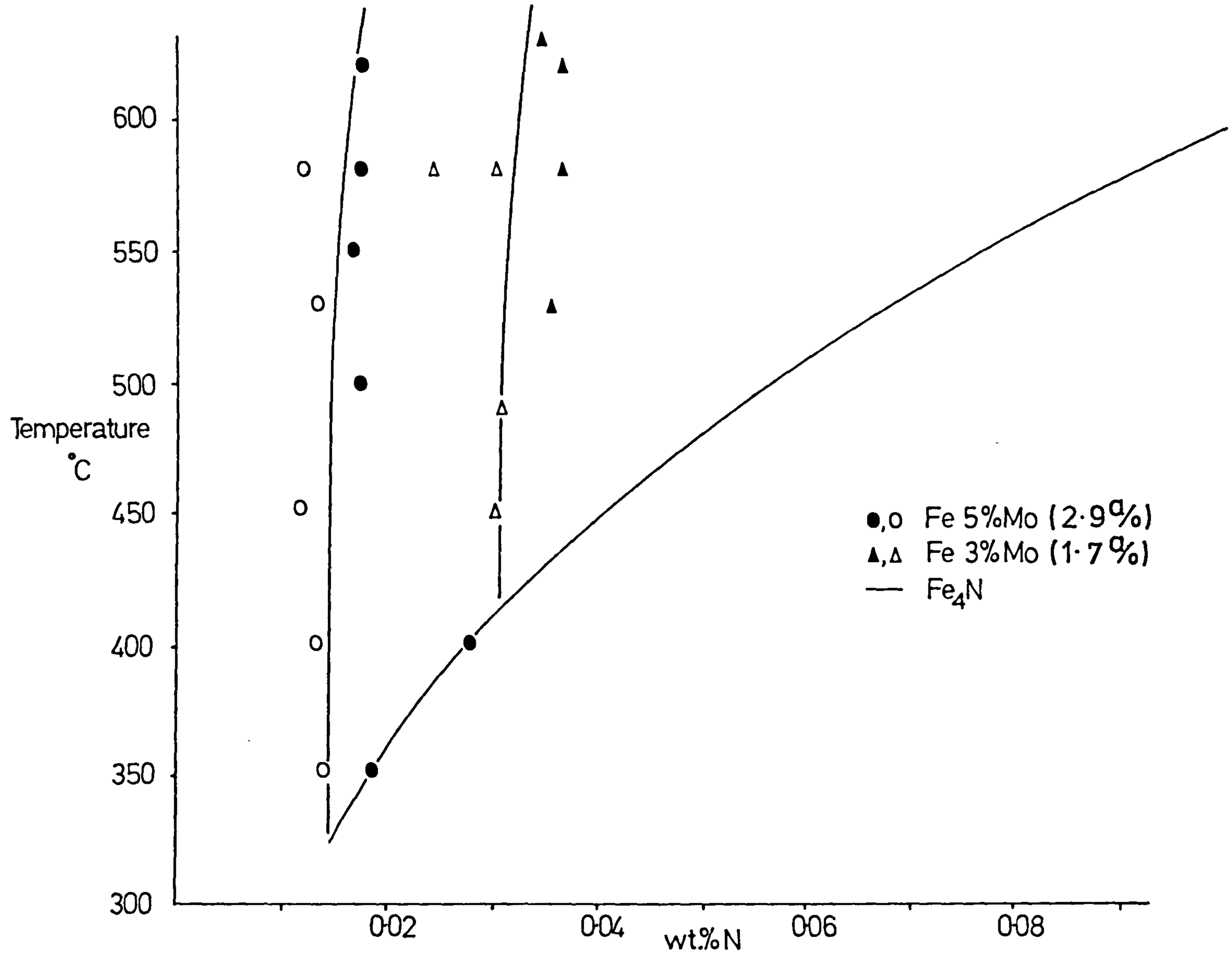

SOLVUS LINES FOR HOMOGENEOUS PRECIPITATION IN Fe-Mo-N ALLOYS.

Fig. II.9.

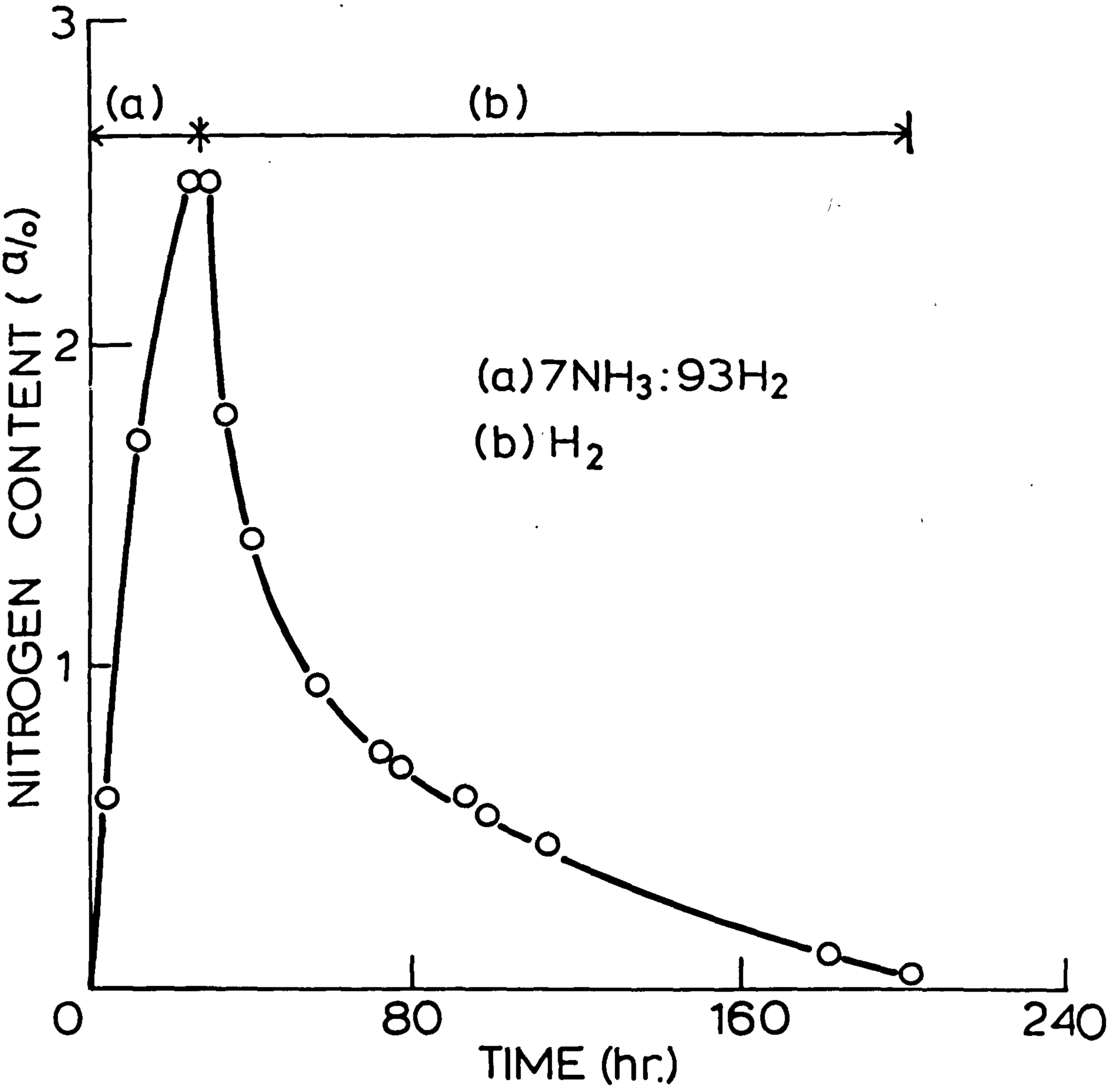

Nitrogen Contents of Fe-2·9 a/o Mo Alloy during Nitriding and Hydrogen Reduction

for Fe-3^{a}/oMo nitrided at 480°C to a nitrogen content of 2.4^{a}/oN and subsequently aged in hydrogen at 500°C. Only 0.4^{a}/oN could be removed in the ageing treatment and Driver et al (1972) suggest that this is due to the higher stability of zones at 500°C than at 580°C.

Driver (1972) reports that after over-ageing an Fe-2.9^{a}/oMo alloy nitrided to 0.8^{a}/oN at 800°C for one hour the precipitate is γ-Mo_2N which has a Bain orientation relationship with the matrix. On further ageing this transforms to η-Fe_3Mo_3N.

Figure II.10 shows the lattice parameters of Fe-2.9^{a}/oMo and Fe-1.7^{a}/oMo nitrided at 450°-580°C as a function of nitrogen content (Driver, 1973). The results for the Fe-2.9^{a}/oMo alloys are consistent, showing an increase in lattice parameter of 0.006Å per N atom per 100 metal atoms. Allowing for experimental error this figure agrees with the figures derived from the data of Jack (1951a,b) and Wriedt & Zwell (1962) for the expansion of the ferrite lattice by nitrogen. At 580°C the nitrided Fe-1.7^{a}/oMo alloys rapidly over-age because this molybdenum concentration barely exceeds the critical limit for zone formation. Thus after a small initial increase, the matrix unit-cell dimension falls rapidly on nitriding because of precipitation.

Fig. II.10.

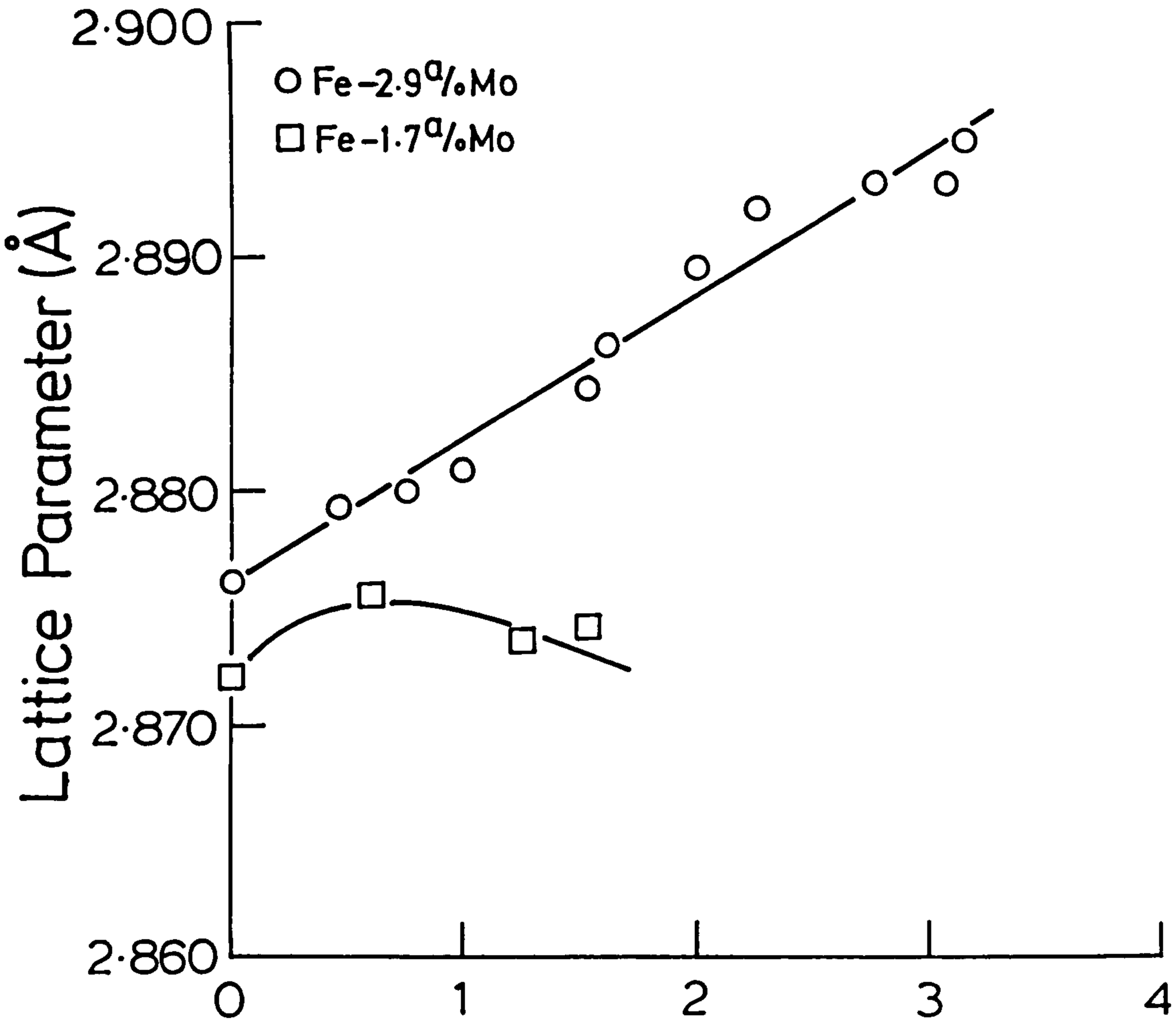

Lattice Parameters of Nitrided Fe-Mo Alloys

[Driver(1973)]

Chapter III

ALLOY MATERIALS

III.1. Binary Alloys

The chemical analyses of iron-titanium alloys supplied by the British Iron and Steel Research Association (B.I.S.R.A.) and iron-molybdenum alloys supplied by the National Physical Laboratory (N.P.L.) are given in Table III.1. These analyses give the total substitutional element contents including any present as carbide. The amount of "active" substitutional element (i.e. the substitutional element in solid solution) was calculated from the chemical analyses by assuming all carbon to be present as TiC, MoC or Mo_2C. Within experimental error the "active" molybdenum contents of the iron-molybdenum alloys are the same as their total molybdenum contents. As well as analyses provided by B.I.S.R.A., chemical analyses on the iron-titanium alloys were carried out in the Department of Metallurgy at the University of Strathclyde. Solvents which would not dissolve titanium carbide, nitride or oxide were used so that the analyses would indicate only the amount of substitutional element in solution i.e. the "active" substitutional element content. Results are given in Table III.1.

The lattice parameters obtained for the iron-molybdenum and iron-titanium alloys are listed in Table III.2.

Table III.1

cast	nominal composition	substitutional element (a/o) Mo	Ti	carbon (a/o)	source of analysis	mean "active" substitutional solute content (a/o) Mo	Ti
K1414	Fe-2a/oTi	-	2.110	0.023	B.I.S.R.A.	-	2.13
		-	2.17*	-	Strathclyde		
K1413	Fe-1a/oTi	-	1.10	0.074	B.I.S.R.A.	-	1.03
		-	1.03*	-	Strathclyde		
K1412	Fe-0.5a/oTi	-	0.595	0.074	B.I.S.R.A.	-	0.55
		-	0.571*	-	Strathclyde		
K2732	Fe-0.2a/oTi	-	0.187	0.1	B.I.S.R.A.	-	0.171
		-	0.167*	0.012	Strathclyde		
39AF2	Fe-3a/oMo	2.92	-	0.005	N.P.L.	2.92	-
39AF3	Fe-2a/oMo	1.72	-	0.009	N.P.L.	1.72	-
40AFI	Fe-1a/oMo	1.26	-	0.014	N.P.L.	1.26	-
FMTI	Fe-1.4a/oMo-1.1a/oTi	1.403	1.113	0.051	Strathclyde	1.40	1.06

* Soluble titanium only.

Table III.2

Alloy	Lattice parameter a/o (Å)
Fe-2^{a}/oTi	2.8716
Fe-1^{a}/oTi	2.8684
Fe-0.5^{a}/oTi	2.8671
Fe-0.2^{a}/oTi	2.8667
Fe-3^{a}/oMo	2.8769
Fe-2^{a}/oMo	2.8724
Fe-1^{a}/oMo	2.8709
Fe-1.4^{a}/oMo-1.1^{a}/oTi	2.8740

The lattice parameter of pure iron is 2.8664 Å

The N.P.L. chemical analyses quoted in Table III.1 and the lattice parameters quoted in Table III.2 for iron-molybdenum alloys are consistent with the data of Bowman, Parke & Herzig (1943); Guljaev & Trusova (1950) and Abrahamson & Lopata (1966). Thus, these values were assumed correct for the present investigation.

The lattice parameters obtained for the iron-titanium alloys are lower than those expected from the data of Abrahamson & Lopata (1966) and Zwell & Wriedt (1966) who observed a lattice parameter variation with titanium content of 0.0031Å/^{a}/oTi. The value obtained for the higher titanium content alloys used in the present investigation is 0.0026Å/^{a}/oTi which is close to the value obtained by Sutton & Hume-Rothery (1955) for alloys of similar titanium content (0.0025Å/^{a}/oTi).

The chemical analyses and lattice parameters for iron-titanium alloys assumed in this investigation are the mean values quoted in Tables III.1 and III.2.

Additional iron-titanium alloys of nominal compositions Fe-1.5^{a}/oTi and Fe-0.75^{a}/oTi were made in small quantities ($\sim$12g.) by arc melting appropriate mixtures of Fe-2^{a}/oTi, Fe-1^{a}/oTi and Fe-0.5^{a}/oTi in a purified argon atmosphere. The lattice parameters of the Fe-1.5^{a}/oTi and Fe-0.75^{a}/oTi alloys were 2.8699Å and 2.8676Å respectively and from these values, together with the data of Tables III.1 and III.2 the compositions were calculated as Fe-1.51^{a}/oTi and Fe-0.70^{a}/oTi in good agreement with the syntheses.

III.2. Ternary Alloys

An iron-molybdenum-titanium alloy was made up from commercially pure iron, Fe-2^{a}/oMo (39AF3) supplied by N.P.L. and commercially pure titanium foil (99.7%) by melting the constituents in the apparatus shown in Figure III.1 in a flow of purified hydrogen. Once the alloy was completely molten the hydrogen flow was stopped and the transparent vitreous silica vessel was flushed with purified argon to "de-gas" the melt. The melt was then allowed to solidify slowly and cool to room temperature in the argon atmosphere. The resultant ingot (~150g.) was hot-forged down to 5mm thick slab, descaled and cold-rolled to 1.5mm strip. Samples taken from both ends and the centre of the strip were analysed.

All three samples had the same composition within experimental error: Fe-1.40^{a}/oMo - 1.11^{a}/oTi - 0.051^{a}/oC of which all the carbon was assumed to be present as TiC. The concentrations of "active" titanium and molybdenum are taken as 1.4^{a}/oMo and 1.06^{a}/oTi so that the nominal composition is Fe-1.4^{a}/oMo-1.1^{a}/oTi. The lattice parameter of as-annealed wire specimens of this alloy was 2.8740Å.

Fig. III.1.

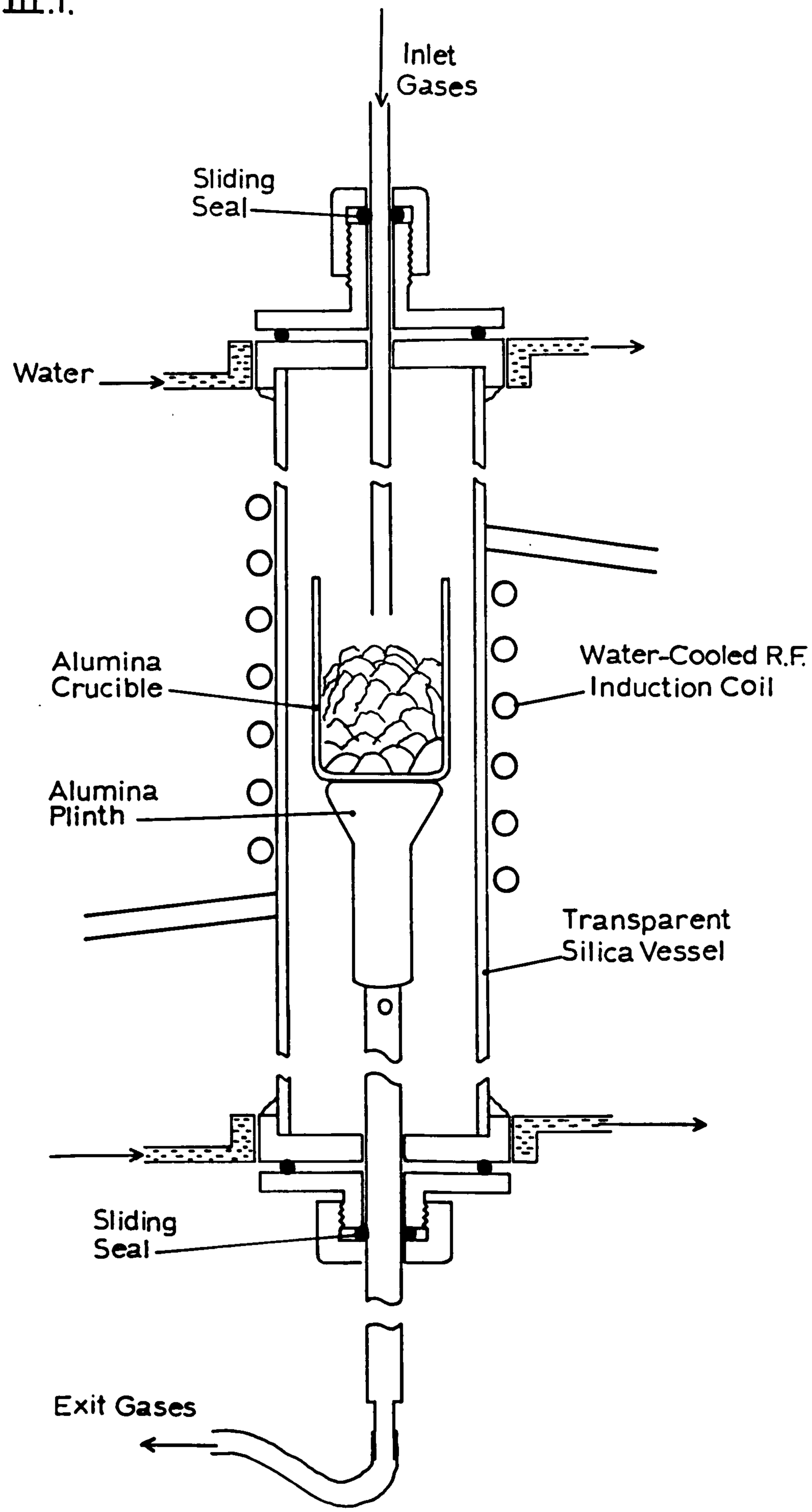

Induction Melting Apparatus

Chapter IV

EXPERIMENTAL METHODS

IV.1. Ammonia-Hydrogen Nitriding

Specimens were nitrided in ammonia-hydrogen gas mixtures of varying proportions at temperatures between 400° and $750^{\circ}C$. The nitrogen activity of an ammonia-hydrogen gas mixture is determined by the ratio of the concentrations of ammonia and hydrogen. The nitriding reaction is:

$$NH_3(g) \rightleftharpoons \underline{N} + 3/2\ H_2(g) \qquad \ldots . \quad \text{IV.1}$$

and at $T^{\circ}K$, the equilibrium constant is given by:

$$K = \frac{a_{\underline{N}} \cdot p_{H_2}^{3/2}}{p_{NH_3}} \qquad \ldots . \quad \text{IV.2}$$

where $a_{\underline{N}}$ is the activity of nitrogen in the nitride phase or solid solution and p_{NH_3} and p_{H_2} are the partial pressures of ammonia and hydrogen respectively. A system can therefore be brought to equilibrium under a predetermined nitrogen activity by controlling the proportions of ammonia and hydrogen.

Figure IV.1 illustrates the phases in the iron-nitrogen system in equilibrium with various ammonia-hydrogen gas mixtures over a range of temperatures (Lehrer, 1930). In the present investigation only nitriding conditions within the α-nitrogen-ferrite phase field of Figure IV.1 were employed.

Since Henry's Law is applicable over the complete range of solubility of nitrogen in ferrite at one atmosphere of nitrogen then:

$$a_{\underline{N}}^{\alpha} = K_h \cdot {}^{w}/_{o}\,\underline{N}^{\alpha} \qquad \ldots . \qquad \text{IV.3}$$

where K_h is the Henry's Law constant. Therefore the ${}^{w}/_{o}$ nitrogen in solution in pure ferrite in ammonia hydrogen gas mixtures is given by:

$${}^{w}/_{o}\,\underline{N}^{\alpha} = K^{1} \cdot \frac{p_{NH_3}}{p_{H_2}^{3/2}} \qquad \ldots . \qquad \text{IV.4}$$

The variation of K^1 with temperature is illustrated in Figure IV.2. The diagram shown in Figure IV.3 derived from equation IV.4 proved useful in determining suitable nitriding conditions. Roberts (1970) has shown that with the flow rates used in the present investigation there is no detectable "cracking" of ammonia below 650°C and hence no reduction in the effective nitriding potential expected for a particular set of nitriding conditions below this temperature.

Fig. IV.1.

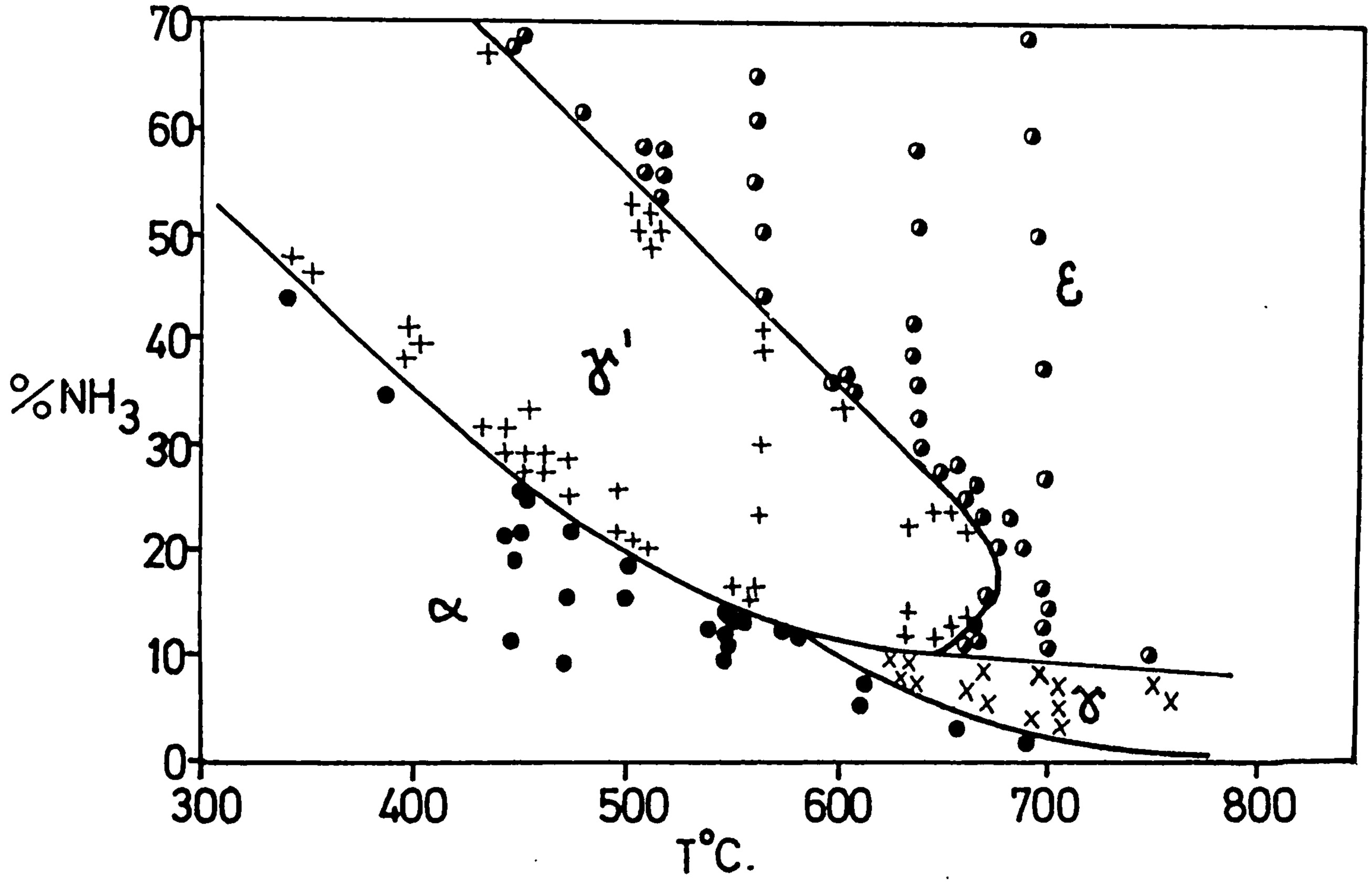

EQUILIBRIUM BETWEEN NH_3–H_2 MIXTURES [1 ATM.] AND SOLID PHASES OF THE IRON-NITROGEN SYSTEM [AFTER LEHRER (1930)].

Fig.Ⅳ.2.

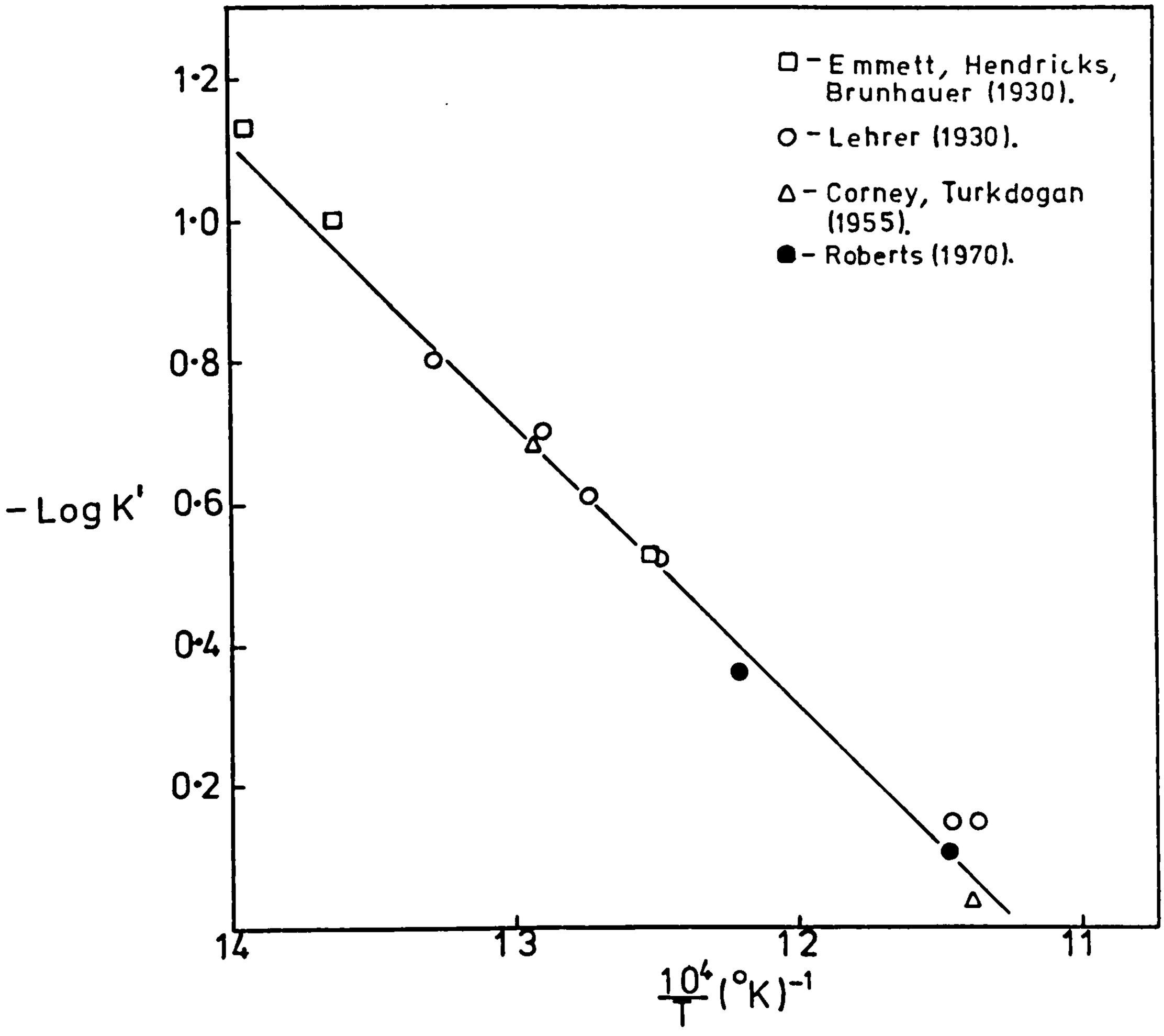

Temperature variation of K'.

Fig. IV.3.

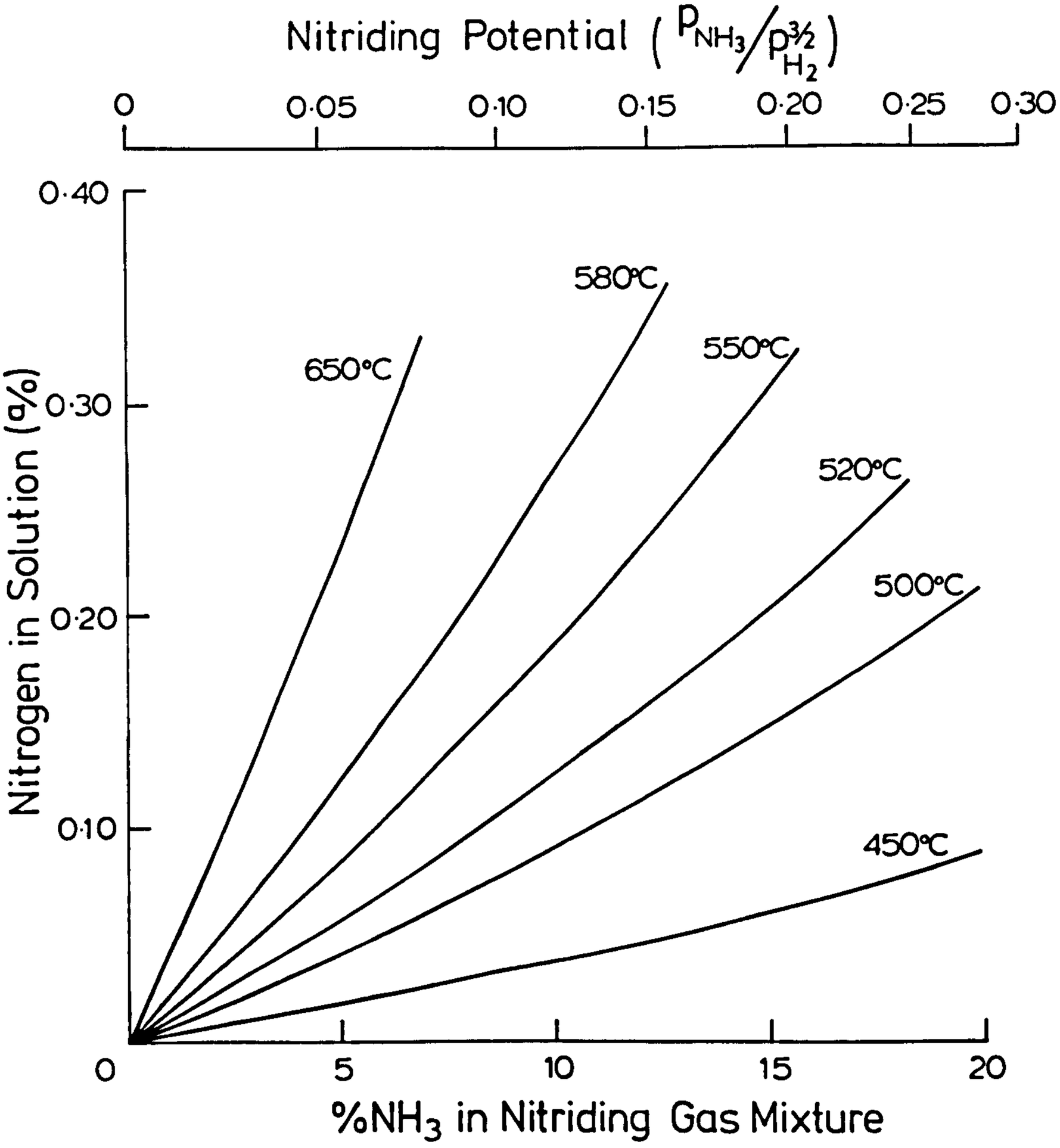

Nitrogen Concentration in Pure Iron in Equilibrium with Ammonia : Hydrogen Gas Mixtures

IV.2. Nitriding Apparatus

A schematic drawing of the nitriding apparatus is shown in Figure IV.4. The vertical reaction tube (25mm i.d.) was made of recrystallised alumina or mullite. Commercial hydrogen, argon,nitrogen and ammonia were purified by standard methods (Schwerdtfeger & Turkdogan, 1970) as illustrated in Figure IV.5. The activated copper was pre-reduced in hydrogen for several days at 160°C and maintained at 120°C during use. Gas flows were measured by capillary flow meters (see Figure IV.6) calibrated by a bubble displacement technique (Darken & Gurry, 1945). Total gas flow rates of 200ml/min were used during nitriding runs.

The temperature of the furnace hot zone (60mm long at 500°C) was controlled to $\pm$ 5°C by a standard "Ether" controller using a Pt/Pt-13%Rh thermocouple situated between the reaction tube and the furnace winding. The specimen temperature was monitored by a chromal/alumel thermocouple in an alumina sheath adjacent to the specimen.

The total gas pressure was maintained at slightly greater than atmospheric pressure by 10-20mm of oil in an exit bubbler.

IV.3. Annealing the Starting Alloys

For nitriding experiments the as-rolled strip or as-drawn wire was abraded, cleaned, degreased, sealed in transparent vitreous silica capsules evacuated to better than 10^{-5}torr, and then annealed at 900°C for 20 minutes by hanging the capsule in the hot zone of a vertical furnace.

Fig. IV.4.

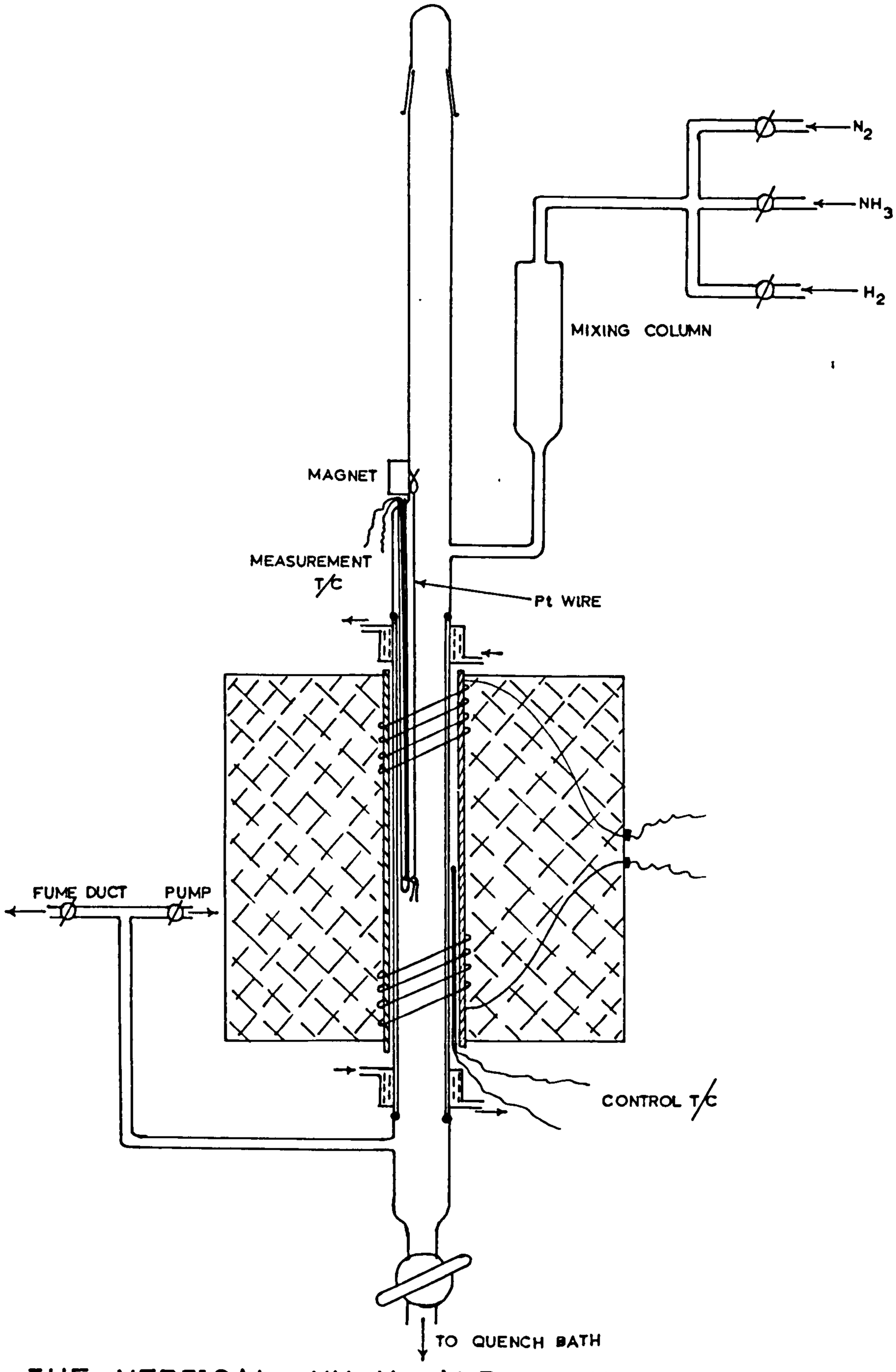

THE VERTICAL NH_3-H_2 AND N_2-H_2 EQUILIBRATION APPARATUS.

Fig. IV.5.

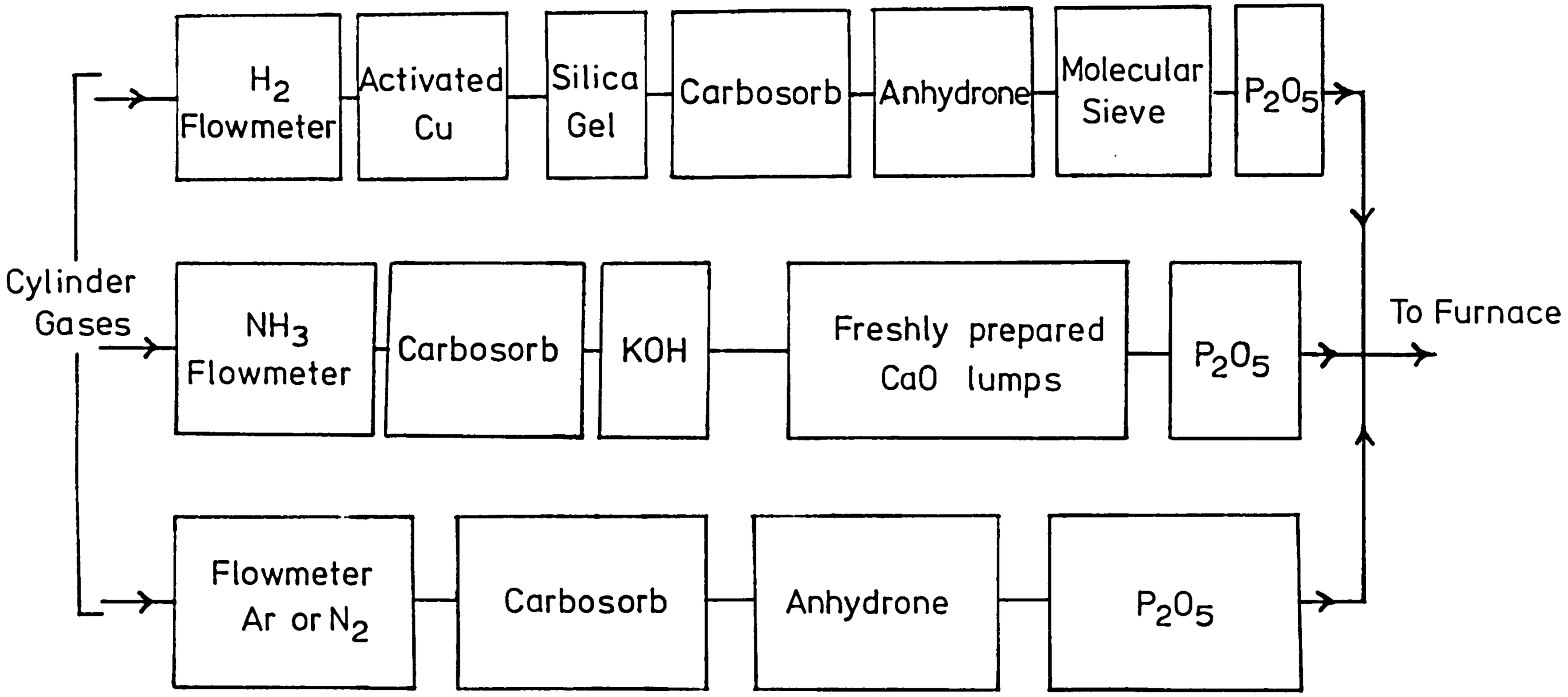

Gas Flow System for NH_3-H_2 and N_2-H_2 Equilibrations.

Fig. IV.6.

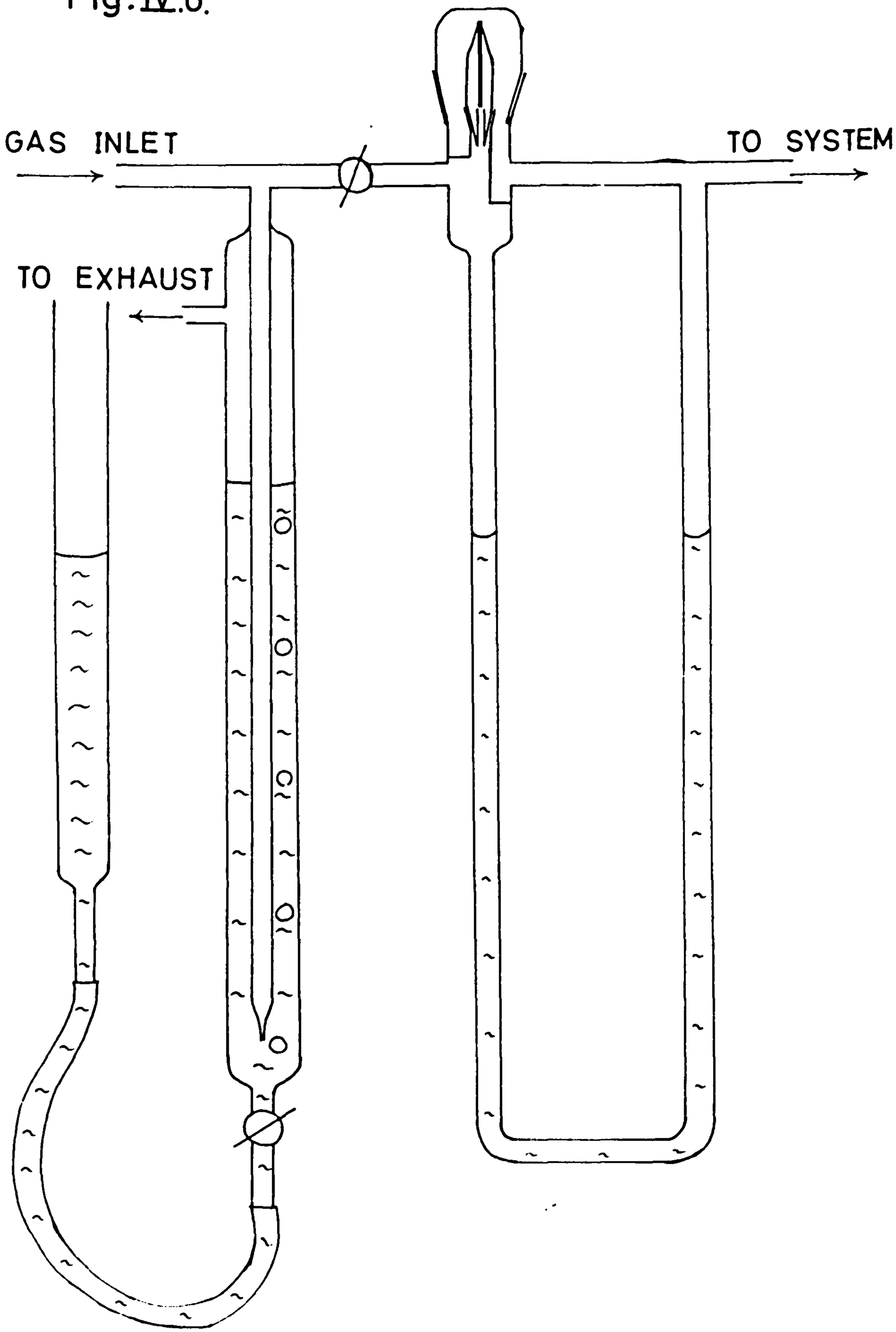

A CAPILLARY FLOWMETER [SCHEMATIC].

Specimens used for mechanical testing subsequent to nitriding were annealed in the nitriding furnace at 800°C for 8 hours in flowing hydrogen.

IV.4. Nitriding Procedure

Annealed specimens were abraded, degreased and given a light electropolish. After weighing they were suspended on a platinum wire and inserted into the cold (upper) end of the furnace and supported there by attachment to a soft iron bob held by a magnet. The system was then evacuated, checked for leaks and flushed with nitrogen. The appropriate ammonia-hydrogen gas mixtures were then passed through the furnace for about one hour before lowering the specimens into the furnace hot zone.

After nitriding, the specimens were raised quickly out of the hot zone and quenched in the incoming gas stream in the cold zone of the furnace. They were left there for 15 minutes before the furnace was evacuated, flushed with nitrogen, and the specimens removed and weighed. Similar procedures were adopted for ageing specimens in other gases.

Similar apparatus and nitriding procedures were used for nitriding tensile specimens for mechanical testing. However the nitriding apparatus was much larger. The furnace reaction tube was 30mm i.d. with a hot zone 250mm long and gas flow rates of 600ml/min were used.

IV.5. Weight Changes

Alloy specimens were weighed prior to and after nitriding treatments to ± 0.0001g on an analytical balance and an average of at least three values was taken as correct. In general nitrogen levels in nitrided alloys are much higher than those in steels (up to nearly 1.5^{w}/o in the present study) and at these values weight differences before and after nitriding give good reproducibility.

IV.6. Optical Metallography

Alloy specimens in the form of strip or wire were mounted vertically in phenolic hot-mounting compound and polished on two grades of emery paper followed by four grades of diamond down to 0.25μ . Specimens were etched in nital for 5-20 seconds.

A Reichart projection microscope was used for optical microscopy and photomicrography at a direct magnification of up to x1200.

IV.7. Hardness Measurements

Hardness measurements were made on etched metallographic specimens using a standard micro-hardness tester fitted to the Reichart microscope and with a load of 80g on the indenter.

IV.8. Mechanical Testing

Tensile tests were carried out on flat tensile specimens of 20mm gauge length and cross-section approximately 5x0.5mm at a nominal strain rate of $1.67\ 10^{-4}$ with an "Instron" type 1115 tensile testing machine. Load-extension curves were automatically recorded and for each observation at least three specimens with identical histories were tested.

IV.9. Preparation of Specimens for Electron Microscopy

Thin foils of nitrided alloy specimens were prepared from strip less than 0.5mm thick. Usually the material was thinned to about 0.1mm by chemically polishing in a mixture 50 parts water:50 parts hydrogen peroxide (100 volumes):2-10 parts hydrofluoric acid. Thin foils were then obtained by electropolishing using a standard "window" technique with a "Shandon" electropolisher power supply at 18-22 volts and -2° to $+3^{\circ}$C in a solution of 68v/o glacial acetic acid:16v/o perchloric acid:16v/o 2-butoxyethanol.

IV.10. Electron Microscopy

Transmission electron microscopy was carried out using a Philips E.M.300 instrument equipped with a goniometer stage.

IV.11. X-ray Diffraction

Specimens examined by X-ray powder photography were wire (0.3-0.6mm diameter) or narrow strip cut from foils.

X-ray powder photographs for determination of ferrite lattice parameters were obtained using Philips 114mm and Unicam 190mm diameter cameras with iron-filtered Co-K_α radiation or LiF crystal monochromated Fe-K_α radiation Lattice parameters were obtained by Nelson-Riley (1945) extrapolation and were found to be self-consistent for different cameras.

For the determination of second phases and the investigation of diffuse scattering effects Unicam 90mm diameter cameras were used with crystal reflected monochromatic Fe-K_α and Cr-K_α radiations.

X-ray diffuse scattering effects were also examined using a Philips diffractometer with Cr radiation from a graphite monochromator.

Chapter V

THE SCOPE OF THE PRESENT INVESTIGATION

Previous investigations at Newcastle have shown that mixed substitutional-interstitial solute-atom clusters are formed when both ferritic and austenitic Fe-X alloys are constant activity nitrided in ammonia:hydrogen gas mixtures at 350-750°C. In the present work similar experimental methods, including electron microscopy, X-ray diffraction, mechanical properties measurements, observation of weight changes, diffuse X-ray and electron scattering and careful lattice parameter measurements, are all used with nitrided Fe-Ti alloys to provide further insight into the structure and properties of mixed substitutional-interstitial solute-atom clusters.

In Chapter VI the planar discontinuities existing in nitrided Fe-Ti alloys are shown to be mixed clusters. The structure of these clusters is deduced from the variation of their N:Ti atomic ratio with nitriding conditions; chemical and crystallographic considerations are also used in proposing a model for the cluster.

In Chapter VII the electron microstructures of Fe-Ti alloys nitrided at both high and intermediate temperatures are examined. Tweed contrast images and diffuse electron scattering effects similar to those observed in aged Cu-2^{w}/oBe alloys indicate the presence of partially ordered arrays of G.P. zones in alloys nitrided at intermediate temperatures. The observed X-ray diffuse

scattering effects are shown to be consistent with this model and are correlated with the changes in microstructure under varying nitriding conditions.

The ageing kinetics of nitrided Fe-Ti alloys at high temperatures (800-850°C) are reported in Chapter VIII.

In Chapter IX it is shown that the dominant strengthening mechanism operating in as-nitrided Fe-Ti alloys, suggested from hardness measurements and tensile tests, is chemical in origin.

In Chapters XI and XII the results of an investigation of homogeneous precipitation in a nitrided Fe-Mo-Ti alloy are presented and compared with those for similar experiments in the ternary Fe-Ti-N and Fe-Mo-N systems. The mutual effect of Mo and Ti on the behaviour of nitrogen in iron alloys is compared with their individual effects in Fe-Ti-N and Fe-Mo-N . To facilitate this comparison the nitriding behaviour of Fe-Mo alloys is described in Chapter X.

Chapter VI

THE COMPOSITION AND STRUCTURE OF ZONES IN NITRIDED Fe-Ti ALLOYS

VI.1. Introduction

Measurements of unit-cell dimensions used in conjunction with electron microscopy and hardness measurements provide a means of identifying mixed substitutional-interstitial solute-atom clusters in ternary ferrites. For Fe-Ti, Fe-Mo, Fe-V and under certain conditions for Fe-Cr alloys the increase in unit cell dimensions of the nitrided alloys is much greater than expected by assuming precipitation of the alloying element nitride together with equilibration of the ferrite matrix with the nitriding atmosphere (Pope, Jones & Jack, 1975). Weight change measurements correlate with unit-cell dimensions to show that the nitrogen is, within experimental error, entirely in solid solution with no precipitation of any substitutional or interstitial solute. Electron micrographs show dense arrays of thin, disc-shaped structures on $\{100\}$ matrix planes which give rise to $\langle 100 \rangle$ streaking of matrix spots on electron diffraction patterns (Speirs et al, 1970 and Jack, D.H., 1971). This evidence together with the high hardness of the nitrided alloys suggests that the solid solutions of substitutional and interstitial atoms are non-random and that the disc shaped structures must be solute-atom clusters.

In the present investigation careful measurements of

nitrogen uptake and loss have also been made during equilibration of Fe-Ti alloys in nitriding and reducing atmospheres to determine the composition of the resultant alloys.

VI.2. Unit-Cell Dimensions of Nitrided Fe-Ti Alloys

Table VI.1 shows the weight, gain measurements, hardness, lattice parameters and increments in lattice parameter per $^{a}/_{o}$ nitrogen for Fe-Ti alloys nitrided in ammonia:hydrogen atmospheres in the temperature range 400-750^{o}C. In no case was heterogeneous precipitation observed and after an initial nitriding period the nitrogen content reached a constant level for a given set of nitriding conditions and remained constant indefinitely. The lattice parameters of the alloys in every case increased during nitriding and high hardnesses were observed.

The introduction of a nitrogen atom into an interstice of b.c.c. iron to form a solid solution distorts the arrangement of surrounding iron atoms into a regular octahedron (see Figure II.4). If all three orientations of octahedra are occupied equally then the isotropic distortion will result in an increase in the mean unit cell dimension of the solid solution i.e. an increase in the lattice parameter of the alloy which will depend on the nitrogen concentration. For Fe-Ti alloys nitrided at 500-580^{o}C the mean increment in lattice parameter is $+0.0064 \pm 0.0005$Å per $^{a}/_{o}$ nitrogen uptake. This value is slightly less than that (0.008 ± 0.0007Å/$^{a}/_{o}$N) predicted for very dilute solutions ($< 0.2^{a}/_{o}$N) of nitrogen in ferrite by Wriedt & Zwell (1962). However for the

Table VI.1

alloy	temp. ^{o}C	v/oNH$_3$	a/oN (by wt.)	a_o(Å)	a_o/N (Å/a/oN)	V.M.H.
Fe-2^a/oTi	750	1	2.46	2.8783	-	750
	650	3.7	3.76	-	-	1200
	580	0.5	2.31	-	-	1030
		1	3.25	-	-	-
		2	3.55	2.8948	0.0065	1175
		4	3.6	2.8938	-	1170
		4.5	4.05	-	-	-
		6	3.6	-	-	-
		6.7	3.94	-	-	1180
		8	4.64	-	-	-
		12	-	-	-	1205
	550	9.2	4.68	-	-	1135
	520	12.8	5.27	-	-	1140
	500	0.5	2.17	2.8846	0.0060	920
		2	3.60	2.8933	0.0060	910
		4	3.75	2.900	0.0075	1030
		8	4.85		-	1080
		12	5.28		-	1025
		16.7	5.72		-	1140
	400	30	6.28	-	-	-

Table VI.1 (cont.)

alloy	temp. ^{o}C	V/oNH$_3$	a/oN (by wt.)	a_o(Å)	a_o/N (Å/a/oN)	V.M.H.
Fe-1a/oTi	750	1	0.98	2.8759	-	580
	650	3.7	1.72	-	-	900
	580	0.5	1.28	-	-	785
		1	1.52	-	-	-
		2	1.71	2.8800	0.0068	855
		4	2.19	2.8812	0.0058	850
		4.5	2.04	-	-	-
		6	2.27	-	-	-
		6.7	2.17	2.8814	0.0060	870
		8	2.41	2.8839	0.0064	-
		12	-	2.8874	-	910
	550	9.2	2.25			835
	520	12.8	2.55			825
	500	0.5	1.18	2.8762	0.0067	675
		2	1.58	2.8812	0.0081	700
		4	1.89	2.8808	0.0066	755
		8	2.54	2.8829	0.0057	790
		12	2.64	2.8879	0.0074	800
		16.7	2.90	2.8875	0.0066	865
	400	30	2.84	-	-	-
		24	2.55	-	-	-

Table VI.1 (cont.)

alloy	temp. °C	v/oNH$_3$	a/oN (by wt.)	a_o(Å)	a_o/N (Å/a/oN)	V.M.H.
Fe-0.5a/oTi	750	1	1.17	2.8705	0.0030	450
	650	2	0.86	2.8725	0.0064	-
		3.7	1.03	-	-	690
		4.5	1.26	2.8737	0.0053	-
	580	0.5	0.60	-	-	600
		1	0.68	-	-	-
		2	0.80	2.8712	0.0051	610
		4	0.92	-	-	640
		4.5	1.00	-	-	
		6	1.08	-	-	
		6.7	1.12	2.8744	0.0065	
		8	1.20	2.8745	0.0062	
		12	-	2.8776	-	
	550	9.2	1.10	-	-	640
	520	12.8	1.32	-	-	615
	500	0.5	0.60	2.8705	0.0056	405
		2	0.81	2.8712	0.0068	515
		4	0.95	2.8731	0.0063	545
		8	1.14	2.8735	0.0056	575
		12	1.18	2.8744	0.0062	590
		16.7	1.34	2.8757	0.0064	650
	400	24	1.35	-	-	-

Table VI.1 (cont.)

alloy	temp. °C	v/oNH$_3$	a/oN (by wt.)	a_o(Å)	a_o/N (Å/a/oN)	V.M.H.
Fe-0.2a/oTi	580	0.5	0.21	-	-	370
		2	0.30	-	-	415
		4	0.38	-	-	440
		6.2	0.47	-	-	440
		10.7	0.61	-	-	485
	500	0.5	0.21	-	-	360
		1	0.22	-	-	350
		2	0.23	-	-	280
		4	0.30	-	-	310
		8	0.39	-	-	350
		12	0.52	-	-	

higher nitrogen concentrations encountered in the present investigation a more reliable value of 0.007 ± 0.0005 Å/^{a}/oN is based on the structures of α'-nitrogen martensite and of α''-$Fe_{16}N_2$ (Jack, 1951a,b). This is in close agreement with that observed for nitrided Fe-Ti alloys. It is concluded that all the nitrogen absorbed during nitriding is in solid solution with titanium in ferrite, yet the high hardnesses of nitrided alloys indicate that the solute atom distribution can not be random. The high hardnesses are therefore due to solute-atom clusters or G.P. zones in the ferrite matrix which would give the same lattice parameter as for a random solid solution of the same concentration (Krawitz & Sinclair, 1975).

The relatively small increase in lattice parameter with nitrogen uptake for alloys nitrided at 750°C indicates that some precipitation has taken place at this temperature.

VI.3. Composition of Zones in Nitrided Fe-Ti Alloys

In general the nitrogen uptake of nitrided Fe-Ti alloys exceeds that required for the formation of stoichiometric TiN plus the amount corresponding to the equilibration of the ferrite matrix with the nitriding atmosphere. The weight increase of Fe-Ti alloys during nitriding depends on the temperature, nitriding potential $p_{NH_3}/p_{H_2}^{3/2}$ of the gas mixture and the titanium content of the alloys. Figures VI.1 and VI.2 show the variation of nitrogen uptake with nitriding potential for Fe-Ti alloys nitrided at 580°C and 500°C. Also shown is the variation of nitrogen in solution in b.c.c. iron in

Fig. VI.1.

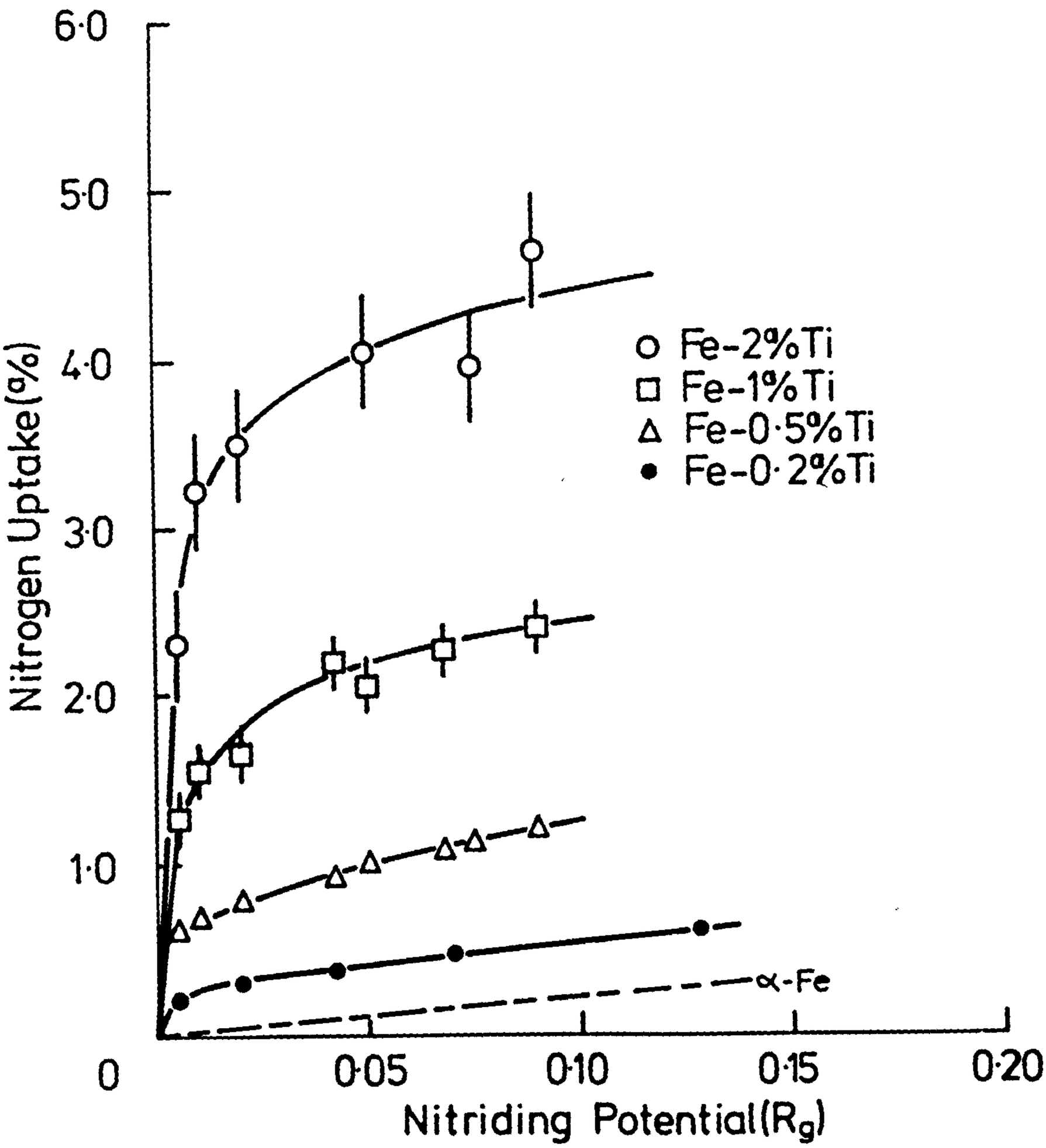

Variation of Nitrogen Uptake with Nitriding Potential(R_g) for Fe-Ti Alloys Nitrided at 580°C

Fig. VI.2.

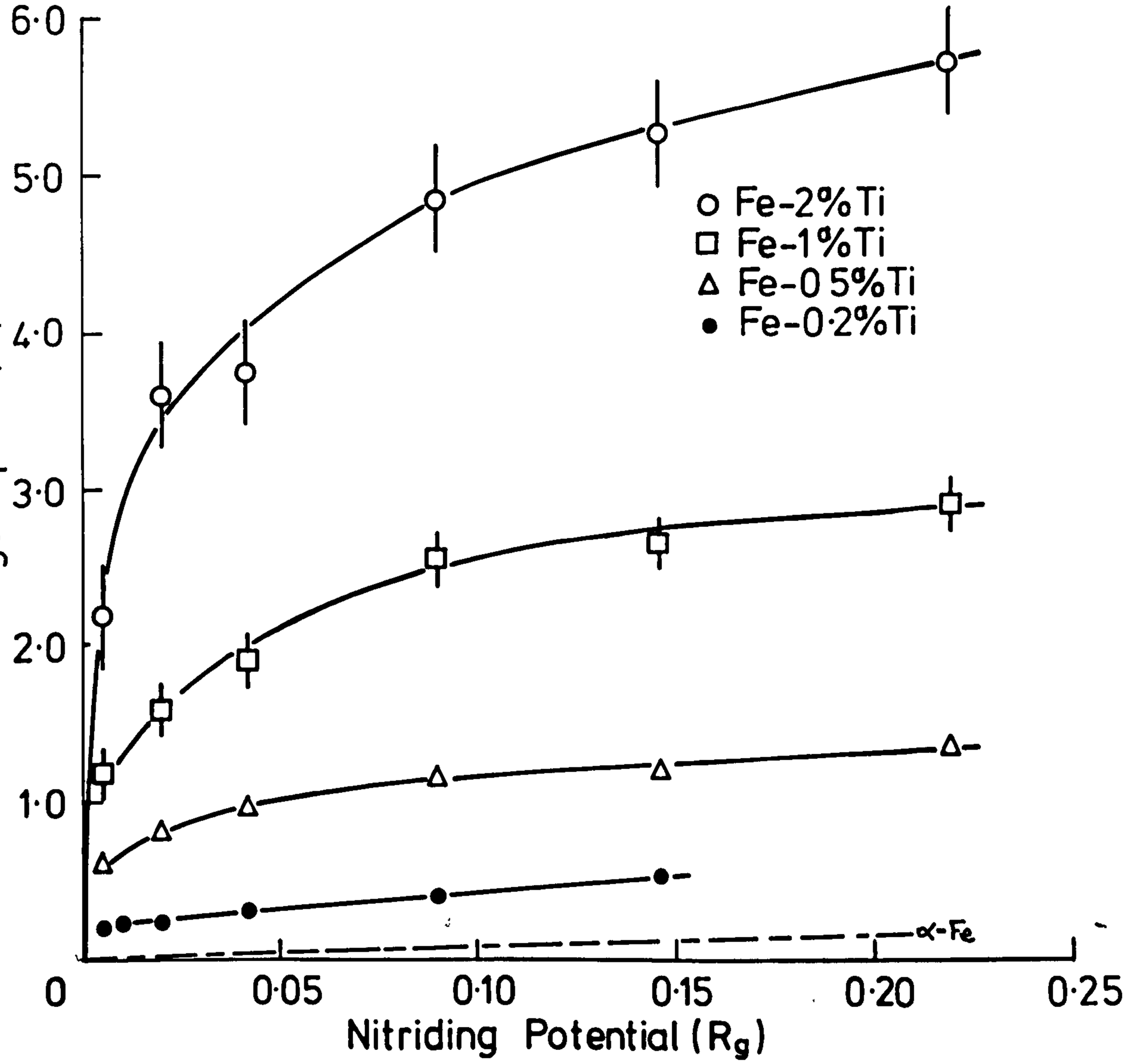

Variation of Nitrogen Uptake with Nitriding Potential (R_g) for Fe-Ti Alloys Nitrided at 500°C

equilibrium with the nitriding atmosphere. The N:Ti atomic ratios vary from about 1:1 at very low nitriding potentials ($0.5NH_3:99.5H_2$) to about 2.7:1 for Fe-2^a/oTi nitrided at 500°C in $17NH_3:83H_2$. For alloys nitrided at 400°C, N:Ti atomic ratios of up to 3:1 are observed. Since the concentration of nitrogen in solution in equilibrium with the nitriding atmosphere at this temperature is negligible the solute-atom clusters in this alloy must have a N:Ti atomic ratio of 3:1.

On ageing nitrided alloys in hydrogen the N:Ti atomic ratios of the alloys are reduced to approximately 1:1 irrespective of the original nitriding conditions i.e. the nitrogen content is always reduced to that which would be obtained by the formation of stoichiometric TiN. However lattice parameter measurements indicate that all the nitrogen and titanium are still in solid solution. At 580°C and below, the hydrogen reduction of the alloys is reversible and the nitrogen content of the alloy can be returned to its original level by re-nitriding. This is illustrated by the results shown in Figure VI.3. Lattice parameter measurements indicate that throughout the nitriding, the hydrogen reduction and the re-nitriding processes the nitrogen in the alloys remains in solid solution and since the changes in lattice parameter with nitrogen content for each step in the process are the same, it must be concluded that the nitrogen atoms occupy the same kind of sites in the lattice at all stages.

The variable composition of nitrided alloys above a 1:1,N:Ti atomic ratio with nitriding potential and the reversible removal of nitrogen in excess of the 1:1,N:Ti atomic ratios implies that this "excess nitrogen" is less strongly bonded than that of the 1:1 stoichiometry, i.e. it exists in a different chemical environment even though

Fig. VI.3.

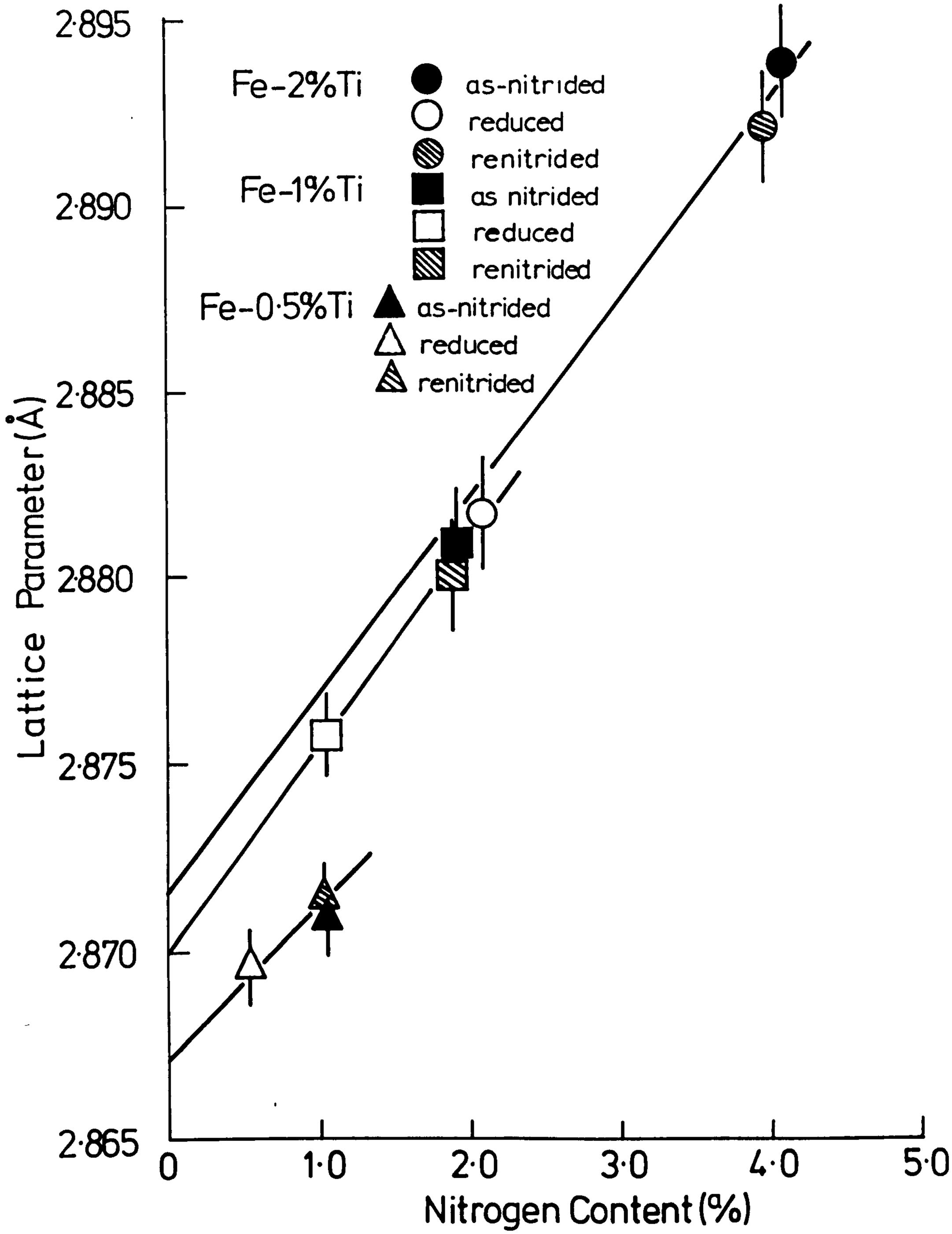

Variation of Lattice Parameter with Nitrogen Content for Fe-Ti Alloys in Various Conditions

the physical environment - evidenced from the lattice parameter values - remains the same. The N:Ti atomic ratio does not fall below 1:1 even after prolonged ageing in hydrogen (up to 280 hours at 580°C) and the relatively small reduction in hardness of the nitrided Fe-Ti alloys after this treatment suggests that the number of obstacles to dislocation movement has not changed appreciably (see Table VI.2); the hardnesses of as-annealed alloys extrapolated to zero titanium concentration provide an estimate of the base alloy hardness (115 V.M.H.). In Figure VI.4 the increase in hardness for nitrided plus hydrogen-reduced alloys is plotted against the square root of nitrogen content, the latter being equivalent to the square root of the volume fraction of Ti-N zones if it is assumed that they are composed of titanium and nitrogen in equal atomic concentrations. This proportionality between hardness and square root of the "TiN" volume fraction is characteristic of alloys containing G.P. zones or coherent precipitates where the strengthening is due to the resistance to shear by strong particles (Brown & Ham, 1971). This is further evidence to suggest that the limiting composition of zones in the hydrogen reduced alloys is "TiN".

VI.4. The Structure of Ti-N Zones

Lattice parameter measurements of the hydrogen reduced alloys indicate that the Ti and N atoms are effectively in solid solution and therefore in the zones they must occupy the same types of crystallographic site as they would in a random solid solution. The Ti atoms in the zones must substitute for Fe atoms in the ferrite lattice and the N atoms in the zones must also occupy octahedral

Table VI.2

alloy	hardness (V.M.H.)		nitrogen loss (a/o)	nitrogen content (a/o)
	as-nitrided	hydrogen reduced		
Fe-2a/oTi	1250	1100	2.47	2.20
Fe-1a/oTi	950	800	1.35	1.05
Fe-0.5a/oTi	720	550	0.66	0.54

Fig. VI.4.

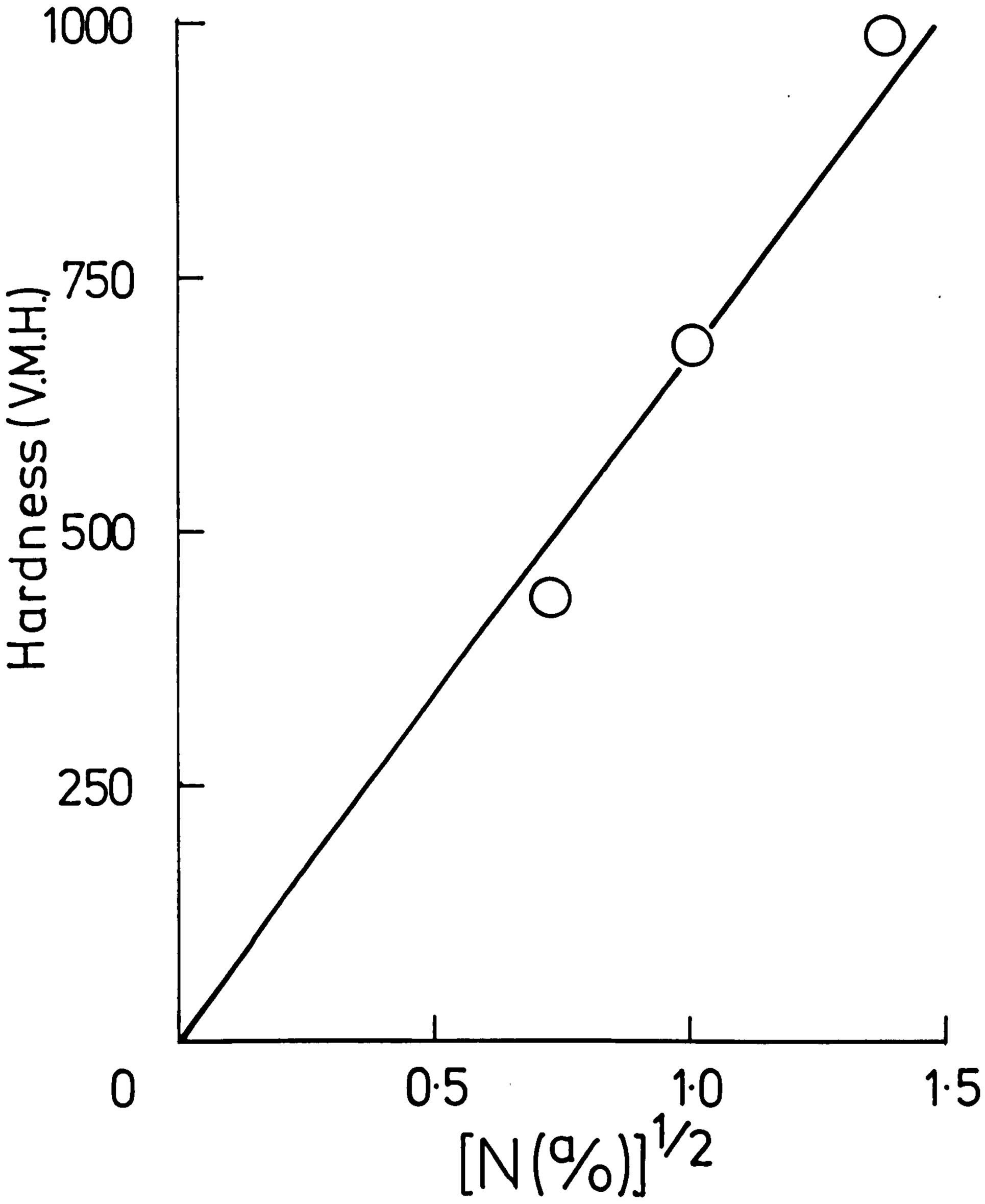

The Increment in Hardness for Nitrided and Hydrogen Reduced Fe-Ti Alloys with Square Root of Nitrogen Content

interstices. The high affinity of Ti atoms for N atoms also implies that the mutual coordination of N and Ti ahould be a maximum.

In an investigation of clustering in Fe-Ti-N alloys concurrent with the present work and covering similar aspects Jack (1976) proposes that the zones are monolayers of composition TiN as shown in Figure VI.5. Each monolayer fits into the ferrite matrix on a (100) plane without causing any structural discontinuity. The Ti atoms substitute for Fe atoms and N atoms occupy octahedral interstices, each coordinated by four Ti atoms in the plane of the zone and by two Fe atoms, one above and one below it. From streaking on electron diffraction patterns Jack estimated the thickness of zones in Fe-2^{a}/oTi nitrided at 575^{o}C to be about 4$\mathring{A}$. This is accounted for if the zone includes the two iron-atom planes and the central Ti-N plane; the three-layer cluster then consists of two 1.94$\mathring{A}$ interplanar spacings i.e. a thickness of 3.88$\mathring{A}$.

In as-nitrided alloys the N:Ti ratio depends upon nitriding potential and temperature (see section VI.3) and reaches a maximum of 3:1, that is, three times the concentration required for a TiN monolayer. Only a negligible proportion of the "excess nitrogen" exists in random solid solution in equilibrium with the gas atmosphere (see Figures VI.1 and VI.2). The remaining nitrogen exists in two types of chemical environment (see Figure VI.6):

(a) nitrogen in the TiN monolayer;

(b) "excess nitrogen" less strongly bonded than monolayer nitrogen where each N atom is coordinated by only one Ti atom. In this model the limiting composition of the zones is Fe_4TiN_3 for as-nitrided alloys and Fe_2TiN for hydrogen-reduced alloys. These compositions satisfactorily account for the experimental observations of the present

interstices. The high affinity of Ti atoms for N atoms also implies that the mutual coordination of N and Ti ahould be a maximum.

In an investigation of clustering in Fe-Ti-N alloys concurrent with the present work and covering similar aspects Jack (1976) proposes that the zones are monolayers of composition TiN as shown in Figure VI.5. Each monolayer fits into the ferrite matrix on a (100) plane without causing any structural discontinuity. The Ti atoms substitute for Fe atoms and N atoms occupy octahedral interstices, each coordinated by four Ti atoms in the plane of the zone and by two Fe atoms, one above and one below it. From streaking on electron diffraction patterns Jack estimated the thickness of zones in Fe-2^{a}/oTi nitrided at 575^{o}C to be about 4Å. This is accounted for if the zone includes the two iron-atom planes and the central Ti-N plane; the three-layer cluster then consists of two 1.94Å interplanar spacings i.e. a thickness of 3.88Å.

In as-nitrided alloys the N:Ti ratio depends upon nitriding potential and temperature (see section VI.3) and reaches a maximum of 3:1, that is, three times the concentration required for a TiN monolayer. Only a negligible proportion of the "excess nitrogen" exists in random solid solution in equilibrium with the gas atmosphere (see Figures VI.1 and VI.2). The remaining nitrogen exists in two types of chemical environment (see Figure VI.6):

(a) nitrogen in the TiN monolayer;

(b) "excess nitrogen" less strongly bonded than monolayer nitrogen where each N atom is coordinated by only one Ti atom. In this model the limiting composition of the zones is Fe_4TiN_3 for as-nitrided alloys and Fe_2TiN for hydrogen-reduced alloys. These compositions satisfactorily account for the experimental observations of the present

Fig. VI.5.

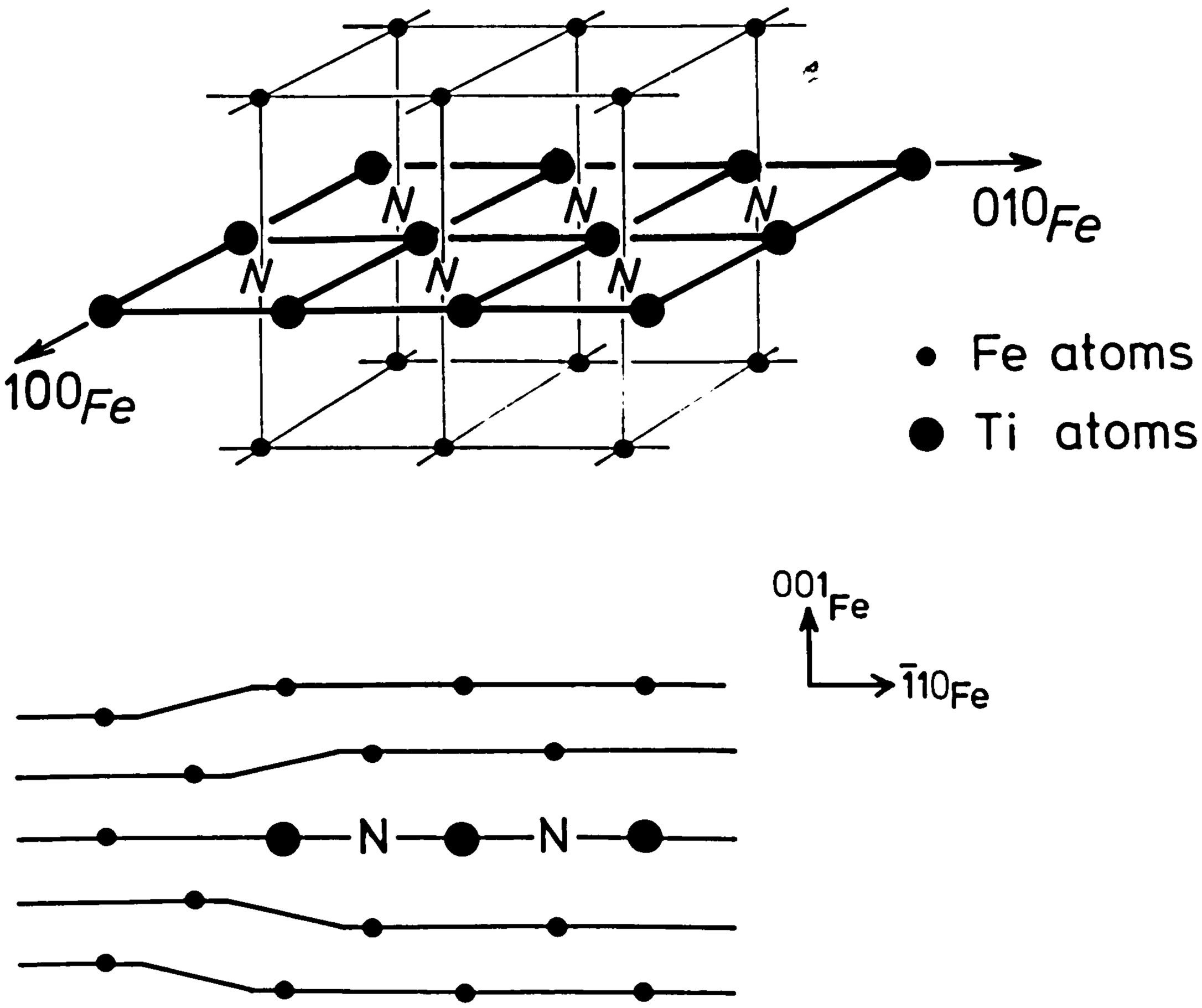

Proposed Model for the Structure of Zones in Nitrided Fe-Ti Alloys

[After D.H. Jack (1974)]

Fig. VI.6.

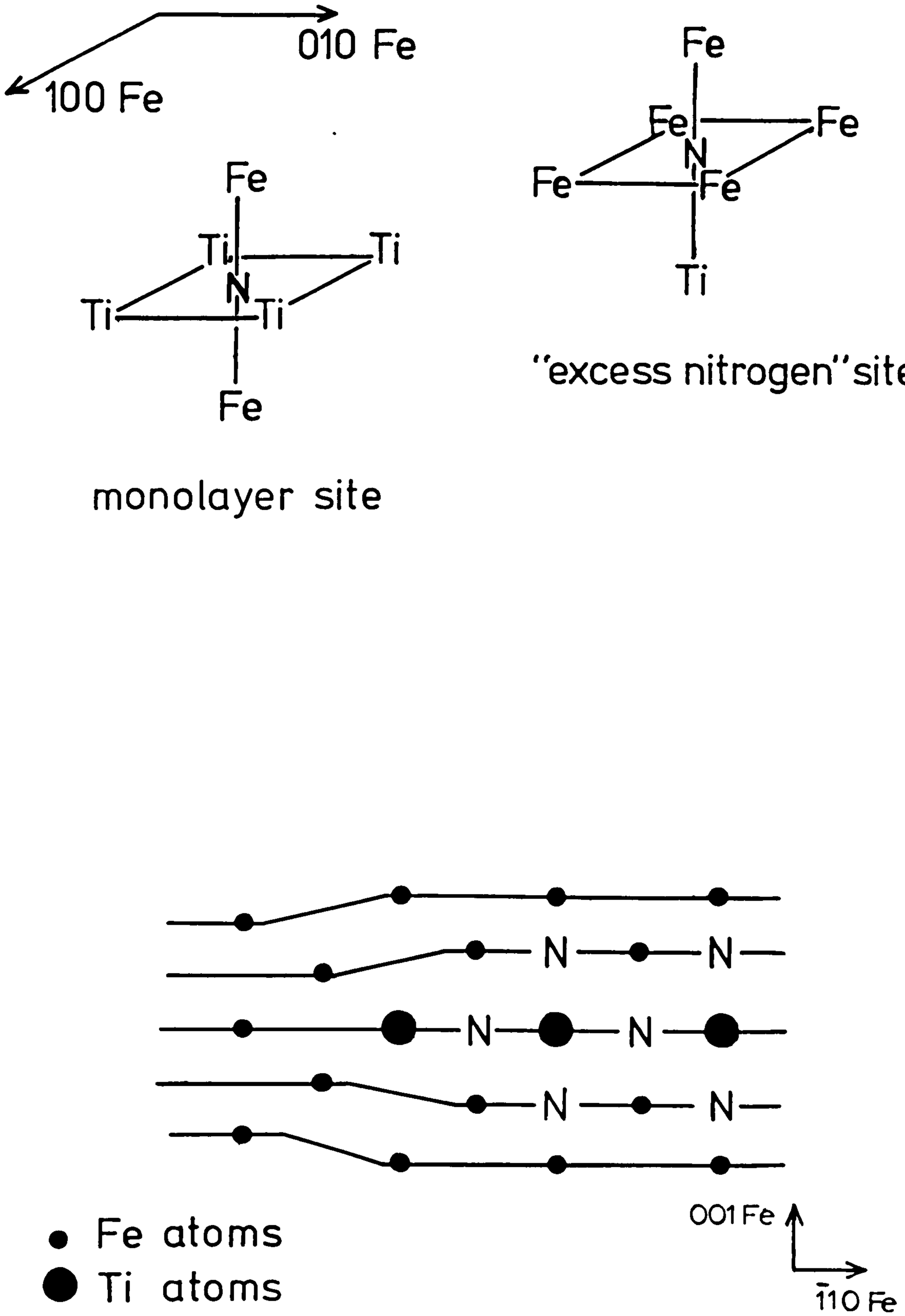

Nitrogen Atom Environments in Nitrided Fe-Ti Alloys

investigation in which the N:T atom ratio approaches a maximum value of 3 with increasing nitriding potential and decreasing temperature.

Jack (1976) proposes a different model for the sites of the "excess nitrogen". In Jack's model the "excess nitrogen" is held in the tensile-strained regions at the periphery of the TiN monolayers because of enhanced solubility of nitrogen. These sites might have the required capacity for the observed "excess nitrogen" concentrations but occupation of these sites merely extends the peripheral strain field further and for each site occupied a new site of enhanced solubility is created. This does not account for the observed limiting nitrogen concentration in nitrided alloys.

VI.5. Conclusions

(i) Thin plate-like zones are formed during the nitriding of Fe-Ti alloys, the composition of which varies from Fe_2TiN to Fe_4TiN_3 depending upon nitriding conditions.

(ii) The nitrogen in nitrided Fe-Ti alloys occupies two different chemical environments

(a) nitrogen in TiN monolayers where each N atom is coordinated by four Ti atoms and two Fe atoms (see Figures VI.5 and VI.6)

(b) nitrogen in sites at the faces of TiN monolayers where each N atom is coordinated by one Ti atom and five Fe atoms (see Figure VI.6).

(iii) Hardening of nitrided Fe-Ti alloys is due principally to the resistance of these disc-shaped zones to shear by dislocation movement.

Chapter VII

THE MORPHOLOGY OF NITRIDED Fe-Ti ALLOYS

VII.1. Electron Microstructure

(i) Alloys nitrided at high temperatures (650°-750°C)

Alloys nitrided at 650°C generally show tweed contrast on electron micrographs. However, in Fe-0.5^{a}/oTi fine plate-like coherent precipitates or zones 100-150Å diameter and less than 20Å thick are resolved parallel to {100} matrix planes in areas close to grain boundaries; see Figure VII.1. Although lattice parameter measurements in conjunction with weight changes indicate that very little precipitation of nitrogen or titanium has taken place during nitriding, intensity maxima are observed on electron diffraction patterns at the expected positions for TiN precipitate reflections; see Figure VII.2. These appear on selected area diffraction patterns for regions in the foil which exhibit tweed contrast and also in regions where precipitates or zones are resolved.

The resolution of "precipitates" in grain boundary areas may be due to the fact that the zones here are coarser than in the remainder of the foil. Since it is known that tweed contrast arises from arrays of fine, closely-spaced coherent precipitates or zones (Tanner, 1966), an alternative explanation may be that the foil is very thin in these grain-boundary areas and there are insufficient precipitates or zones to produce the tweed contrast.

Fig. VII.1.

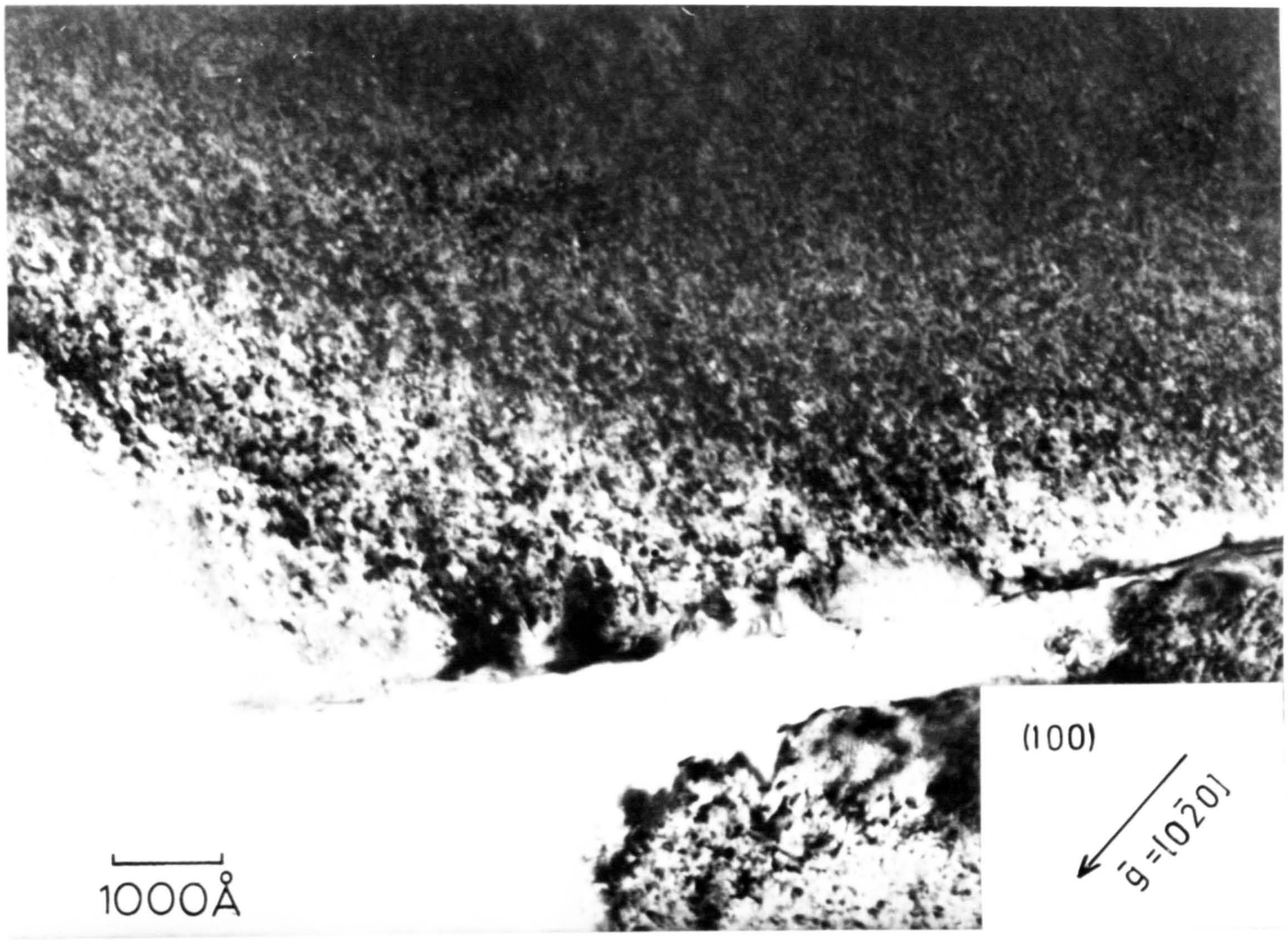

Bright Field Micrograph of Fe-0·5%Ti Nitrided at 650°C in $4{\cdot}5NH_3:95{\cdot}5H_2$

Fig.VII.2.

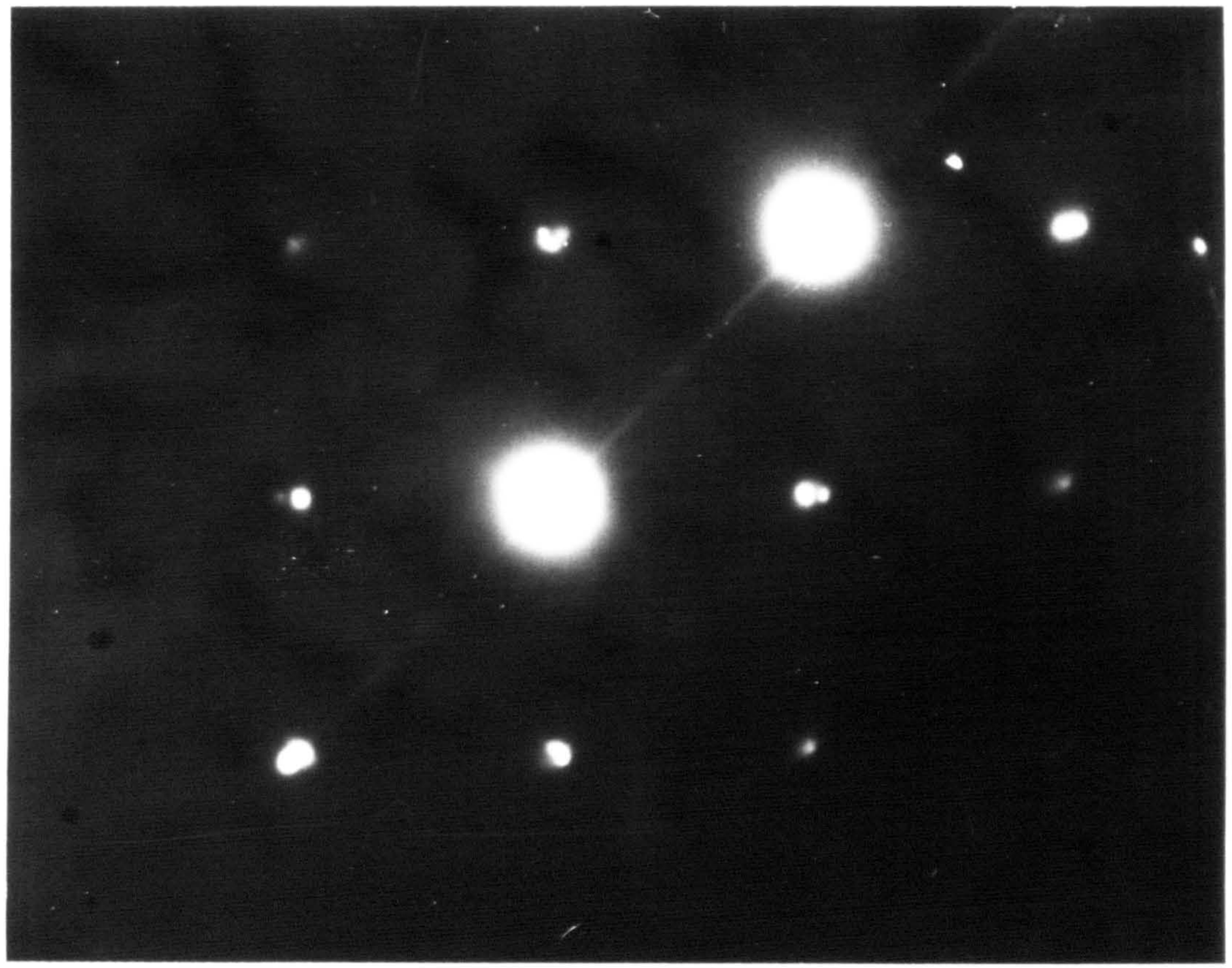

Electron Diffraction Pattern of Fe-0·5%Ti
Nitrided at 650°C in $4{\cdot}5NH_3{:}95{\cdot}5H_2$
($[001]_\alpha$ zone)

Tweed structures are not observed at all in Fe-0.5^{a}/oTi nitrided at 750°C in $1NH_3:99H_2$. The microstructure consists of a dense array of plate-like coherent precipitates or zones lying on $\{100\}$ matrix planes and about 120-200Å diameter (see Figure VII.3). Lattice parameter measurements of this alloy (see Table VI.1) indicate that some of the nitrogen has precipitated from solid solution and very strong intensity maxima streaked along $\langle 100 \rangle$ matrix directions are observed on electron diffraction patterns at positions corresponding to those of TiN precipitate reflections. This is illustrated by the electron diffraction pattern in Figure VII.4. The electron beam is approximately parallel to a $\langle 120 \rangle$ matrix direction and the central part of a $\{120\}_{\alpha}$ reciprocal lattice plane is shown. The streaks along $[00\bar{2}]$ adjacent to the zero order reflection are probably due to double diffraction effects from the main TiN reflections. The two medium intensity spots (marked Λ) on each side of the zero order reflection in a $\langle 210 \rangle$ direction are probably due to intensity maxima adjacent to $\{110\}$ reflections in the $\{110\}$ matrix reciprocal lattice plane. A centred dark field image derived from a streaked intensity maximum adjacent to a (002) reflection in a $\{110\}$ reciprocal lattice plane shows plate-like precipitates aligned along $\langle 100 \rangle$ matrix directions (Figure VII.5).

(ii) Alloys nitrided at intermediate temperatures (400°-650°C)

Under general imaging conditions Fe-2^{a}/o, 1^{a}/o and 0.5^{a}/oTi alloys nitrided in the temperature range 400°-650°C show an apparently random, fine-dot contrast similar to that reported by Phillips & Seybolt (1968). However, under two beam dynamical conditions tweed contrast is

Fig. VII.3.

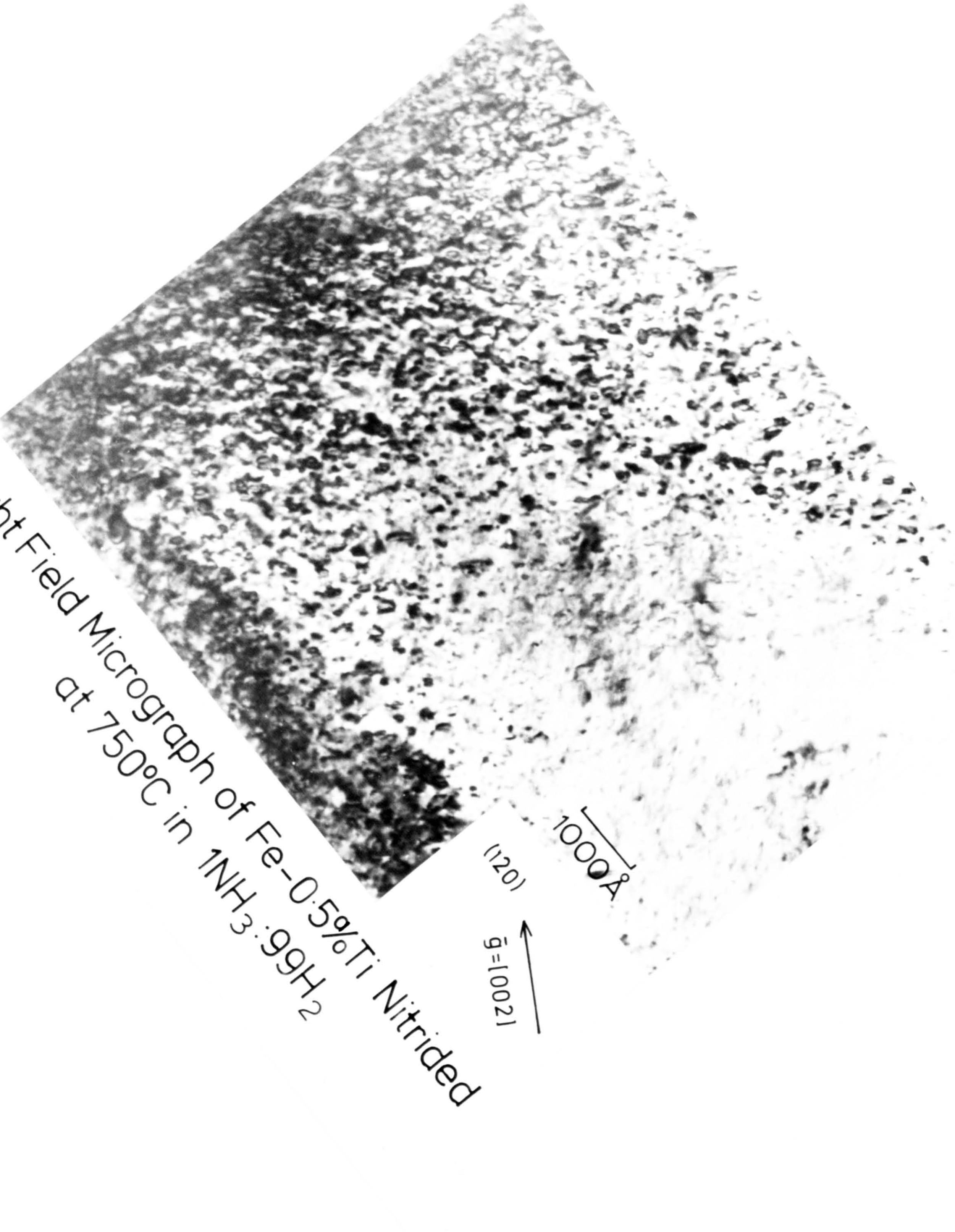

Bright Field Micrograph of Fe-0.5% Ti Nitrided at 750°C in $1NH_3:99H_2$

Fig. VII.3.

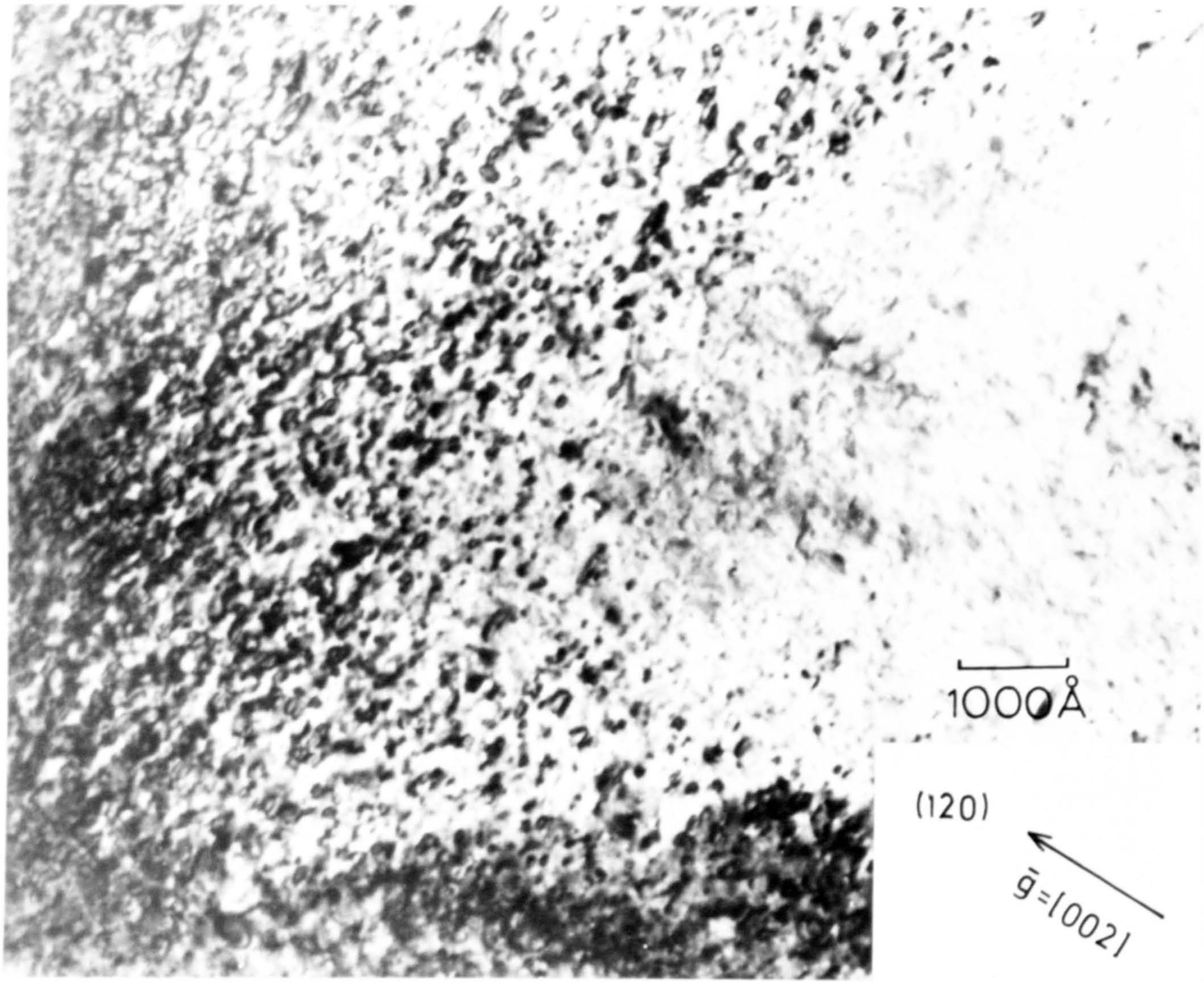

Bright Field Micrograph of Fe-0·5%Ti Nitrided at 750°C in $1NH_3:99H_2$

Fig. VII.4.

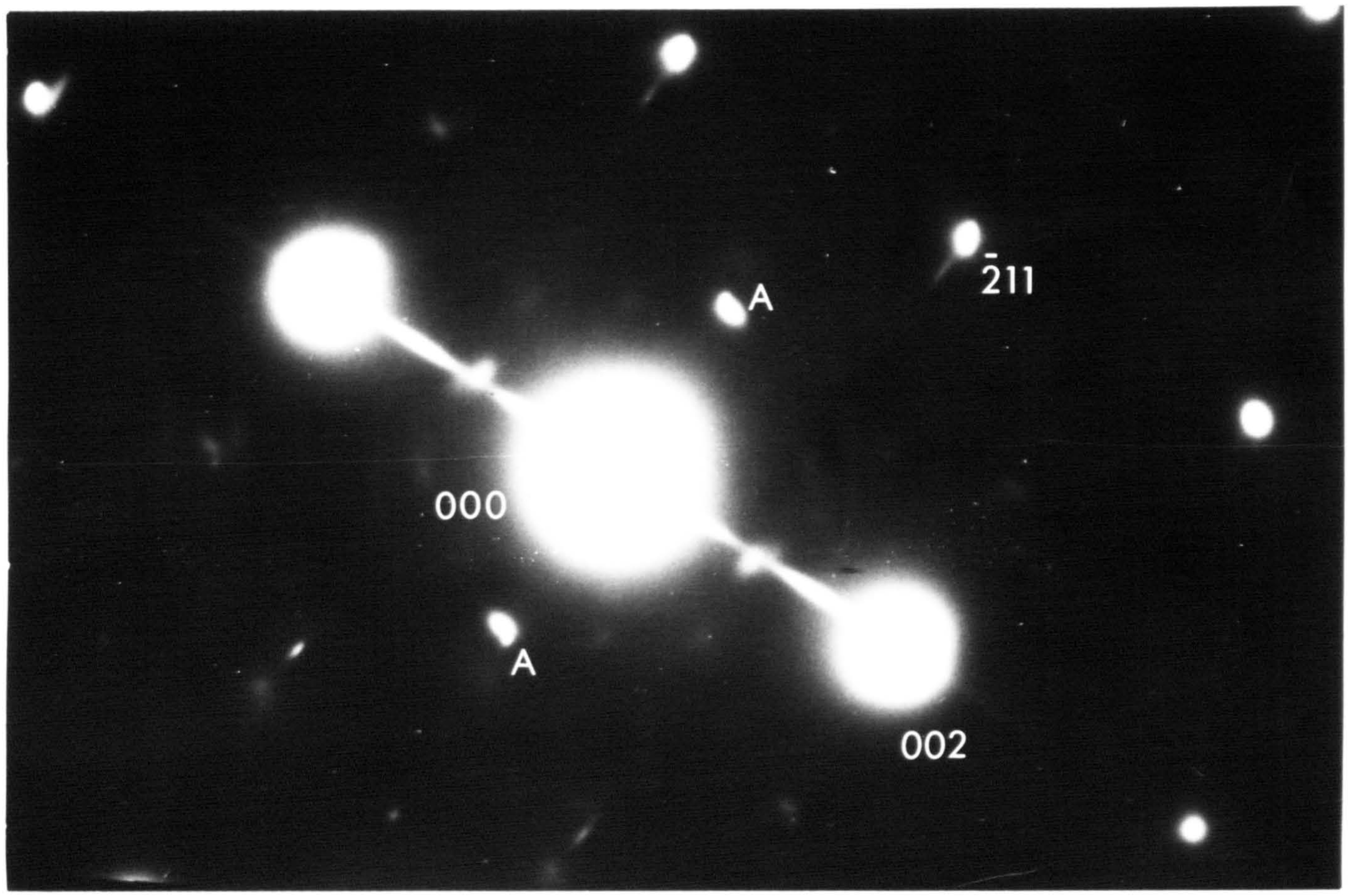

Electron Diffraction Pattern of Fe-0·5%Ti
Nitrided at 750°C in $1NH_3:99H_2$ ($[120]_\alpha$ zone)

Fig. VII.5.

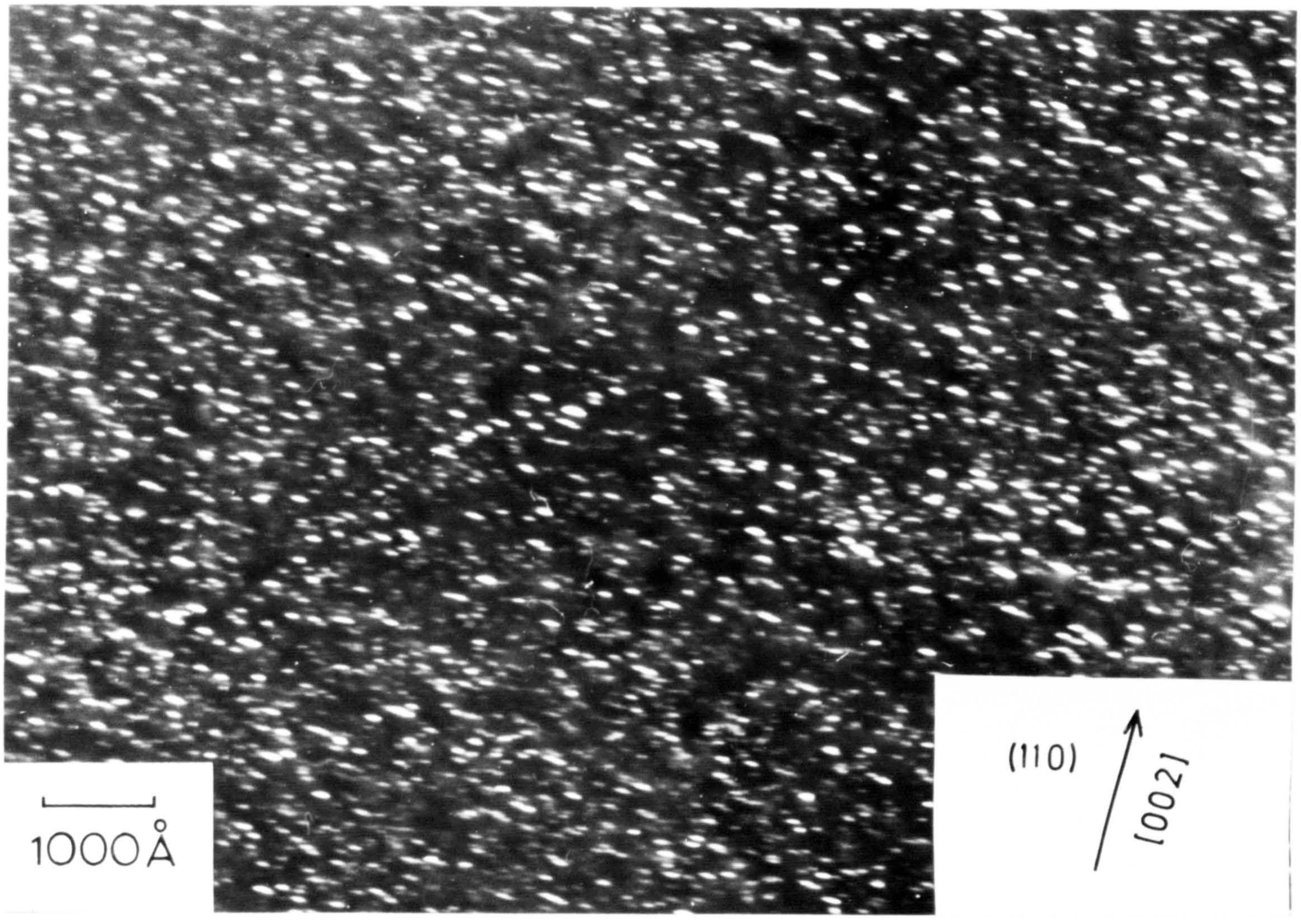

Centred Dark Field Micrograph of Fe-0·5%Ti
Nitrided at 750°C in $1NH_3:99H_2$ ((002) TiN Reflection)

observed similar to that reported for aged Cu-2^{W}/oBe alloys (Tanner, 1966; Phillips & Tanner, 1971). The foil orientation is critical for observation of well-developed tweed contrast. Typical examples of the tweed microstructures observed are shown in Figures VII.6-8.

In Figure VII.6 the plane of the foil is parallel to an $\{001\}$ ferrite plane ($[001]_{\alpha}$ zone) and the operating $\underline{g}$ vector is $[020]$. The microstructure has an orthogonal basket weave texture whose weave directions are parallel to $\langle 110 \rangle$ directions. This type of microstructure is only observed when the plane of the foil is parallel to a $\{001\}$ ferrite plane with strong two beam imaging conditions and a $\langle 200 \rangle$ $\underline{g}$ vector.

Figure VII.7 shows a similar microstructure in which the plane of the foil is parallel to a $\{111\}$ ferrite plane ($[\bar{1}11]_{\alpha}$ zone) and the operating $\underline{g}$ vector is $[\bar{1}01]$. The angle of zig-zag is different to that observed in the type of microstructure shown by Figure VII.8.

Tweed constrast similar to that observed in electron micrographs of aged Cu-2^{W}/oBe alloys (Phillips & Tanner, 1971) arises from a pseudo-periodic array of thin plate-like zones or coherent precipitates on cube planes (Jack, D.H., 1976). Continuous streaking of matrix spots along $\langle 100 \rangle$ directions was observed on electron diffraction patterns for alloys nitrided under all the conditions investigated, see Figure VII.9. The intensity distribution of this streaking was diffuse compared with that observed for nitrided Fe-3^{a}/oMo alloys (Driver & Papazian, 1973), but generally the $\langle 100 \rangle$ streaking is less diffuse for alloys nitrided at the higher temperatures and with lower titanium contents. For

Fig. VII.6.

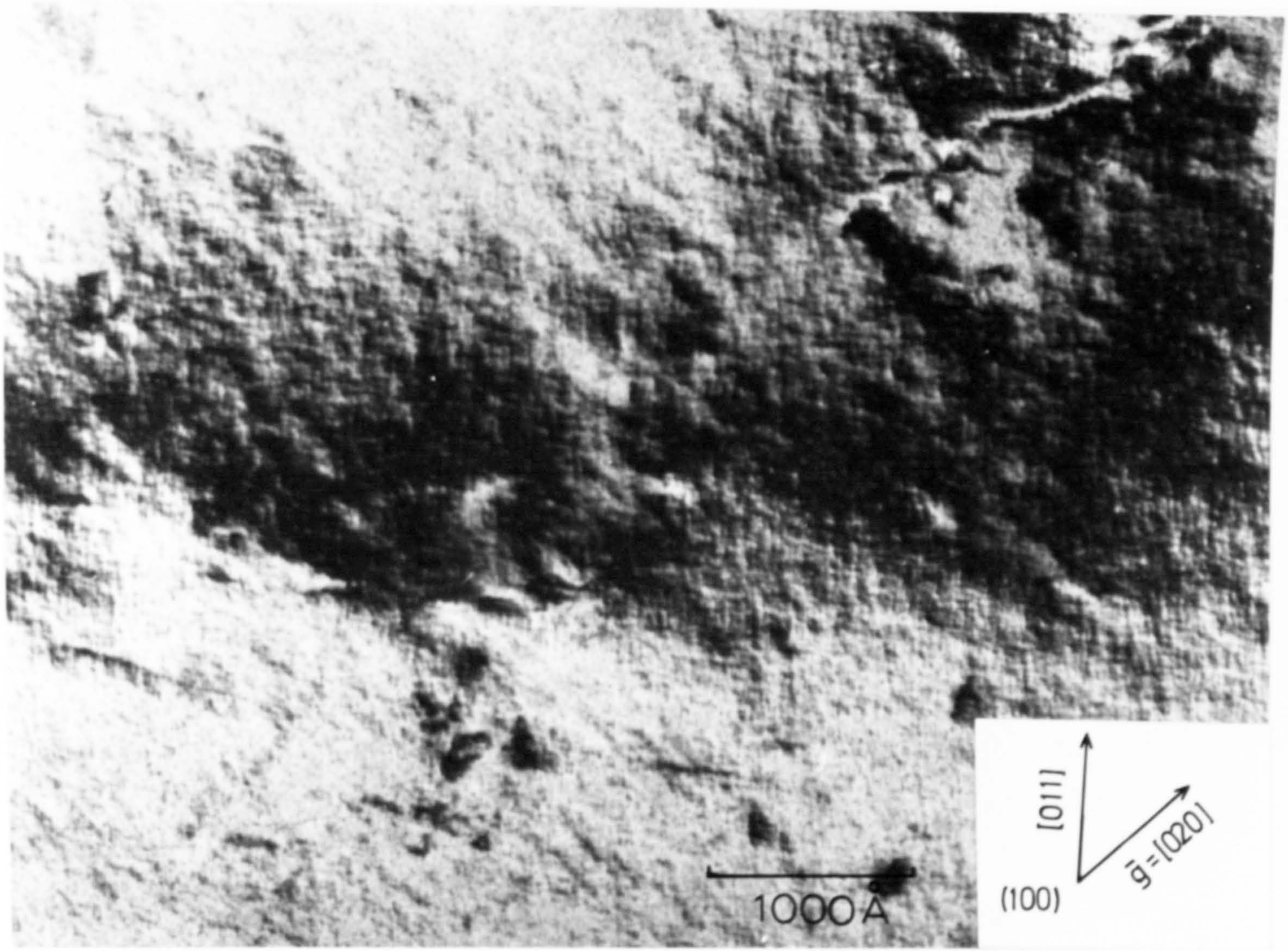

Bright Field Micrograph of Fe – 2% Ti Nitrided at 400°C in 30 NH_3:70 H_2

Fig. VII.7

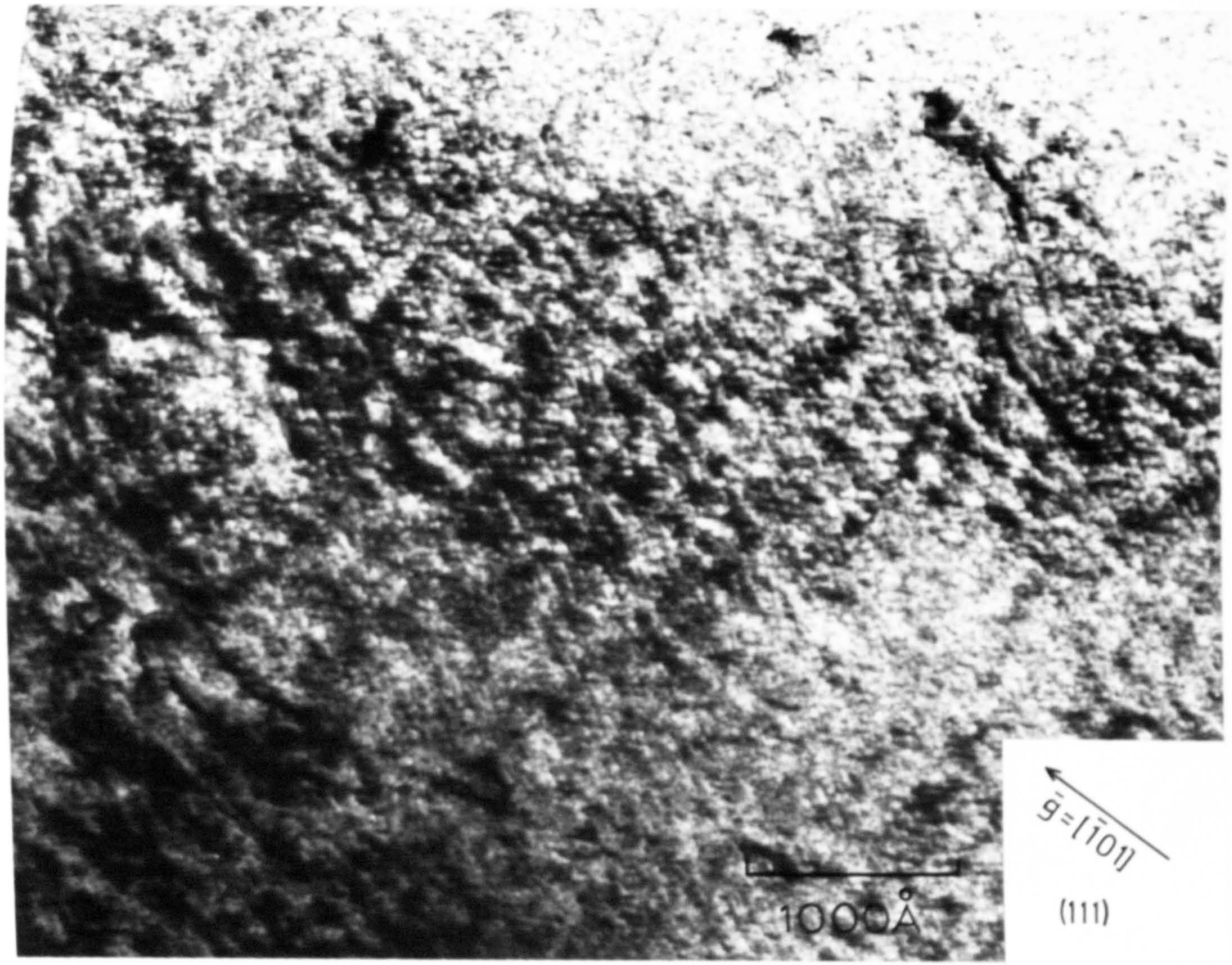

Bright Field Micrograph of Fe-2%Ti Nitrided at 400°C in $30NH_3 : 70H_2$

Fig. VII.8.

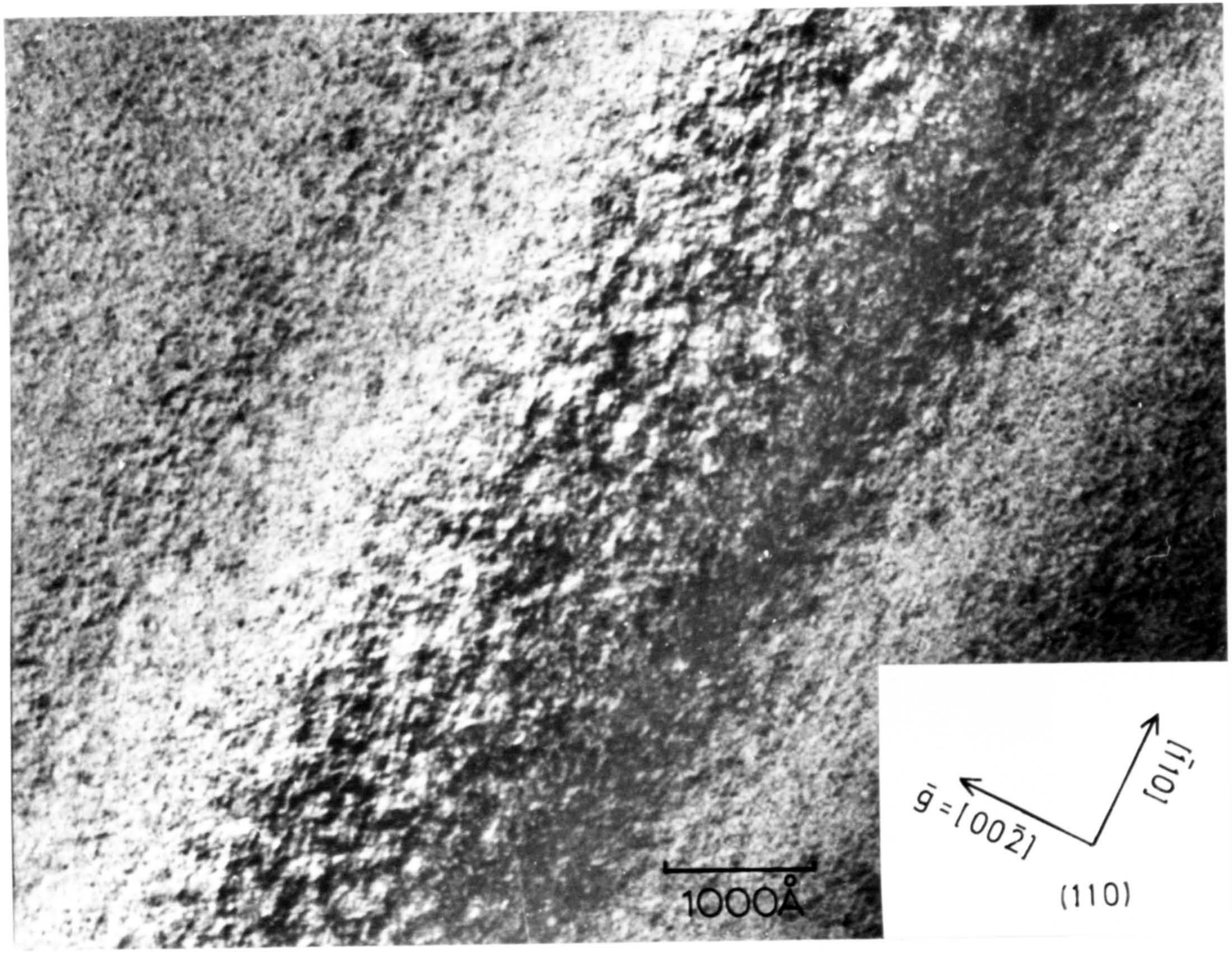

Bright Field Micrograph of Fe-0·5% Ti Nitrided at 650°C in $2NH_3 : 98H_2$

Fig. VII.9.

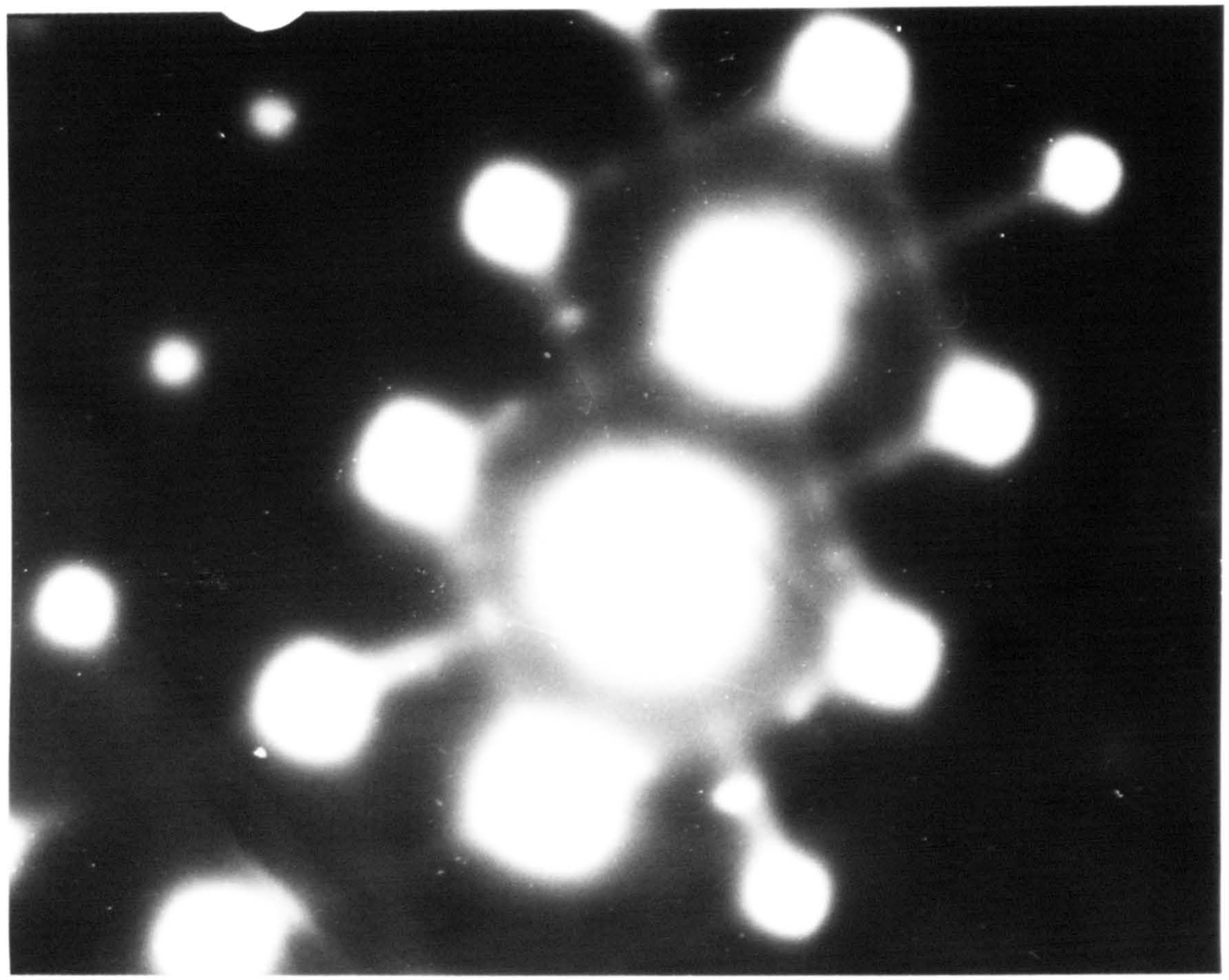

Electron Diffraction Pattern of Fe-2% Ti
Nitrided at 580°C in $7NH_3$:$93H_2$ ($[001]_\alpha$ zone)

Fe-2^{a}/oTi nitrided at 400°C the ⟨100⟩ streaking was barely detectable. This streaking is caused by planar discontinuities parallel to {100} matrix planes which for alloys nitrided at intermediate temperatures must be mixed substitutional-interstitial G.P. zones (see Chapter VI.2). Undoubtedly it is these zones which give the tweed contrast observed in bright field electron micrographs. Fillingham, Leamy & Tanner (1971) have demonstrated that this type of contrast can result from a suitably ordered array of disc shaped zones which gives a tetragonal distortion of the matrix. They suggest that partially ordered arrangements based on relative precipitate orientations shown in Figure VII.10(a) and VII.10(b) may account for experimentally observed contrast morphology in Cu-2^{W}/oBe alloys. The two dimensional array (see Figure VII.10(c)) of disc-shaped particles having an edge-face configuration gave simulated contrast morphologies close to those experimentally observed in the investigation of Cu-2^{W}/oBe and the present investigation.

Close examination of matrix spots on electron diffraction patterns of the nitrided alloys reveals additional diffraction effects which are more marked for alloys nitrided at low temperatures (400°-500°C) and higher titanium contents; see Figure VII.11. The effects are:

(i) short streaks along ⟨211⟩ directions on matrix spots when the main electron beam is parallel to a ⟨110⟩ ferrite direction;

(ii) "satellite" spots around matrix spots when the electron beam is almost but not exactly parallel to a ⟨100⟩ ferrite direction.

These effects are similar to those observed in Cu-2^{W}/oBe by Phillips & Tanner (1973) who concluded that they were cross sections of ⟨110⟩ relrods

Fig. VII.10.

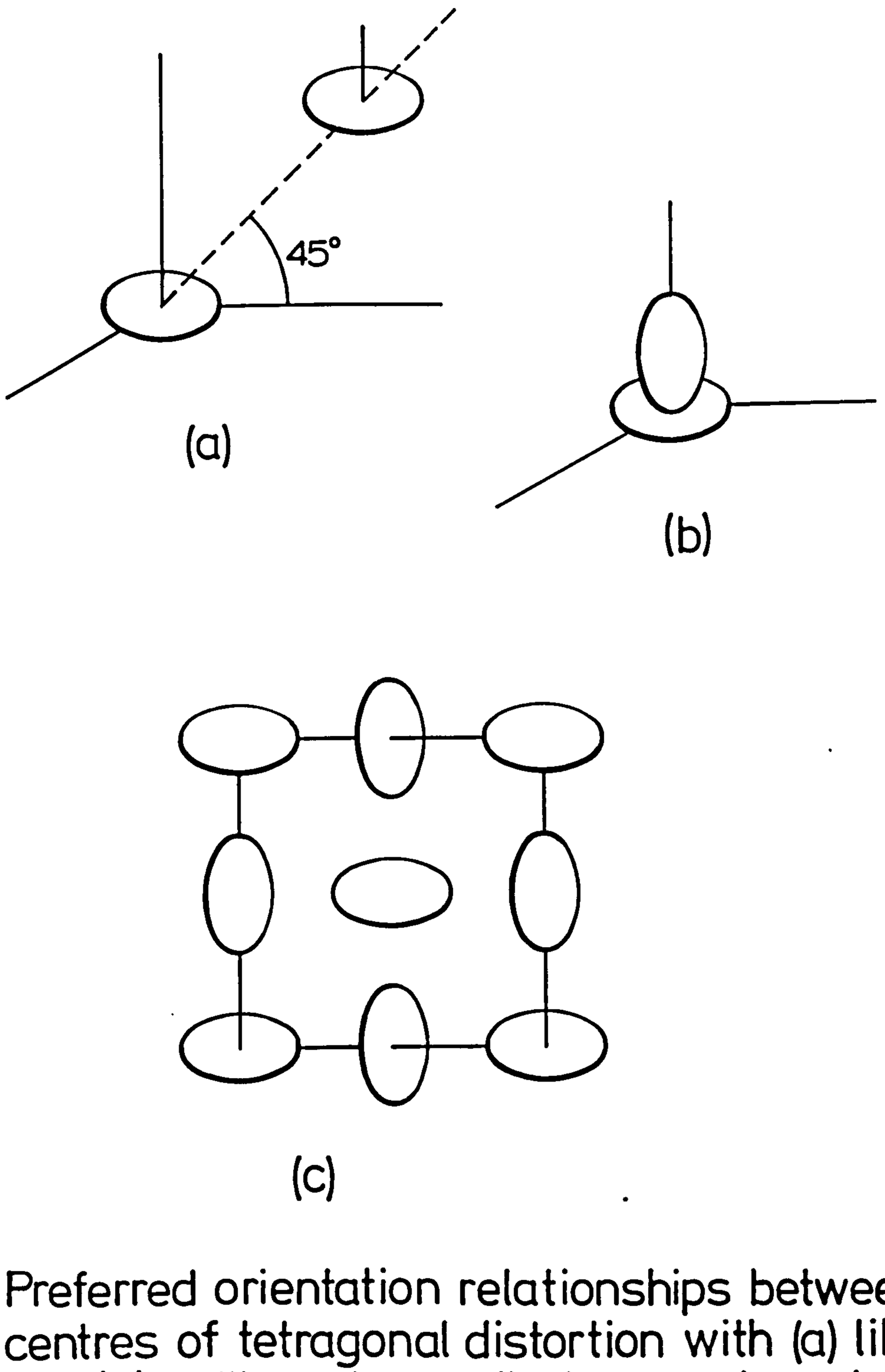

(a)

(b)

(c)

Preferred orientation relationships between centres of tetragonal distortion with (a) like and (b) unlike primary displacement vector
(c) A two-dimensional array derived from (a) and (b)

Fig. VII.11.

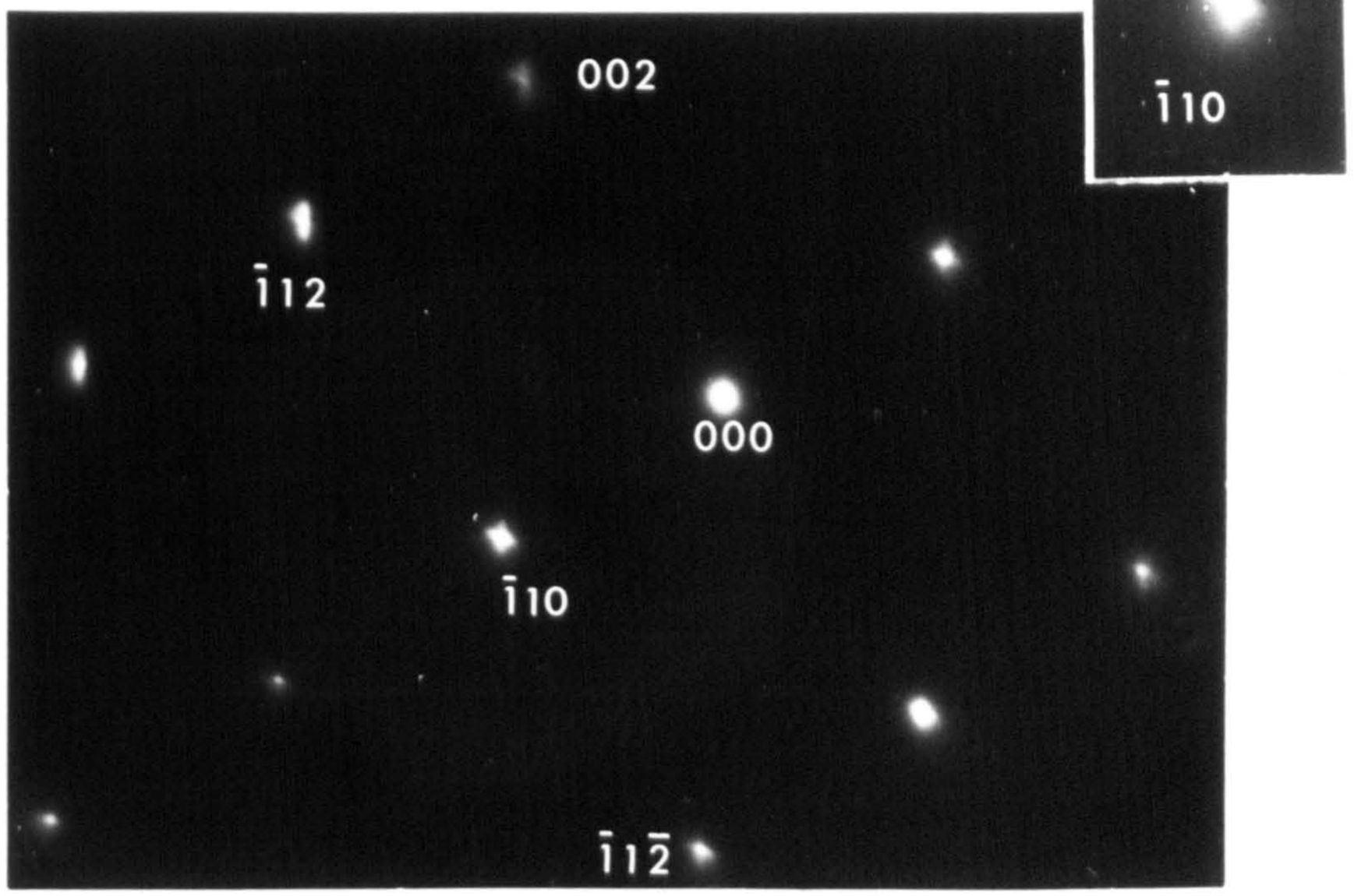

(a)

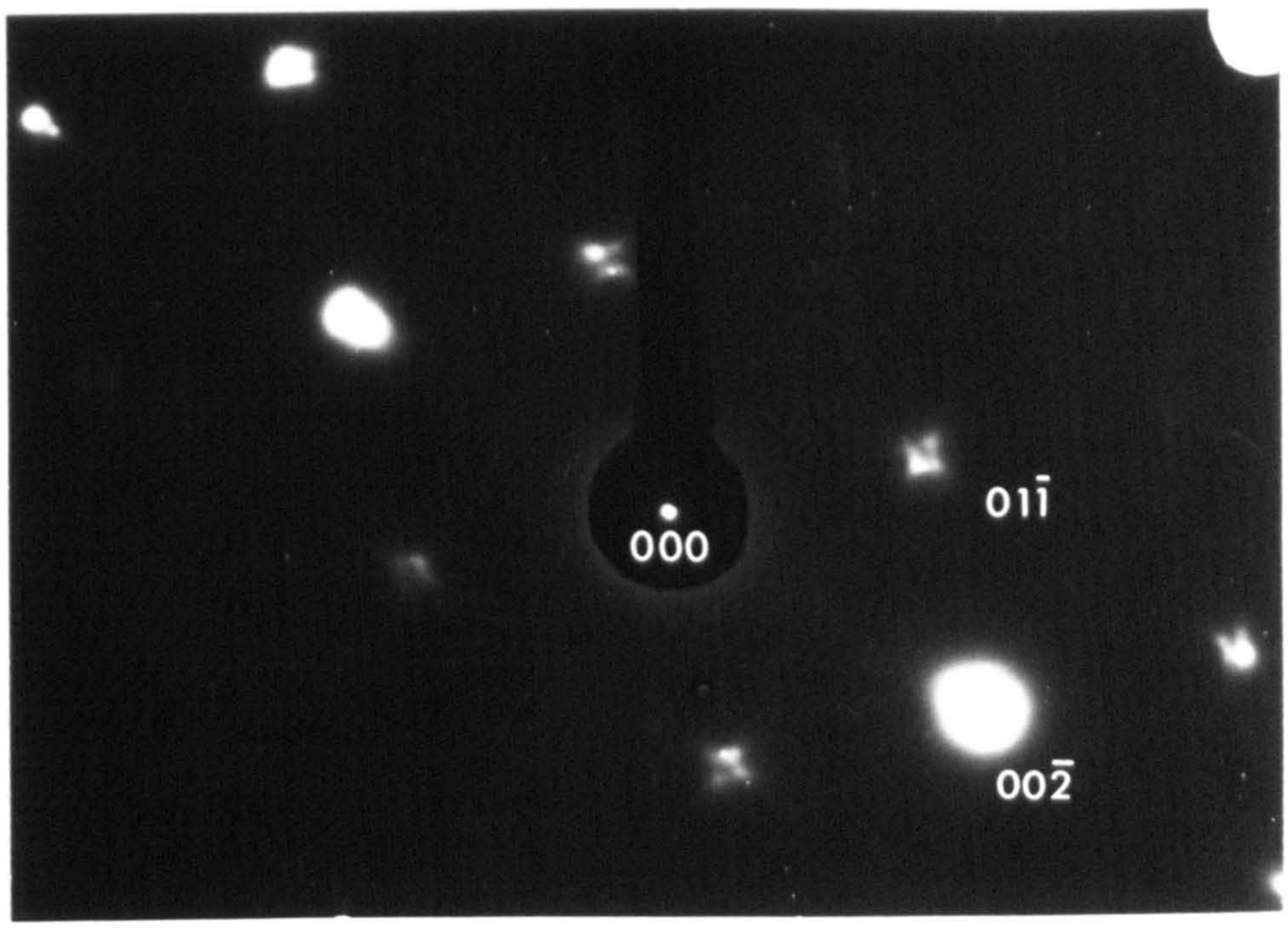

(b)

Electron Diffraction Patterns of Fe-2%Ti Nitrided at 400°C in $30NH_3:70H_2$
(a) $[110]_\alpha$ zone (b) $[100]_\alpha$ zone

cutting the Ewald sphere. The ⟨211⟩ streaks in Figure VII.11(a) coincide with the projections of ⟨110⟩ relrods but no streaking is observed along ⟨110⟩ directions on the diffraction pattern itself. The diffuse scattering effects observed about matrix reflections in Figure VII.11(b) resemble "satellite" reflections but these are only observed on electron diffraction patterns for which the electron beam is not exactly parallel to ⟨100⟩ directions in the foil. These "satellite" reflections are also probably sections of ⟨110⟩ relrods. The observation of ⟨110⟩ matrix streaking implies the presence of some regular strain variations in the alloys (Phillips & Tanner, 1973).

Since aged Cu-2^{w}/oBe alloys and nitrided Fe-Ti alloys both consist of dense arrays of clusters lying on {100} matrix planes and both alloys exhibit similar diffuse electron scattering effects it is reasonable to assume that these effects have similar causes in both systems. The zones in Cu-2^{w}/oBe and Fe-Ti-N both produce tetragonal distortions of the matrix and Phillips & Tanner (1973) have suggested that these elastic distortions are responsible for the observed diffuse electron scattering effects. Eurin, Penisson & Bourret (1973) show that elastic interactions between precipitates which cause tetragonal distortions are responsible for the regular arrangement of nuclei in CoPt alloys and conclude that they arrange themselves in a pseudo-periodic array so as to maximise the number of edge-face configurations. Such a morphology would also minimise the strain energy created by the tetragonal distortion at the faces of the dense arrays of coherent clusters. The most probable arrangement of the ordered nuclei in CoPt is shown schematically in Figure VII.12 as a projection onto a {100} cube plane. This arrangement is consistent with the production of

Fig. VII.12.

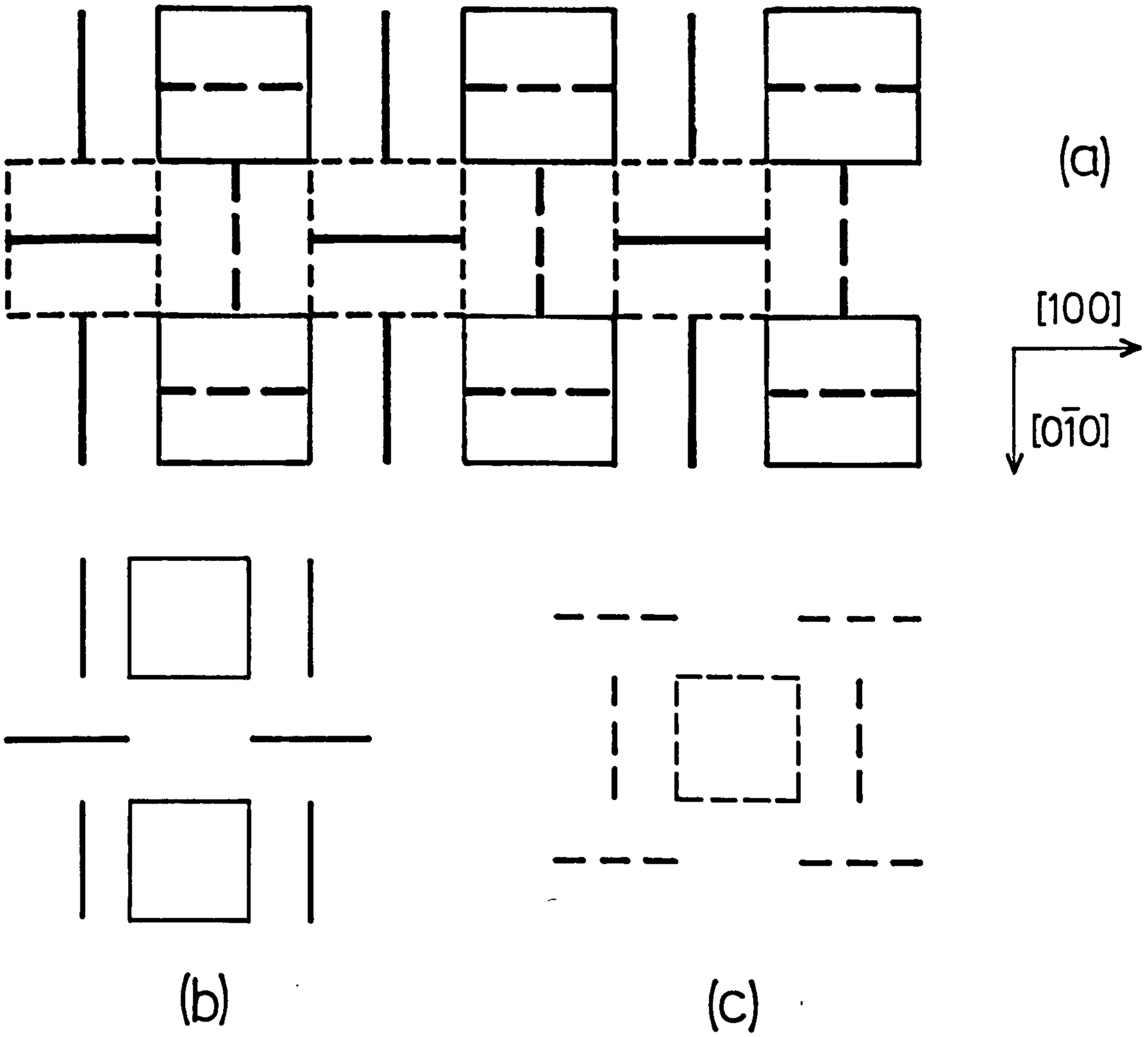

A pseudo-periodic array of plates projected onto a (001) cube plane

tweed contrast images and diffuse electron scattering effects observed in nitrided Fe-Ti alloys; it is also similar to the model proposed by Fillingham, Leamy & Tanner shown in Figure VII.10.

In an investigation concurrent with the present work Jack D.H. (1976) has obtained similar results. From the array shown in Figure VII.12 and by superimposing the simple black-white strain contrast for each plate Jack has derived a schematic picture of the final electron image. For the two imaging conditions applied ($\underline{g}$ = 200 and $\underline{g}$ = 110) the contrast corresponds to the tweed contrast actually observed.

VII.2. X-Ray Diffuse Scattering Effects

(i) Results

On monochromatic X-ray powder photographs of nitrided Fe-Ti alloys regions of diffuse scattered intensity are observed on the high angle side of each of the b.c.c. α-phase Bragg reflections (see Figure VII.13). This effect is associated with zone formation and for high solute concentrations this diffuse scattering is separated from the Bragg reflection by a low intensity region. Similar effects are observed by X-ray diffractometry (Figure VII.14) but careful step scanning also reveals a much lower intensity diffuse scattering on the low angle side of each Bragg reflection. The centres of gravity of the low and high angle regions of diffuse scattering are approximately equidistant from the Bragg peak. Diffuse scattering is detected more readily on a diffractometer trace because the diffracted beam is

Fig. VII.13.

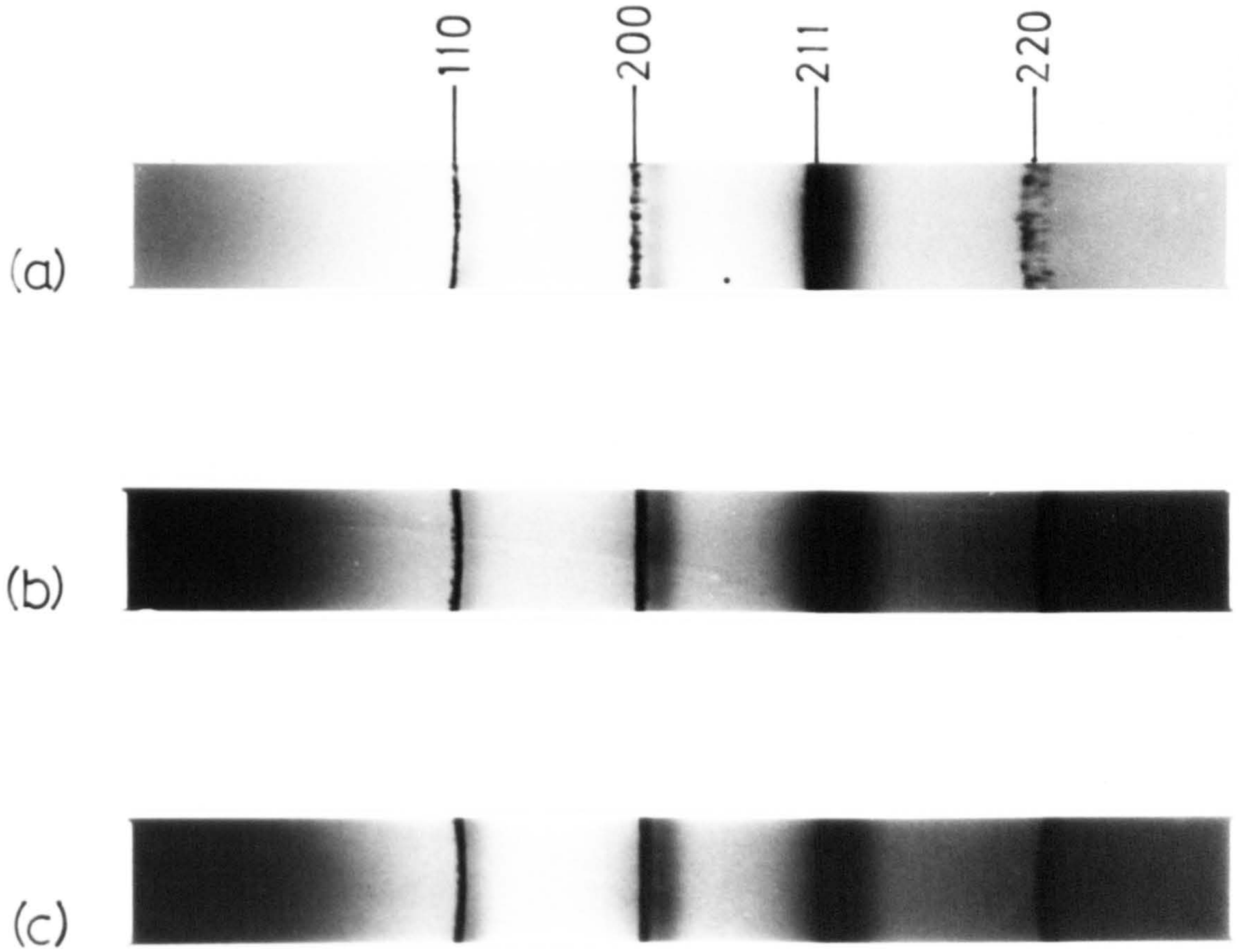

X-ray Powder Photographs of Fe–2at%Ti:

(a) As nitrided at 580°C in $8NH_3:92H_2$

(b) Nitrided and Aged at 580°C in H_2 for 150hr.

(c) Nitrided and Aged at 580°C in H_2 for 280hr.

Fig. VII.14.

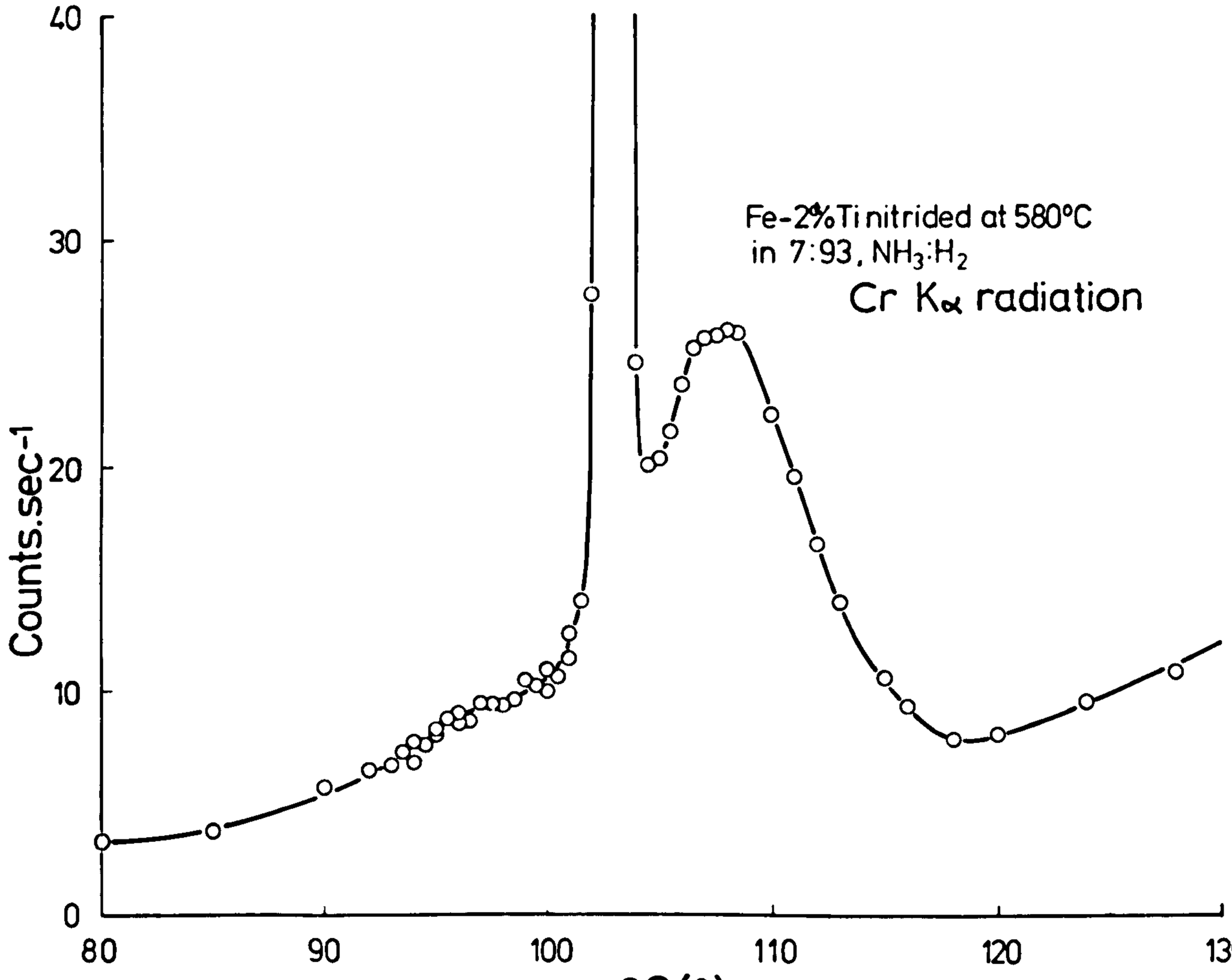

X-ray Diffraction Profile of {200} Reflection

monochromatised and background fluorescence counted is cut to a minimum whereas in X-ray powder photography the incident beam is monochromatised so that background fluorescence as well as the diffracted beam hits the film.

Kirkwood et al (1974) have also observed the high-angle diffuse scattering effects (see Chapter II) but attribute these to tetragonal distortion of the ferrite matrix adjacent to the faces of fine plate-like TiN precipitates. For the $\{200\}$ reflection the high-angle diffuse intensity peak is attributed to (020) and (200) tetragonal reflections and the lower angle high intensity peak is attributed to (002). However the relative intensities of these peaks are quite different from those expected for a tetragonal distortion of the matrix. Kirkwood et al also point out that their observations of the microstructures of overaged alloys are not consistent with this interpretation. The observation of low angle diffuse scattering in the present investigation suggests that the Kirkwood interpretation is incorrect since only two discrete $\{200\}$ reflections are expected for a tetragonal phase.

It is proposed from the present observations that these diffuse scattering effects are side-bands caused by a structure modulation e.g. by periodic variations of composition, lattice parameter or X-ray scattering factor. Daniel & Lipson (1943) first proposed such a model to explain diffuse X-ray scattered intensity occurring on both sides of Bragg reflections of Cu_4FeNi_3 in the early stages of decomposition; copper-rich and copper-poor regions occur in the lattice with a well-defined periodicity. It was shown that the wavelength (λ_m) of the periodic structure variation is

given by:

$$\lambda_m = \frac{h.\tan\theta}{N\ \Delta\theta}\ a_o \qquad \ldots\ . \quad \text{VII.1}$$

where h = highest Miller index of the Bragg reflection $\{h,k,l\}$

$N = h^2 + k^2 + l^2$

θ = Bragg angle for the h,k,l reflection

$\Delta\theta$ = angular separation (radians) of the side-band and Bragg reflection

a_o = mean lattice parameter of the material determined from the Bragg reflections

Applying equation VII.1 to Fe-Ti-N alloys, the values of λ_m calculated using the side-band spacings of different Bragg reflections and using different X-ray wavelengths are found within experimental error, to be the same for any given alloy. Results obtained from both high and low angle side bands on X-ray diffractometer traces also correspond closely with those obtained from X-ray powder photographs. This self-consistency supports the suggestion that the X-ray diffuse scattering effects are in fact side-bands. Further support for this is obtained by comparison with other systems investigated at Newcastle where periodic substitutional-interstitial solute-atom clusters are observed (Driver, Handley & Jack, 1976; Jack, 1975; Handley, 1974). In these systems, as in nitrided Fe-Ti alloys, the side-band intensities are asymmetric about the Bragg reflection.

(ii) Interpretation of X-ray diffuse scattering effects

Two groups of models have been proposed to explain experimental observations of side-bands on X-ray diffraction patterns. The first group (see Figure VII.15) postulates crystal structures modulated by a periodic fluctuation of composition about an average and individual models differ mainly in the nature of the periodic fluctuation. The model of Daniel & Lipson (1943) fits into this first group and they point out that two types of variation may arise from periodic composition fluctuations viz. variations in atomic scattering factor and variations in lattice parameter (or strain) which are analogous to amplitude (A.M.) and frequency (F.M.) modulations respectively in radio transmission. The second group of models postulates random composition fluctuations statistically distributed throughout the matrix (see Figure VII.16). In the present investigation the regular tweed contrast images and diffuse electron scattering effects observed by electron microscopy suggest an ordered or partially ordered dense array of G.P. zones and regular strain variations. Therefore the side-bands observed in the present investigation are probably due to a periodic variation of crystal structure. Since the scattering factors of iron and titanium atoms are very similar and the scattering factor of nitrogen atoms is too low to have more than a very small effect on X-ray intensities, the lattice parameter or strain variations arising from the periodic structure are probably the main cause of the side-bands observed for Fe-Ti-N alloys.

De Fontaine (1966) has developed a general theory of diffraction for one dimensional modulated structures and applied electronic analogues to evaluate the scattered intensity. The intensity profiles observed for nitrided alloys in the present investigation correspond closely to

Fig. VII.15.

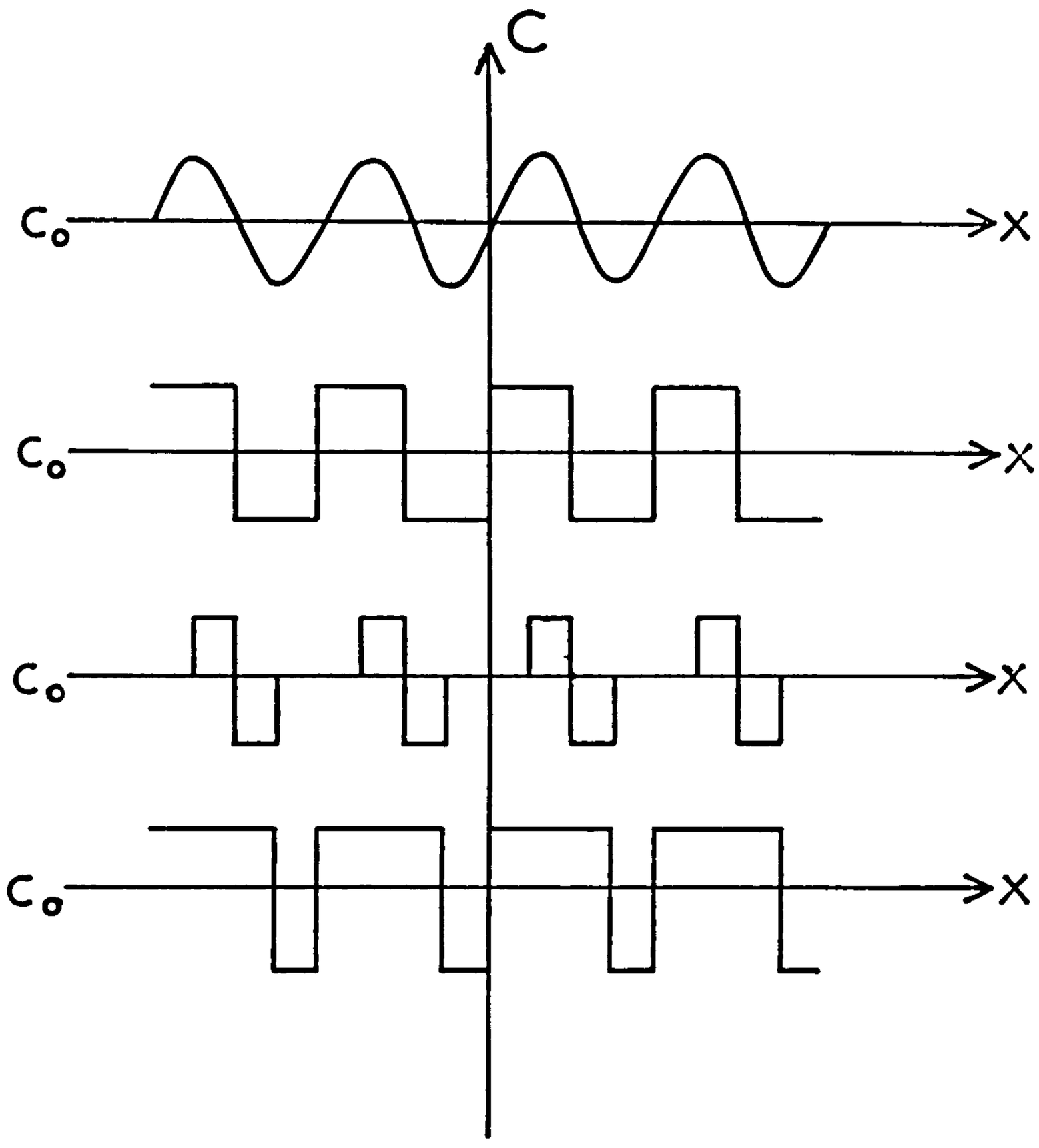

Daniel & Lipson (1943)

Hargreaves (1951)

Hargreaves (1951)

Balli & Zakharova (1954)
Tiedema et al (1957)
Biedermann (1960)

Proposed Models of Clustering in Solid Solutions

(a) Periodic Variation of Composition About a Mean (C_o)

Fig. VII.16.

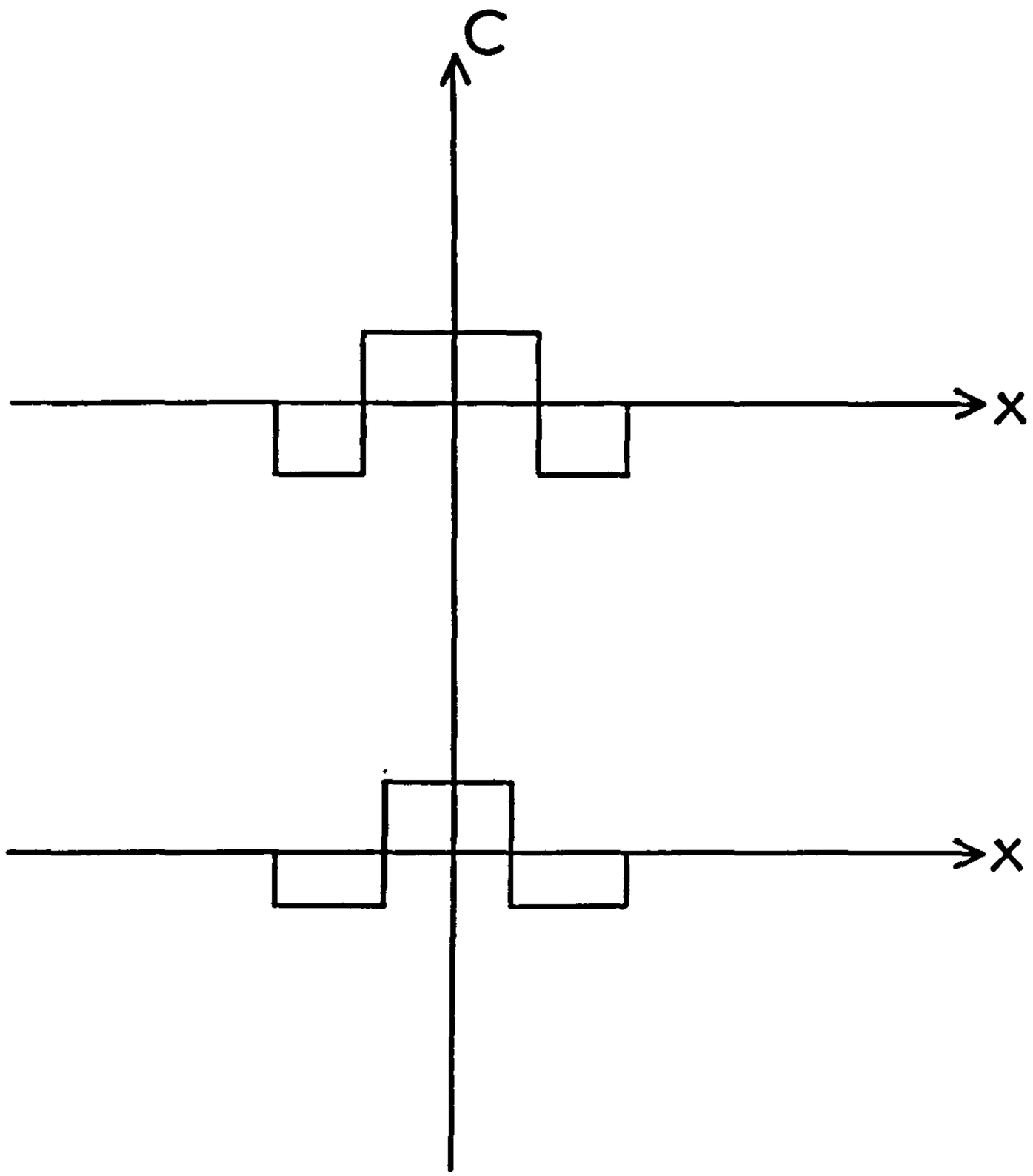

Guinier (1955)

Hillert et al (1961)

Proposed Models of Clustering in Solid Solutions

(b) Isolated Fluctuations of Composition Randomly Distributed in the Untransformed Matrix

the type obtained for lattice parameter (F.M.) variations in a modulated domain structure and for periodic arrays of coherent precipitates; this is illustrated in Figure VII.17. Periodic arrays of G.P. zones would give similar results since these also give rise to regular lattice parameter or strain variations. The interpretation is consistent with the morphology inferred from electron micrographs in which there is a pseudo-periodic array of very thin plate-like zones accompanied by regular strain variations.

(iii) Variation of side-band spacing with nitriding conditions

Although the parameter λ_m in equation VII.1 is probably not simply related to inter-zone spacing in nitrided Fe-Ti alloys it still can be used as a measure of the pseudo-periodicity of the crystal structure or as a guide for comparison of the inter-zone spacing of different alloys.

Information obtained in the present investigation about X-ray scattered intensity profiles is insufficient to allow a detailed interpretation of the type of structure variations which occur but the variation of side-band separation under different nitriding conditions has been studied. Structure modulation periods (λ_m) have been calculated to provide a correlation of inter-particle spacing with nitriding conditions and alloy composition.

Most of the work has been carried out using long exposure X-ray powder photography and appreciable errors of measurement are inevitable, especially for side-bands with small separations from the main Bragg reflections.

Fig. VII.17.

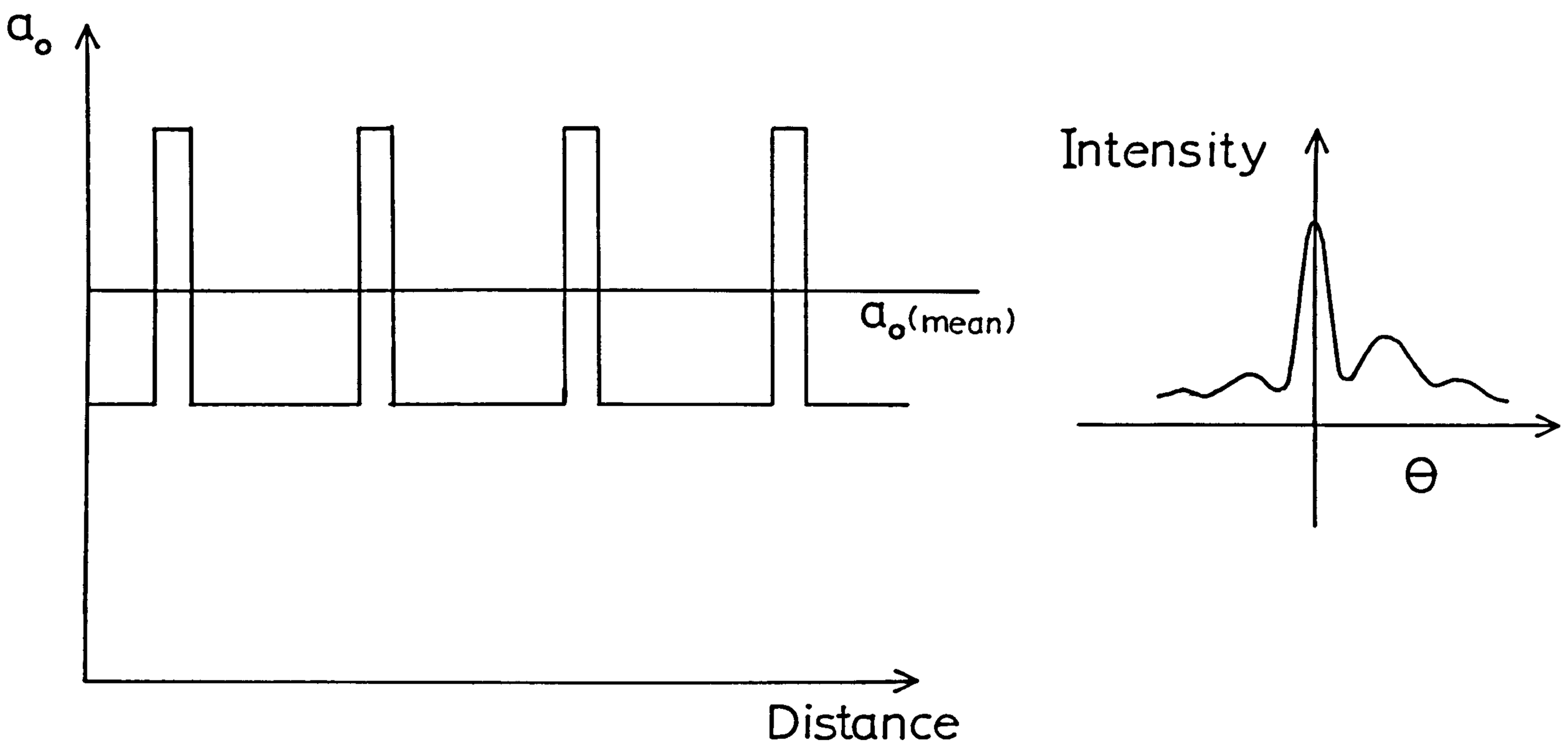

(a) One dimensional Model of Periodic Lattice Parameter Variation

(b) Schematic Representation of X-ray Scattered Intensity Profile Obtained for (a)

This occurs because the main Bragg reflections on the X-ray powder photographs are very broad and overexposed (see Figure VII.17) which makes determination of the position of peak intensity difficult. It is also difficult to determine the position of peak intensity of the relatively weak, diffuse side-bands.

Figure VII.18 shows the variation of modulation period (λ_m) with titanium content for nitrided alloys. It can be seen that λ_m is inversely proportional to titanium content, which is consistent with classical theories of nucleation and growth where the frequency of nucleation of the precipitating species is controlled by the supersaturation of the solid solution. The theory predicts for nitrided Fe-Ti alloys that the critical solubility product $[Ti] . [N]$ necessary for nucleation of stable Ti-N clusters is attained at lower nitrogen supersaturations for higher titanium content alloys. Therefore the frequency of nucleation is greater for higher titanium content alloys nitrided in a given set of conditions and results in finer clusters and smaller inter-particle spacings. This would give the kind of variation of modulation period shown in Figure VII.18.

Figure VII.19 shows the variation of λ_m with nitriding potential for Fe-2a/oTi nitrided at 500°C. Despite large errors in the measurement of λ_m it can be seen that there is a small decrease in λ_m with increasing nitriding potential i.e. the inter-particle spacing decreases as the nitrogen supersaturation of the alloy increases. However no regular variation of λ_m with nitriding potential was detectable for Fe-2a/oTi alloys nitrided at 580°C. At this temperature the variation is likely to be smaller because of the smaller variation of nitrogen content with nitriding potential and

Fig. VII.18.

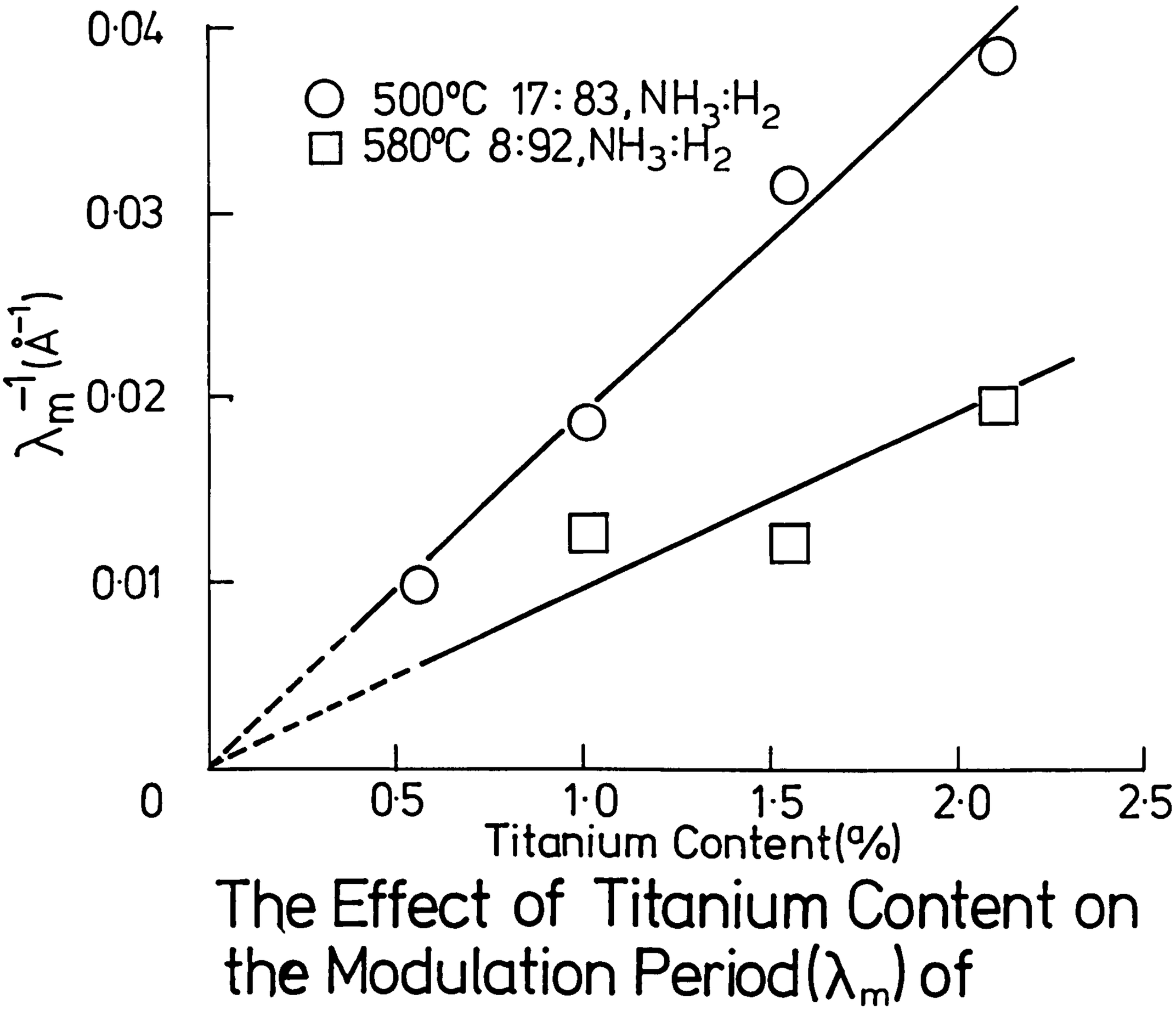

The Effect of Titanium Content on the Modulation Period(λ_m) of Nitrided Fe-Ti Alloys

Fig. VII.19.

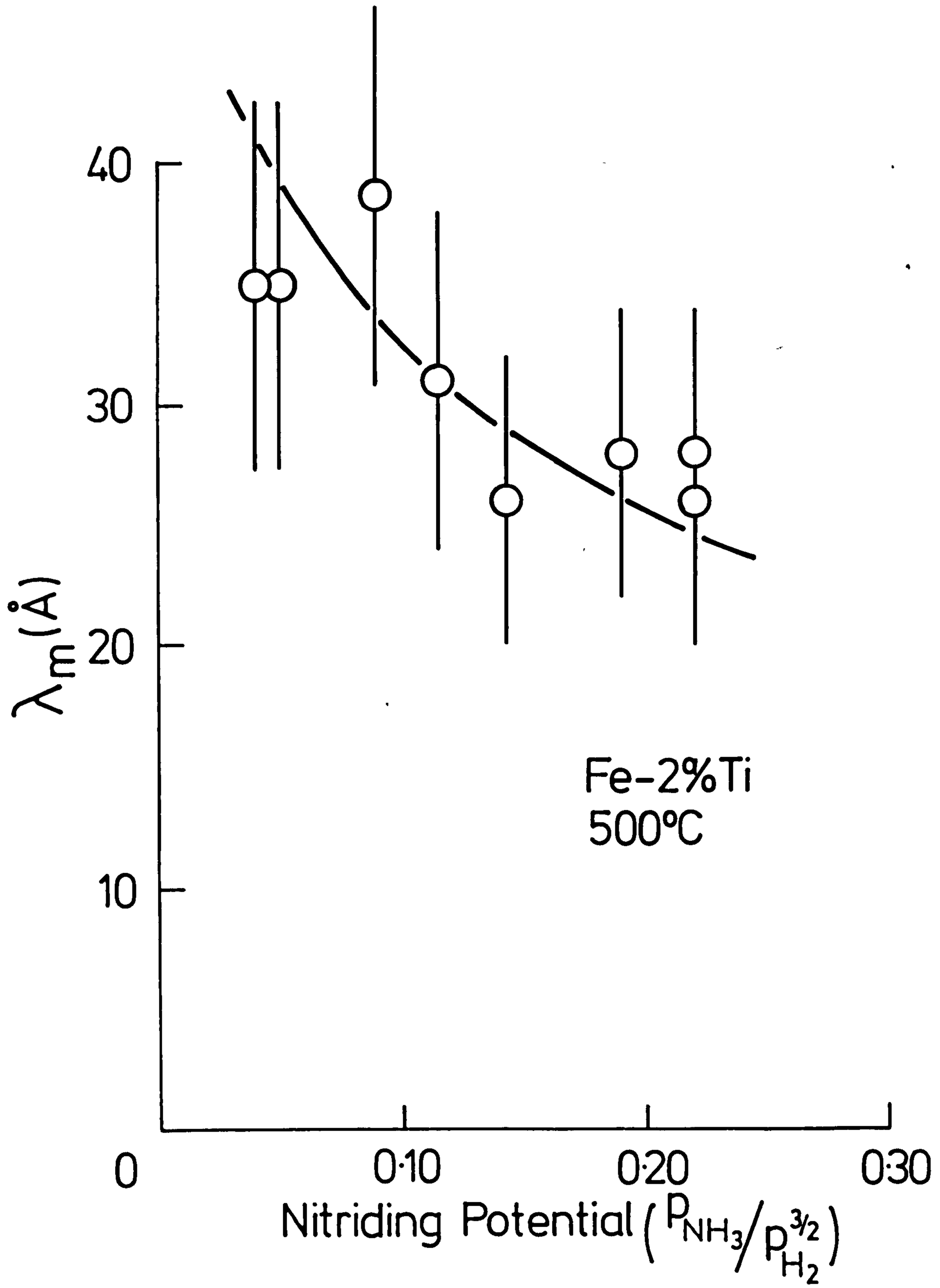

Variation of Modulation Period (λ_m) with Nitriding Potential

any regular variation could be obscured by the large errors in measurement of the modulation period λ_m.

The variation of modulation period λ_m with nitriding temperature for Fe-2^a/oTi and Fe-1^a/oTi alloys was studied by measuring the side-band separations for alloys nitrided in gas atmospheres calculated to be in equilibrium with the same concentration of nitrogen in solution in pure iron (0.17^a/o) at each temperature. The results are shown in Figure VII.20. Generally the higher the nitriding temperature the longer is the observed λ_m. The relative coarseness of the structure of alloys nitrided at higher temperatures may be due to the lower supersaturation of nitrogen and the larger critical nucleus size for stable zone formation.

VII.3. Discussion

Lattice parameter and hardness measurements of Fe-Ti alloys nitrided at 400°-650°C suggest the presence of solute atom clusters. The $\langle 100 \rangle$ streaking of matrix spots on electron diffraction patterns indicates that the clusters are in the form of thin discs lying on $\{100\}$ matrix planes. Although the clusters can not be resolved directly by electron microscopy the regular tweed contrast images suggest that the morphology consists of a dense, ordered array of G.P. zones. The $\langle 110 \rangle$ streaks on electron diffraction patterns are probably caused by periodic elastic distortions of the matrix due to the ordering of the zones. This ordering is itself a result of the tetragonal distortion of the matrix by individual zones.

Fig. VII.20.

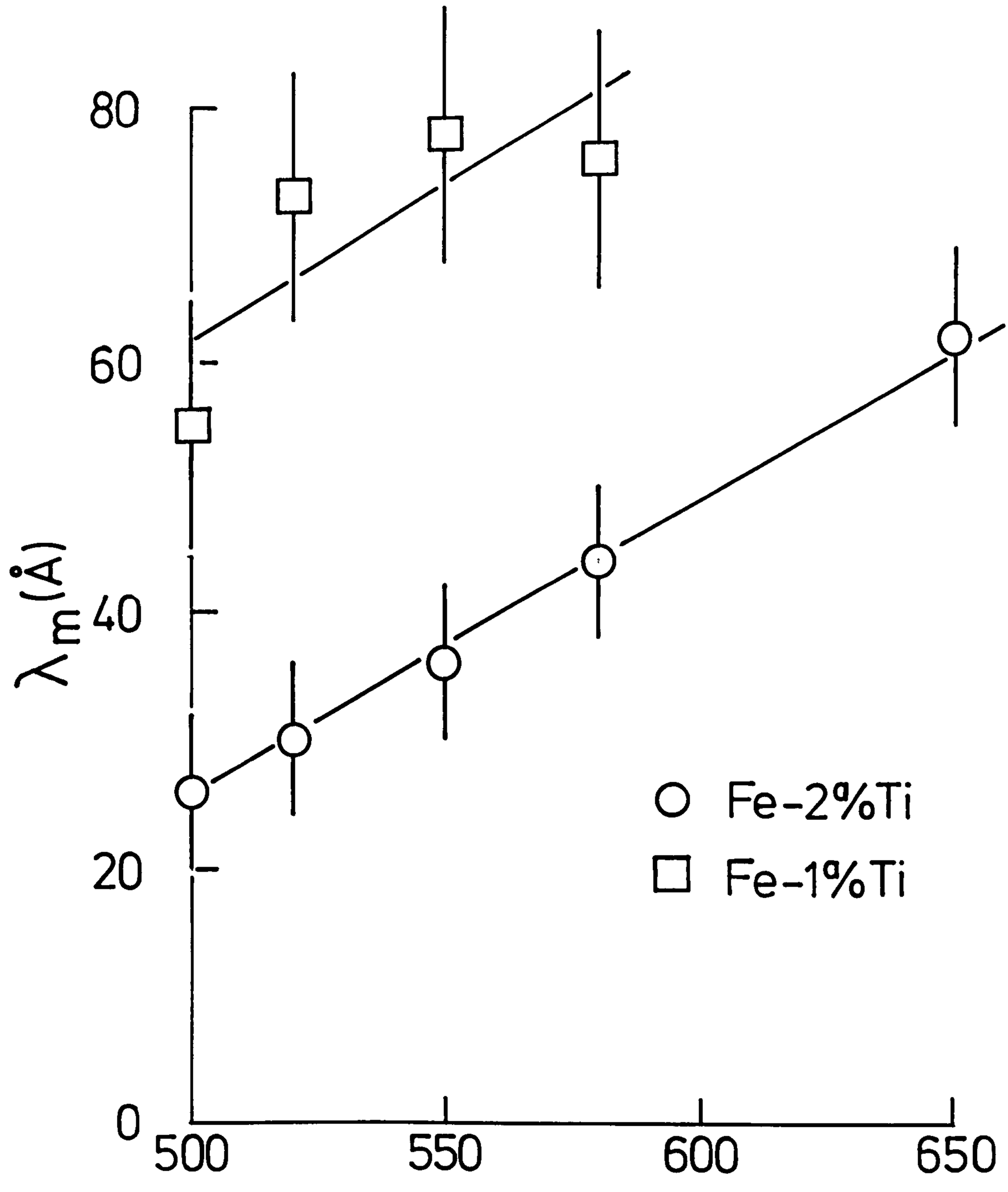

Variation of Modulation Period (λ_m) with Nitriding Temperature for Fe-Ti Alloys

The observation of side-bands on X-ray diffraction patterns of the nitrided alloys is consistent with the observation of tweed contrast images by electron microscopy, since both effects arise from ordered or partially ordered arrays of G.P. zones or coherent precipitates.

The modulation period λ_m is a measure of the separation of the G.P. zones and its variation with alloy composition and nitriding conditions agrees well with that predicted from classical nucleation theory. The structure of Fe-Ti-N alloys is coarser at higher nitriding temperatures and this explains why the zones are resolved in Fe-0.5^a/oTi nitrided at 650^o and 750^{o}C. In general, the electron microstructures of Fe-Ti alloys nitrided at high temperatures are very similar to those of other Fe-X alloys nitrided at intermediate or low temperatures e.g. Fe-V, Fe-Mo, Fe-Cr. It is worth noting that for all these systems the fineness of the microstructure produced at a given nitriding temperature is related to the affinity of the substitutional solute for nitrogen (Pope et al, 1975).

Chapter VIII

THE AGEING KINETICS OF NITRIDED Fe-2^{a}/oTi ALLOYS

VIII.1. Introduction

The ageing of nitrided Fe-Ti alloys in hydrogen for long periods at 580°C (see Chapter VI) demonstrates the great stability of the zone structures since no changes in lattice parameter or hardness are observed up to 280 hours. The rates of ageing at 400-750°C are too low to be followed in reasonable times. However, the reaction rates might be expected to vary exponentially with temperature, enabling the kinetics of ageing processes to be followed in relatively short times at higher temperatures (>750°C). A knowledge of the kinetics of ageing processes at these high temperatures should provide quantitative evidence of the stability of the zones and their ageing sequence at lower temperatures.

In an ageing process the reaction rate may be determined by measuring the concentration of transformed (or untransformed) material as a function of time as the reaction proceeds. This is often difficult to measure directly but can be deduced from the variation of some physical property that is a function of the degree of transformation.

VIII.2. Results

Prolonged ageing at 580°C of hydrogen reduced Fe-Ti alloys has no measurable effect. As expected from the model for Ti-N zones (see Chapter VI) hydrogen reduction has no effect on the modulation period λ_m of nitrided Fe-Ti alloys (see Figure VII.13) and prolonged ageing in hydrogen (up to 280 hours) has no further effect on the modulation period λ_m, the N:Ti atomic ratio (1:1) or the hardness of the alloy. This is probably due to the very strong Ti-N interaction which stabilizes the zones both in composition and size. The alloy morphology thus remains unchanged.

The ageing kinetics of nitrided Fe-2^a/oTi at 800°C and 850°C were studied by following the changes in lattice parameter and hardness. Wires nitrided in $4NH_3:96H_2$ at 580°C were hydrogen-reduced at the same temperature to remove all excess nitrogen above the 1N:1Ti atomic ratio and subsequently aged in argon at 800° or 850°C. The variation of lattice parameter with time is shown in Figures VIII.1 and VIII.2.

The alloys were hydrogen-reduced in order to avoid austenite formation during ageing. Since the nitrogen remaining effectively in solid solution in the alloy is strongly associated with the titanium, then ageing at high temperatures should not cause any further loss of nitrogen. Lattice parameter changes must therefore be due to the transformation of the Ti-N zones to a discrete precipitate.

Figures VIII.1 and VIII.2 show initial rapid decreases in lattice parameter with time for the alloys aged at 800° and 850°C, tending to constant values at longer

Fig. VIII.1.

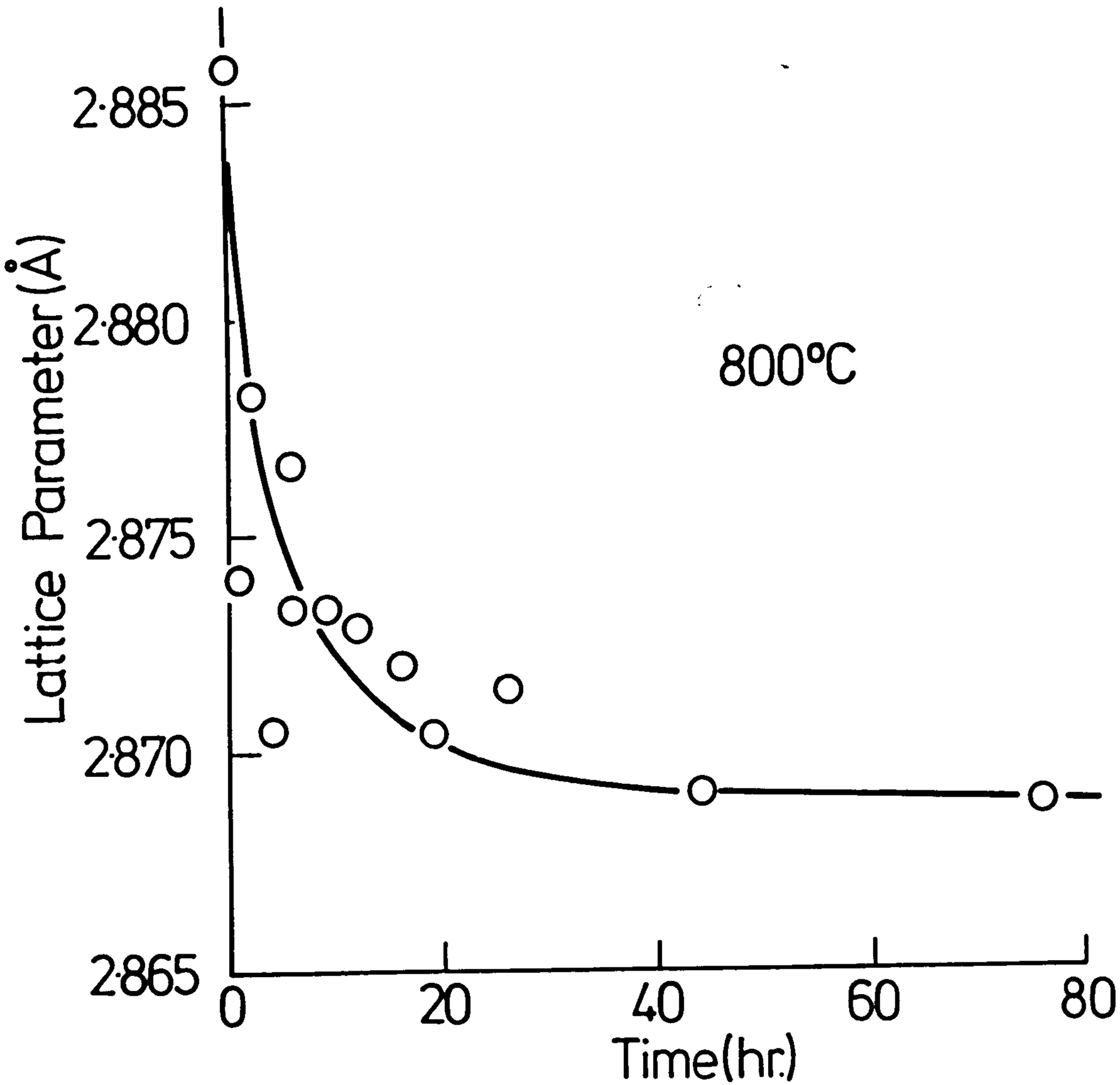

Variation of Lattice Parameter with Ageing Time

Fig.VIII.2.

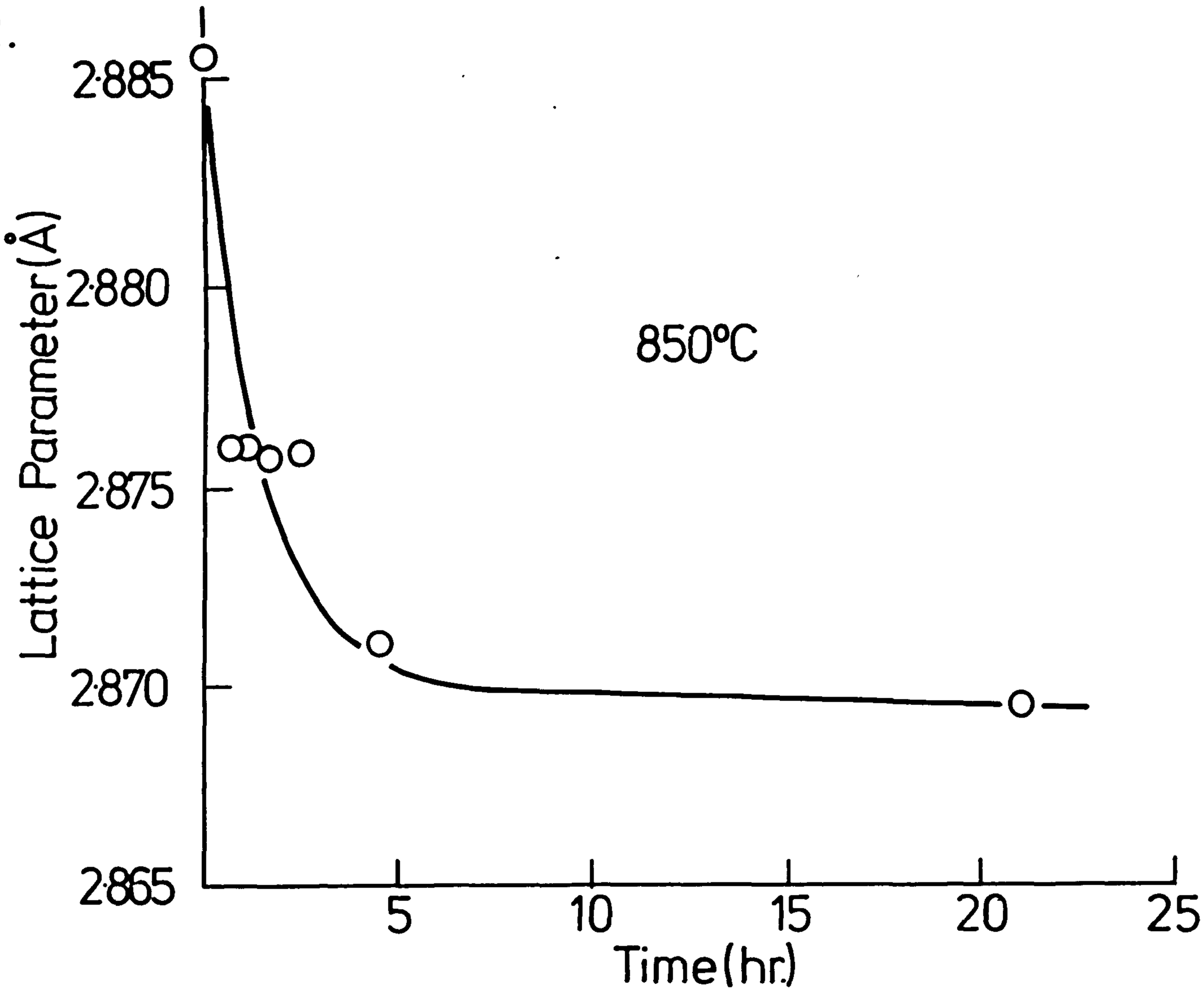

Variation of Lattice Parameter with Ageing Time

times. These constant values are much higher than those expected if all of the titanium and nitrogen present is precipitated, even though the shapes of the graphs suggest that the ageing process is complete. Persistent "high" lattice parameters for aged alloys have also been observed in the Fe-Ti-C system (Hendry, 1974) and in internally oxidised silver alloys (Tillman, 1974) where, in both cases, alloys before ageing contain mixed substitutional-interstitial solute-atom clusters.

Curves drawn through the experimental points of Figures VIII.1 and VIII.2 were used to determine the transformation rates. Y_t, the fraction of the alloy transformed after any time t during the ageing treatment is defined as:

$$Y_t = \frac{\Delta a_o}{a_f - a_i} \quad \ldots . \quad \text{VIII.1}$$

where Δa_o = increase in lattice parameter after time t

a_i = the lattice parameter at time $t = 0$

a_f = the lattice parameter when the ageing process is complete

Assuming that the ageing process is complete when all of the substitutional and interstitial solute is precipitated and that a_f is the lattice parameter of pure iron (2.866Å) the results can be fitted to a complex empirical kinetics equation of the form derived by Austin & Ricketts (1939):

$$dY_t/_{dt} = (1-Y_t)^2 . K_A^n . t^{(n_A-1)} \quad \ldots . \quad \text{VIII.2}$$

which when integrated gives:

$$\frac{Y_t}{1-Y_t} = (K_A'. t)^{n_A} \quad \ldots\ldots \text{VIII.3}$$

if K_A and n_A are constant and n_A is taken into the rate constant (K_A'). The plot of log $(Y_t/1-Y_t)$ against log t is shown in Figure VIII.3. For the alloy aged at 850°C there is a change in slope (n_A) after 6 hours. The behaviour of the alloy aged at 800°C is similar except that the change in slope occurs at about 26 hours after which the data are coincident with those for the alloy aged at 850°C. For each ageing temperature the change in slope of the graphs coincides with the time taken for the lattice parameters to fall close to their lowest observed values. The change in slope must therefore mark the end of the ageing process being followed.

For the alloy aged at 800°C, Figure VIII.4 shows a linear variation of hardness with log (t+1) where t is the ageing time in hours. There is a change in slope after about 20 hours.

Figure VIII.5 shows the electron microstructure of Fe-2^a/oTi nitrided and then hydrogen reduced at 580°C and aged in argon at 850°C for 4 hours; lattice parameter measurements show that the ageing process is almost complete although considerable solute still remains in non-random solid solution. The microstructure consists of plate-like precipitates about 200Å in diameter lying on $\{100\}$ ferrite matrix planes. The precipitates give rise to TiN reflections on electron diffraction patterns (see Figure VIII.6a) which are streaked along $\langle 100 \rangle$ directions. The thickness of the precipitates estimated

Fig. VIII.3.

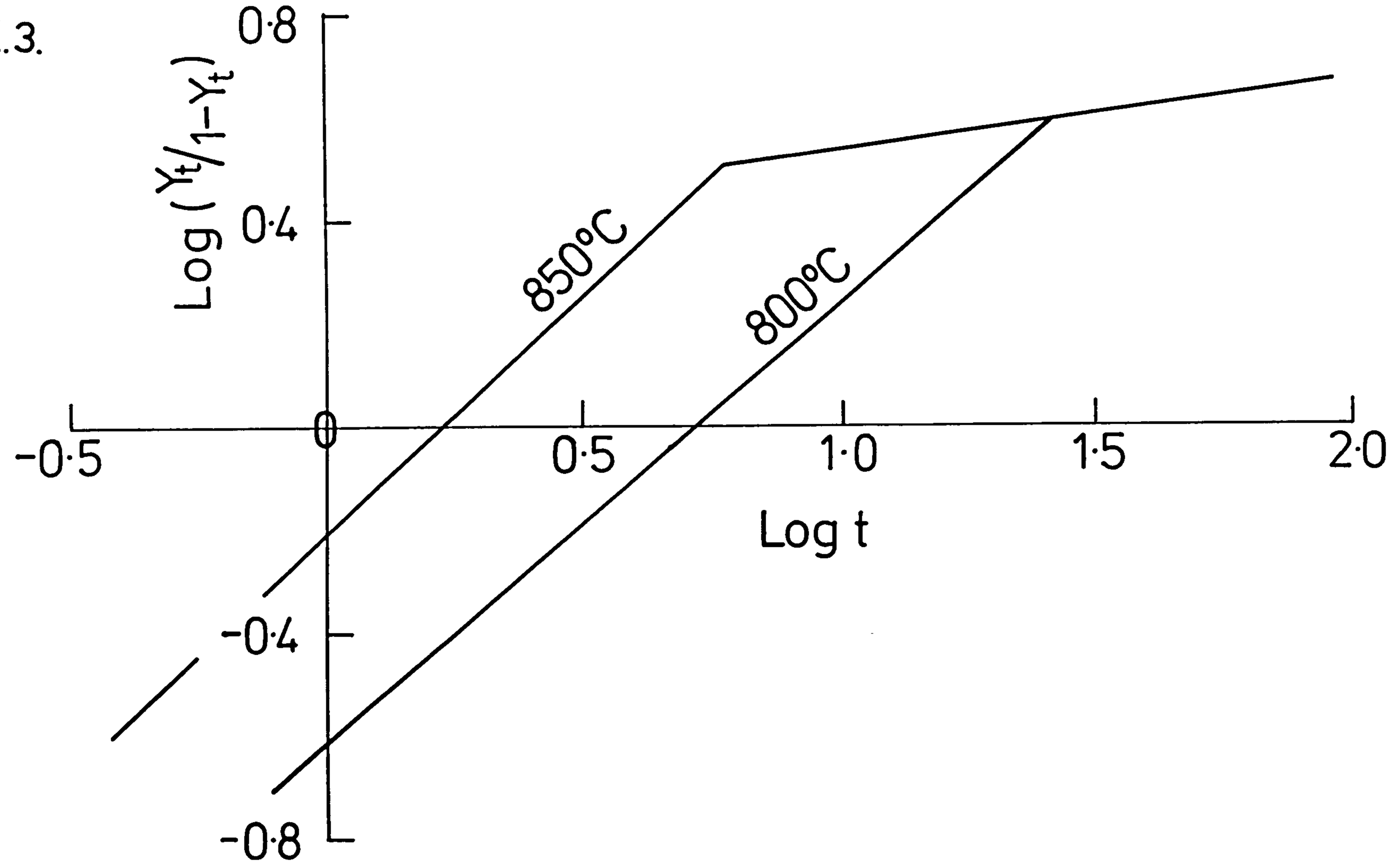

Ageing Kinetics of Nitrided and Hydrogen Reduced Fe-2%Ti (Austin-Ricketts Model)

Fig.VIII.4.

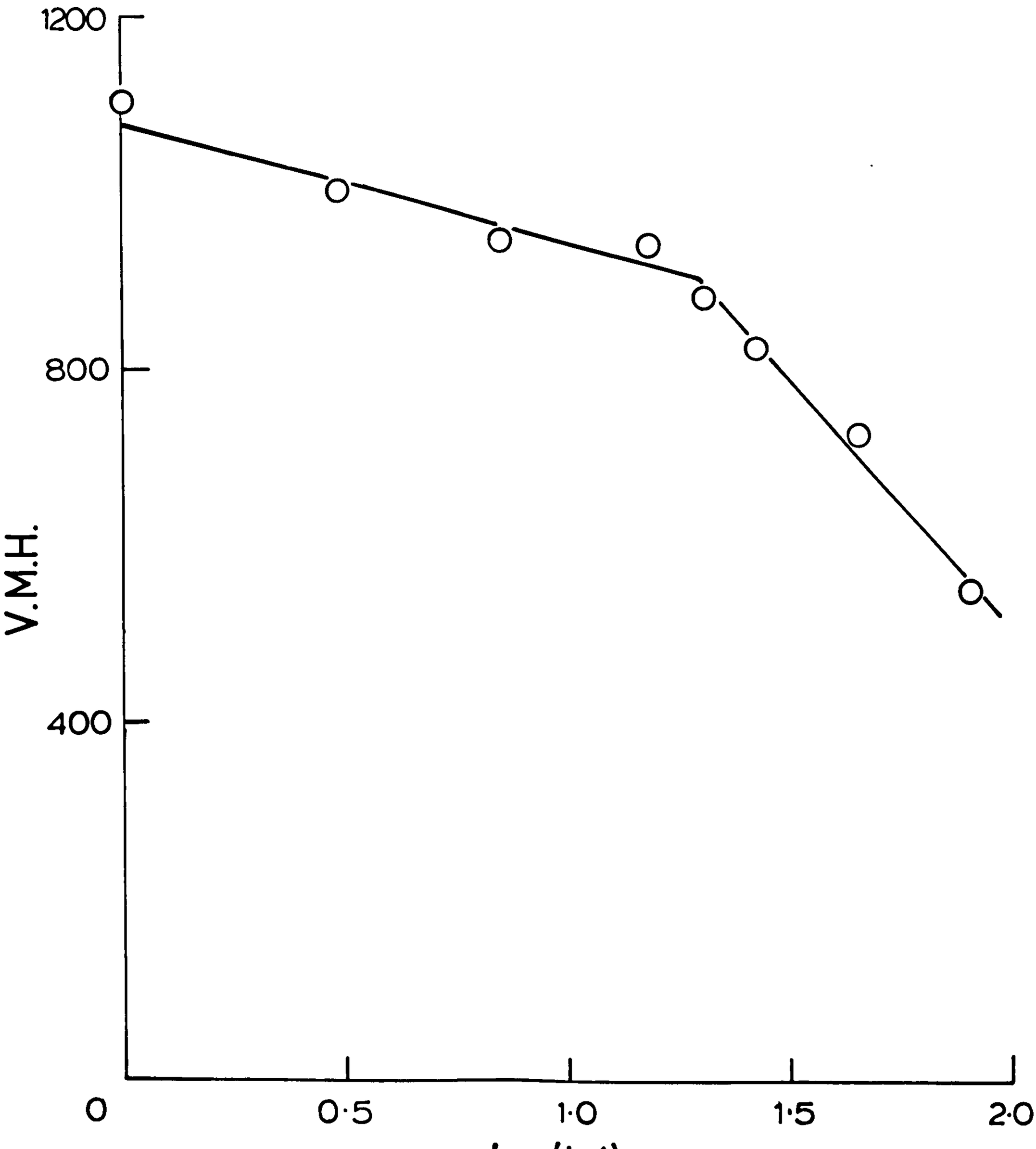

Variation of Hardness with Ageing Time for Fe-2%Ti Nitrided at 580°C, Hydrogen Reduced at 580°C and Aged in Argon at 800°C

Fig. VIII. 5.

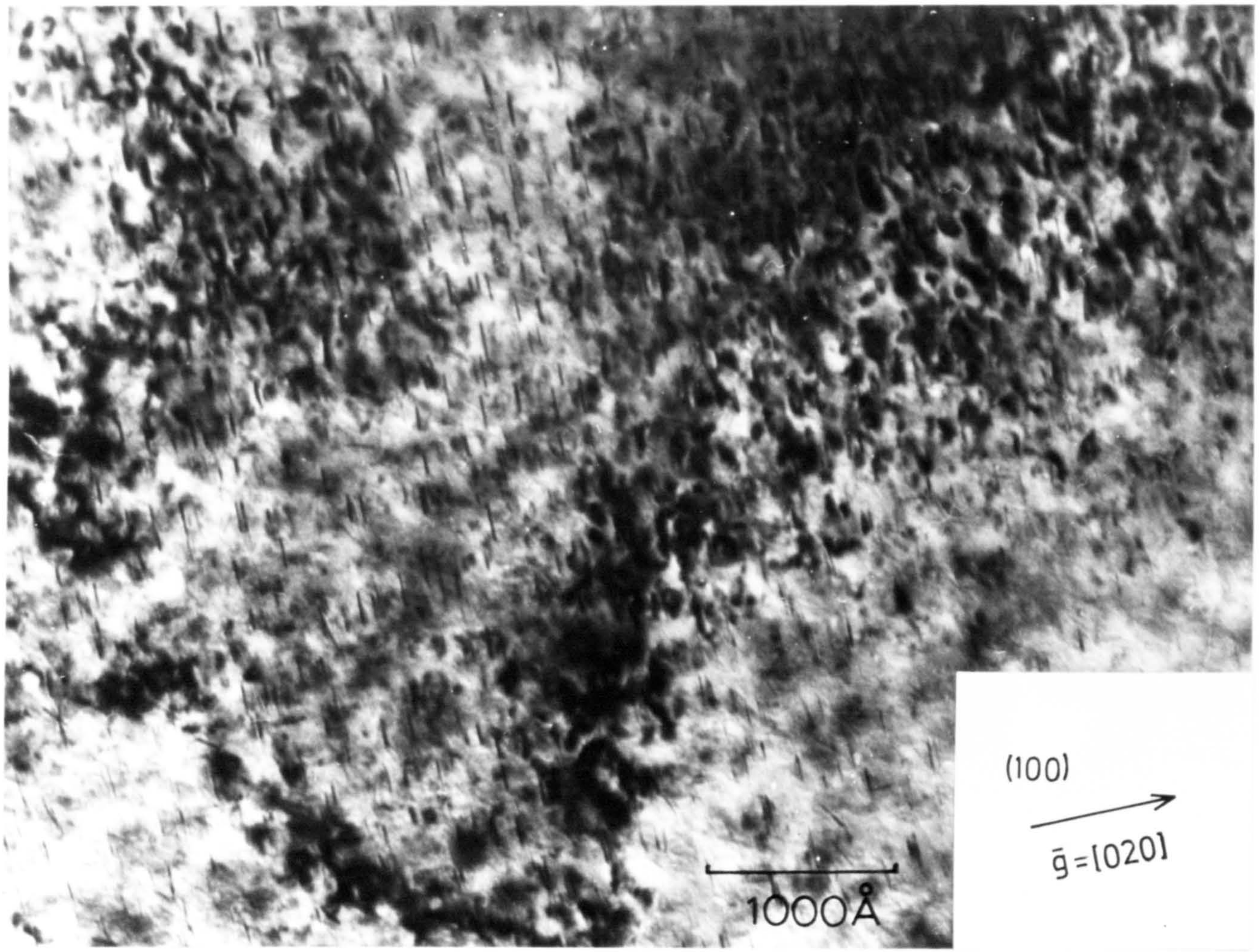

Bright Field Micrograph of Fe-2%Ti Nitrided at 580°C in $4NH_3:96H_2$ and Aged at 850°C in Argon for 4 hours

Fig. VIII. 6.

(a)

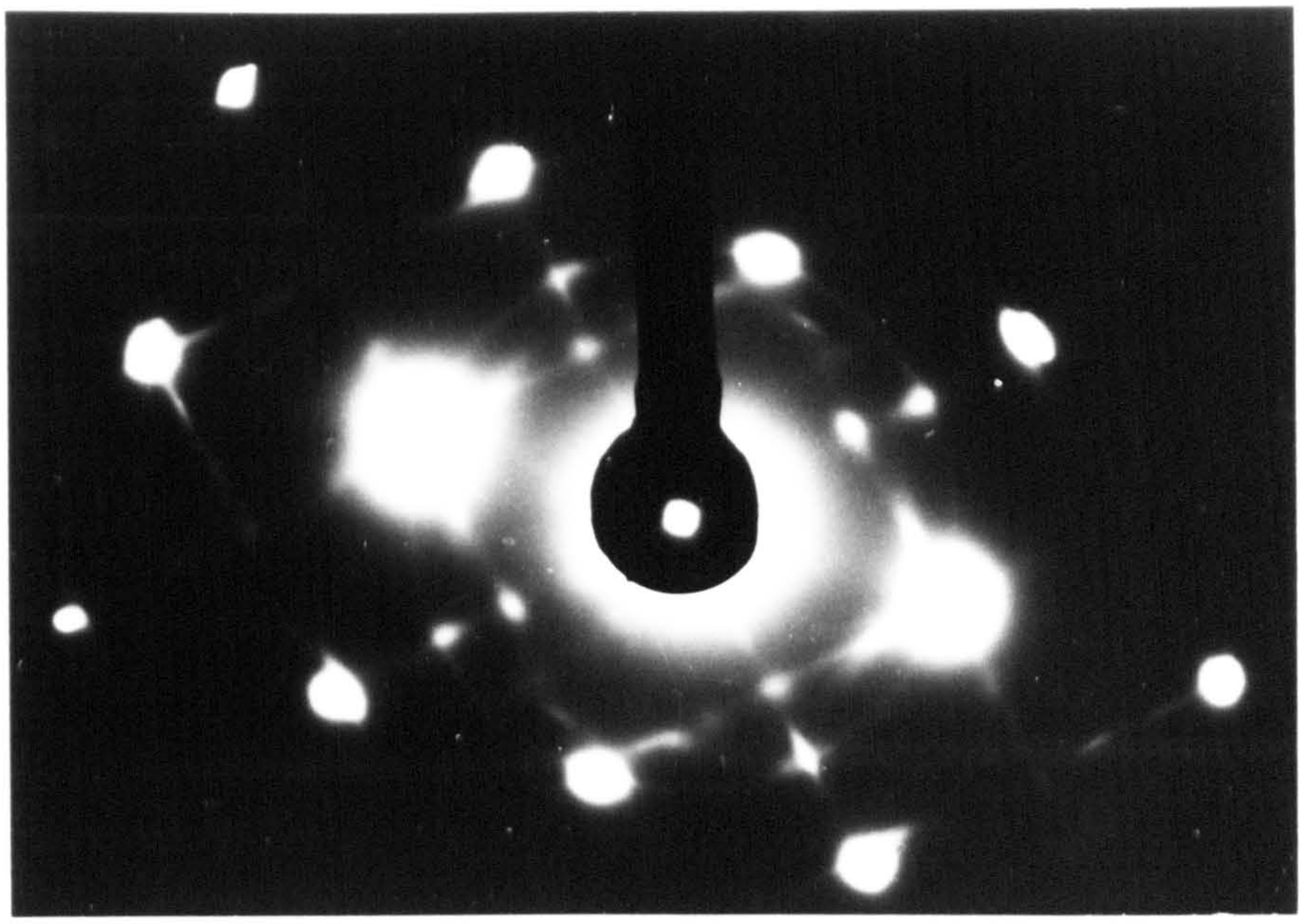

(b)

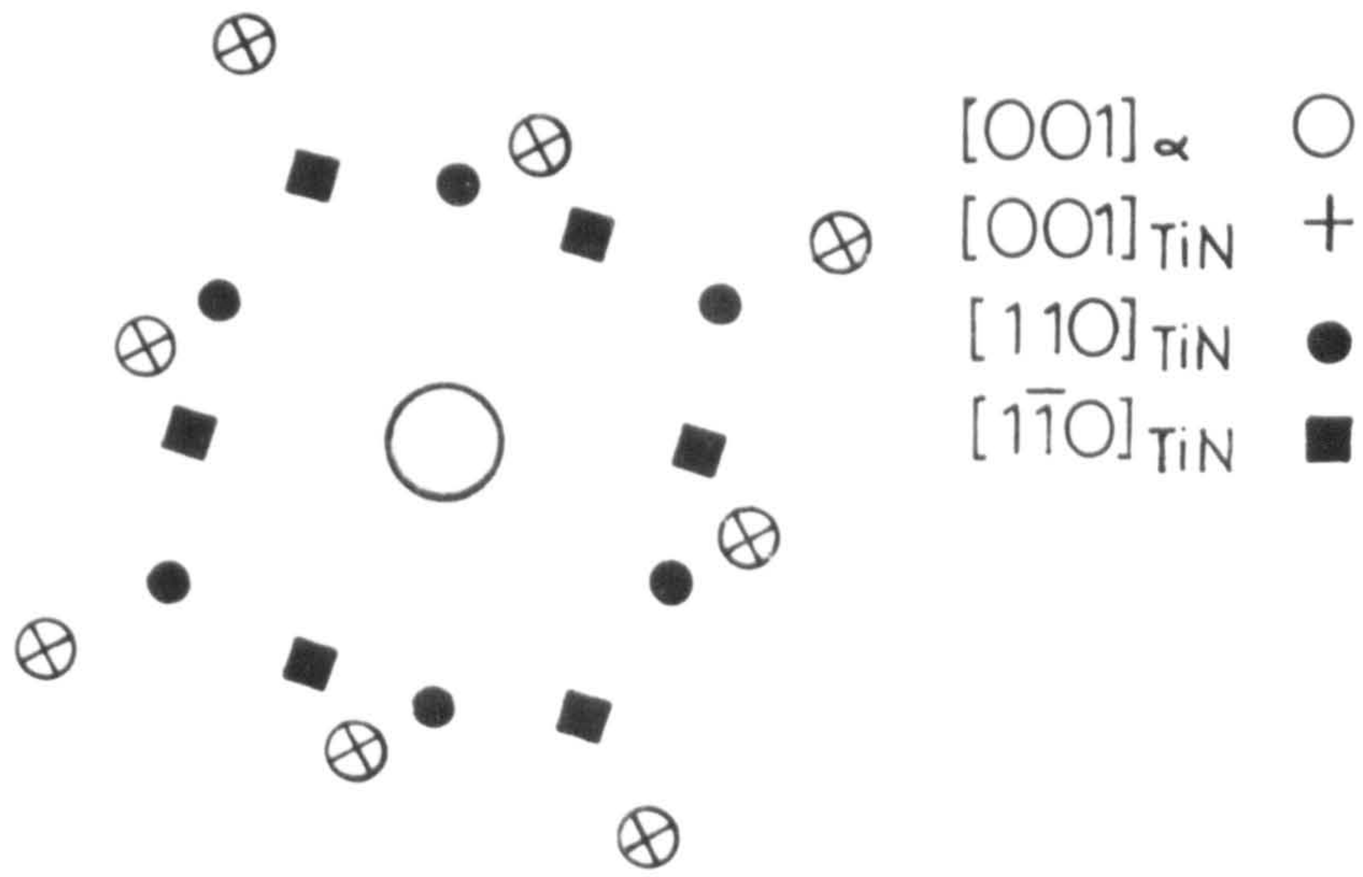

(a) Electron Diffraction Pattern of Fe-2%Ti Nitrided, Hydrogen Reduced at 580°C and Aged in Argon for 4hr. at 850°C

(b) Schematic Representation of (a)

from the length of the streaks (Hirsch, Howie and Whelan, 1965) is approximately 30Å. The precipitates have a Bain orientation relationship with the matrix, the three variants of which are:

$[001]_\alpha \parallel [001]_{TiN}$	$[001]_\alpha \parallel [1\bar{1}0]_{TiN}$	$[00\bar{1}] \parallel [1\bar{1}0]_{TiN}$
$(100)_\alpha \parallel (1\bar{1}0)_{TiN}$	$(100)_\alpha \parallel (001)_{TiN}$	$(100)_\alpha \parallel (110)_{TiN}$
$(010)_\alpha \parallel (110)_{TiN}$	$(010)_\alpha \parallel (1\bar{1}0)_{TiN}$	$(010)_\alpha \parallel (001)_{TiN}$

Figure VIII.6(b) is a schematic representation of Figure VIII.6(a) showing the TiN reflections due to $[1\bar{1}0]_{TiN}$ and $[110]_{TiN}$ zones in a $[001]_\alpha$ zone. The reflections due to $[00\bar{1}]_{TiN}$ zone are almost coincident with the matrix reflections.

VIII.3. Discussion

In Chapter VI it was suggested that elastic interactions between the plate-like Ti-N zones were responsible for their regular arrangement and the observed tweed contrast on electron micrographs of nitrided Fe-Ti alloys. Brown et al (1973) have shown for tetragonal matrix distortions by coherent precipitates that elastic interactions cause a stabilization of the structure at a critical particle size and separation. A similar situation may exist in nitrided Fe-Ti alloys. This would account for the resistance to coarsening of the structure of nitrided and hydrogen-reduced alloys during ageing at 580°C and also the resistance to further change in lattice parameter after short ageing times at 850° and 800°C.

Determination of the ageing kinetics of nitrided

and hydrogen-reduced Fe-2^a/oTi by following the change in lattice parameter of the material with time only takes into account depletion of the titanium and nitrogen effectively in solid solution. Other properties such as size, shape, distribution or volume fraction of phases present can not be measured directly. Hardness measurements are sensitive to such properties and so it is possible that the ageing processes followed by the changes in hardness of the material are completely different from those examined by changes in lattice parameter.

There is no evidence to suggest that any stable phase other than f.c.c. TiN is precipitated during the ageing. The stable precipitate has a distortion of the same atomic arrangement as the non-random solid solution and there is no abrupt change between a fine coherent plate-like precipitate and the mixed substitutional-interstitial solute-atom cluster. The distinction only becomes clear cut when the precipitate becomes incoherent because well-defined phase boundaries then exist and coherency strains relax to allow the precipitate to attain its equilibrium f.c.c. structure. There is probably a continuous transformation in the ageing sequence of Fe-Ti-N alloys involving the clustering and ordering of solute atoms followed by coherent f.c.c. TiN precipitates. Depending on their size and misfit with the matrix, coherent TiN precipitates may completely or partially diffract X-rays with the matrix and behave as if they were still in solid solution. Electron microscopy of the aged Fe-2^a/oTi alloys indicates that during ageing at high temperatures the zones coarsen and that the internal elastic strain which gave rise to tweed contrast in the as-nitrided alloys is considerably reduced. As the zones coarsen, they may then begin to diffract X-rays as f.c.c. TiN causing the

observed decrease in lattice parameter of the ferrite matrix. The driving force for the coarsening process might be the reduction of the total strain energy of the system. This driving force decreases as the ageing process progresses and might be counteracted by stabilization of the structure of the alloy at definite particle size and separation by elastic interactions in the matrix (Brown et al, 1973). This might account for the very slow decrease of lattice parameter at longer ageing times and also the change in the slope of the Austin-Ricketts graph (Figure VIII.3). If the precipitates in the stabilized structure were still partially coherent with the matrix, this might account for the observed persistent high lattice parameters of the aged alloys.

The persistent high lattice parameter of the alloy could also be explained by the existence of a range of precipitate sizes with different degrees of coherency. Because of the limited amount of information available about the ageing of Fe-X-N alloys and changes in lattice parameter explanations of the present observations can only be speculative.

The strengthening mechanism predominant in nitrided and hydrogen reduced alloys is resistance to particle shear (see Chapter IX) and that predominant in such alloys aged for long periods at high temperatures ($>800^{o}$) is the Orowan mechanism (Chen, 1965). The change in slope (at 20 hrs) of the hardness vs log (t + 1) graph (Figure VIII.4) is probably due, therefore, to a change in strengthening mechanism. After about 20 hours ageing the average interparticle spacing may be such that dislocation movement within the alloy can most readily occur by bowing between particles.

Properties such as particle-matrix coherency which may affect the mean lattice parameter of the alloy would no longer significantly affect the strength of the alloy.

ChapterIX

THE MECHANICAL PROPERTIES OF NITRIDED IRON-TITANIUM ALLOYS

IX.1. Introduction

The results of hardness tests have already been used to provide evidence for the composition of zones and the strengthening mechanisms occurring in nitrided Fe-Ti alloys (see Chapter VII). Fundamentally more meaningful mechanical properties such as yield stress, proof stress and work hardening rates can be determined from tensile tests of nitrided alloys and the results should provide further evidence of the structure and chemical nature of the zones and precipitates.

Apart from internal friction studies very little systematic work has been carried out on the mechanical properties of nitrided binary ferrites. Szabo-Miszenti (1971) and Pope, Jones & Jack (1973) report abnormal Snoek peaks in internal friction studies and the latter workers attribute these to stress-induced diffusion of nitrogen atoms at the periphery of solute-atom clusters. Chen (1965) investigated the tensile properties of nitrided Fe-2^{a}/o, 1^{a}/o and 0.5^{a}/oTi alloys aged at high temperatures ($>800^{o}C$) because the as-nitrided alloys were extremely brittle and fractured before yield. In the present investigation this problem has been overcome by using a dilute Fe-0.2^{a}/oTi alloy. Tensile tests were carried out after nitriding at 500^{o} and $580^{o}C$ and the 0.05% proof stresses were determined. Hardness tests have

also been used to assess the mechanical properties of nitrided Fe-2^{a}/o, 1^{a}/o and o.5^{a}/oTi alloys.

IX.2. Results

The electron microstructure of Fe-0.2^{a}/oTi nitrided at 500°C shows an irresolvable non-uniform texture and dot contrast similar to that observed by Phillips & Seybolt (1968) for iron-nitrided alloys. No regular texture or tweed contrast is observed. The electron microstructure of the Fe-0.2^{a}/oTi nitrided at 580°C consists of plate-like zones about 50-90Å diameter lying on {100} ferrite matrix planes (see Figure IX.1). This implies that the zones formed at 580°C are coarser than those at 500°C. The absence of well-defined tweed contrast on electron micrographs is due to the low density and relative coarseness of zones in Fe-0.2^{a}/oTi compared with nitrided Fe-2^{a}/o, 1^{a}/o, and 0.5^{a}/oTi alloys.

Figure VI.4 shows that for nitrided and hydrogen-reduced alloys the hardness increase compared with the annealed un-nitrided alloy is proportional to the square root of the nitrogen concentration which is equivalent to the square root of the volume fraction of the Ti-N zones. This relationship is characteristic of a strong particle cutting strengthening mechanism. Results of tensile tests on nitrided Fe-0.2^{a}/oTi are consistent with this mechanism. The stress-strain curves of the nitrided Fe-0.2^{a}/oTi alloys are similar in shape to those of the as-annealed alloys and the work hardening rates (0.15-0.05% proof stress) are approximately the same (10-30N.mm^{-2}) for both annealed and nitrided alloys which suggests that the dislocation interactions in the nitrided alloys are the

Fig. IX.1.

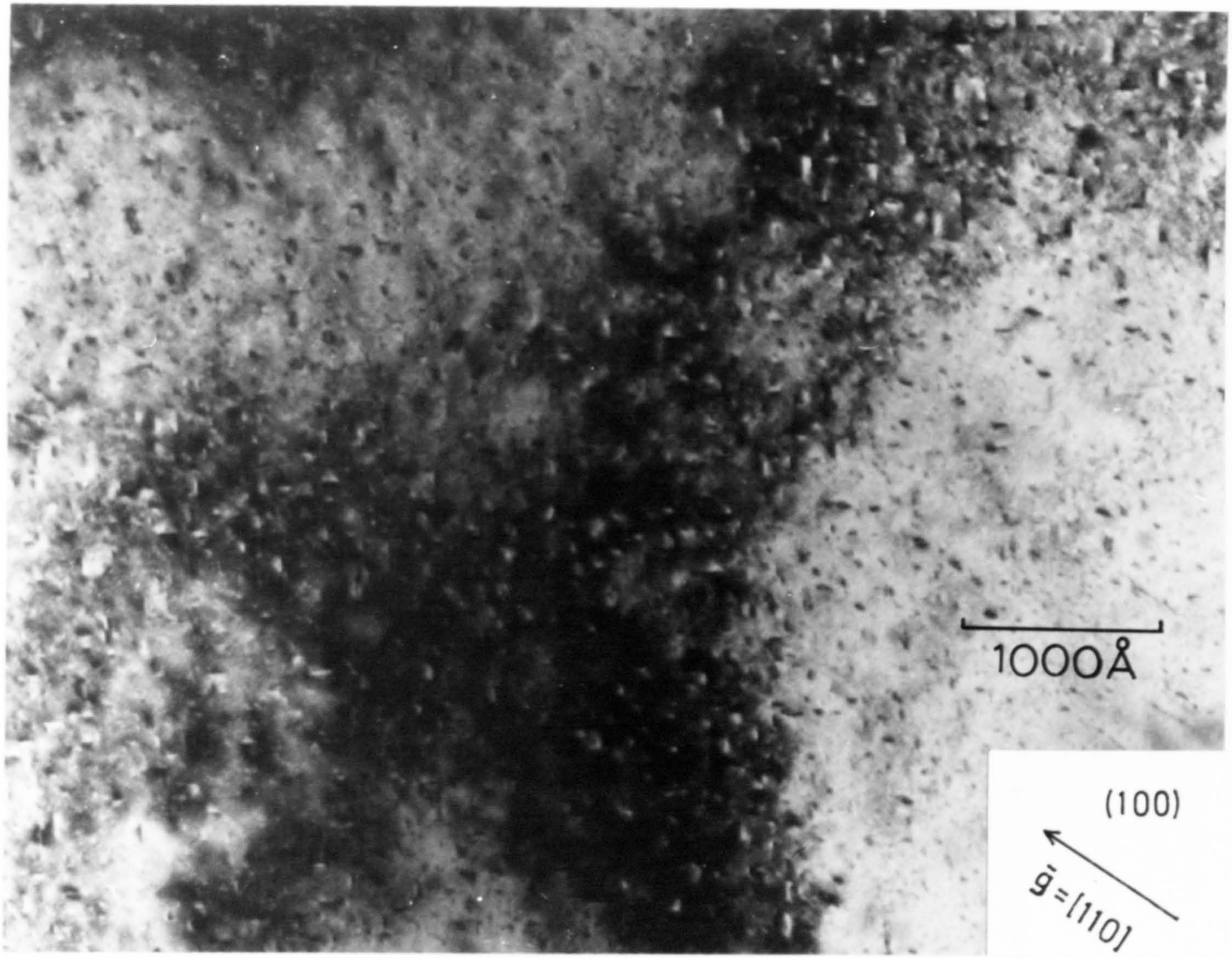

Bright Field Micrograph of Fe-0·2%Ti Nitrided at 580°C in $0{\cdot}5NH_3:99{\cdot}5H_2$

same as those in the annealed alloys. However, the 0.05% proof stress of the annealed alloys is only $57\pm5 N.mm^{-2}$ compared to $550-760 N.mm^{-2}$ for the nitrided alloys. Thus, there is ample evidence for a particle cutting or chemical strengthening mechanism where the resistance to dislocation movement is greatly increased by the need to break strong Ti-N chemical bonds in the zones. On general grounds this mechanism seems the most likely for alloys containing such high densities of very fine particles.

The electron microscopy of the strained nitrided Fe-0.2^{a}/oTi is compatible with slip due to screw dislocations in $\langle 111 \rangle$ directions on $\{110\}$ matrix planes (see Figure IX.2). The dislocation traces are generally long and straight with no evidence of bowing between particles. This is further evidence for a mechanism based on particle shear and chemical strengthening.

Figure IX.3 shows the variation of 0.05% proof stress with nitrogen concentration for Fe-0.2^{a}/oTi nitrided at 500°C. The strength of the nitrided alloys increases only slightly with nitrogen content. Figure IX.4 shows the variation of hardness with nitriding potential for Fe-2^{a}/o, 1^{a}/o and 0.5^{a}/oTi alloys nitrided at 500° and 580°C. The hardness of the nitrided alloys increases only slightly with nitriding potential but it is known that the modulation period (λ_m) and therefore the inter-particle spacing is approximately constant (see Chapter VII) for all nitriding potentials at 580°C. The increase in hardness must be due to "excess nitrogen" in the zones (see Chapter VI) and since this nitrogen is only weakly bonded in the zones their strength is only slightly increased. The hardnesses of the nitrided alloys extrapolated to zero nitriding potential are close to

Fig. IX.2.

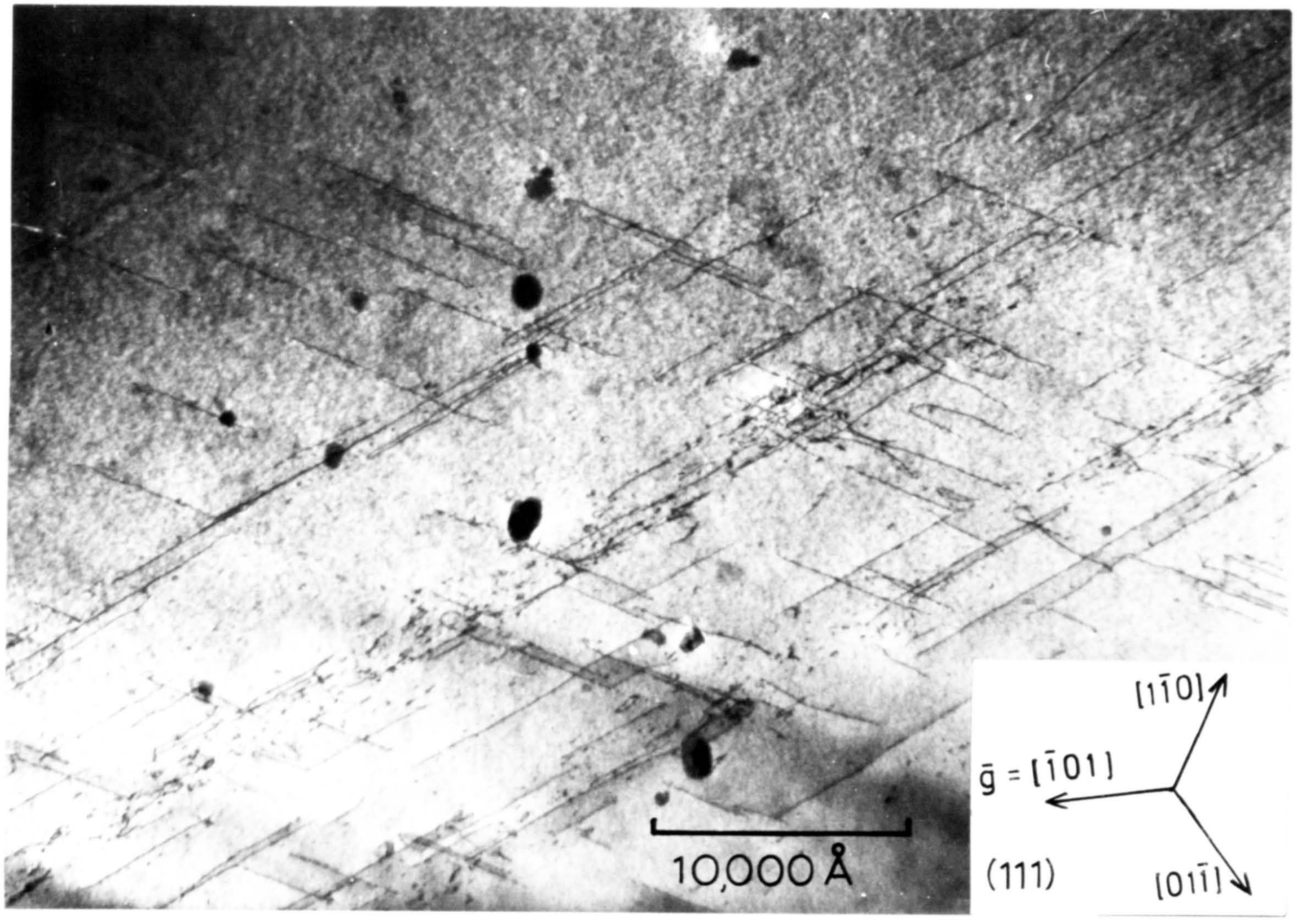

Bright Field Micrograph of Fe−0·2% Ti Nitrided at 500°C in $1NH_3 : 99H_2$ and Strained to 0·25%

Fig. IX.3.

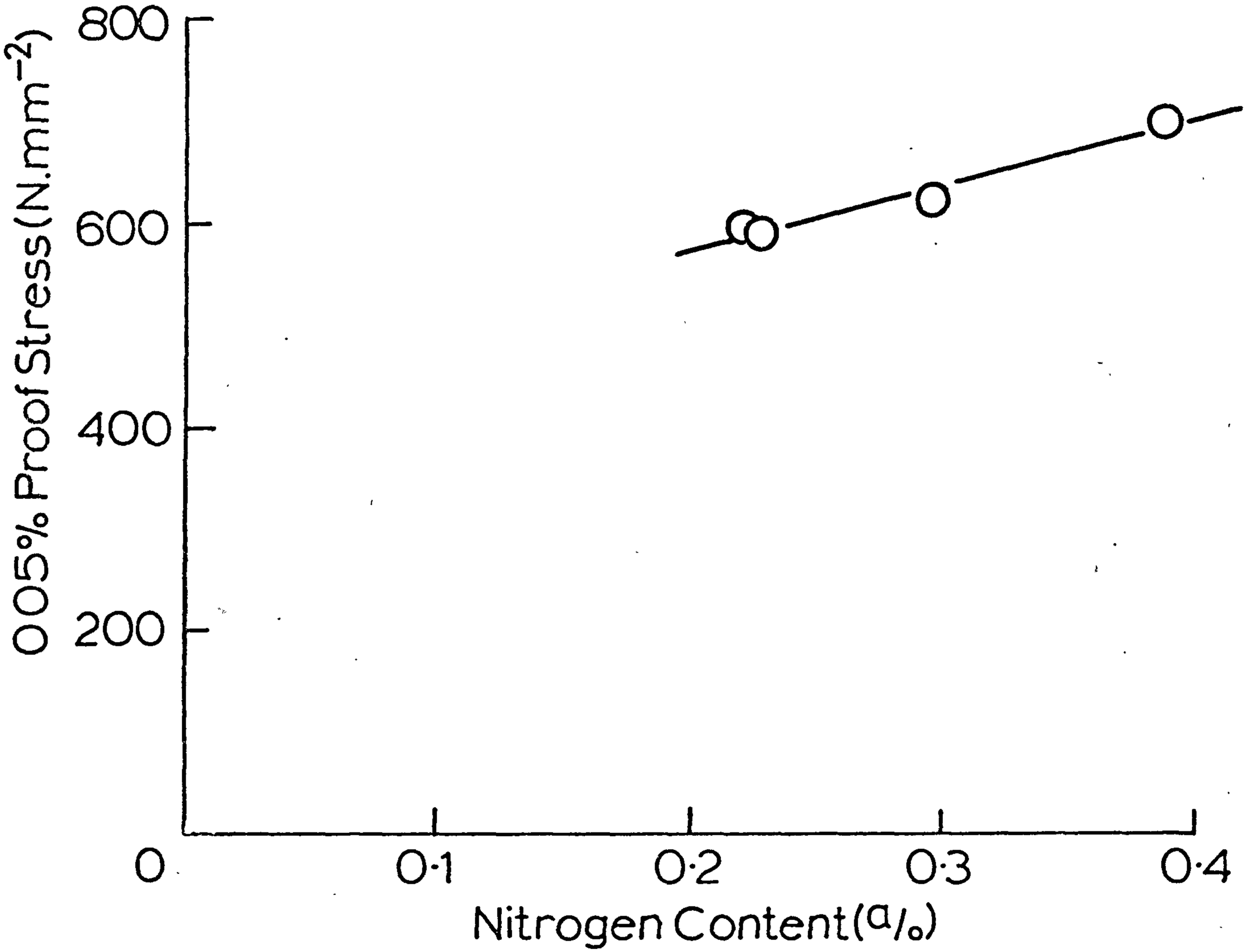

Variation of 0·05% Proof Stress with Nitrogen Content for Fe–0·2%Ti Nitrided at 500°C

Fig. IX.4.

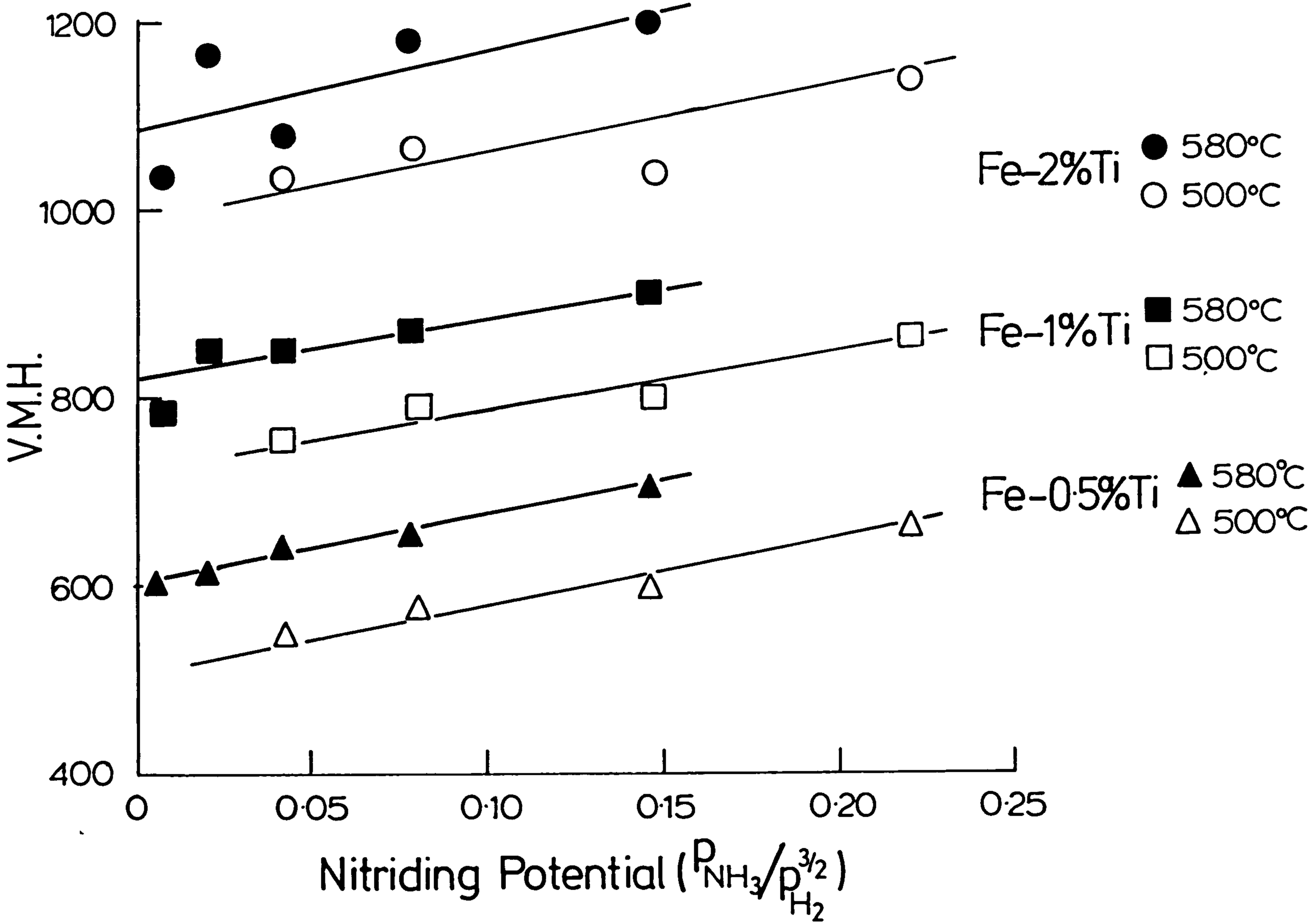

Variation of Hardness with Nitriding Potential for Fe-Ti Alloys

those of the hydrogen-reduced alloys, which might be expected, since in both cases the limiting composition of the zones is the same (Fe_2TiN).

In Figure IX.4 it can be seen that the alloys nitrided at 580°C are harder than those nitrided at 500°C. Also the 0.05% proof stress of Fe-0.2^a/oTi nitrided in $0.5NH_3:99.5H_2$ at 580°C is 760N.mm^{-2} compared to 550N.mm^{-2} for Fe-0.2^a/oTi nitrided in $2NH_3:98H_2$ at 500°C even though the nitrogen concentrations in both alloys are the same. Figure IX.5 shows the variation of hardness with nitriding temperature for Fe-2^a/o, 1^a/o and 0.5^a/oTi nitrided in atmospheres calculated to be in equilibrium with the same concentration of nitrogen in solution in pure iron (0.17^a/oN) at each temperature. Although for the nitriding conditions used (e.g. $13NH_3:87H_2$ at 520°C) the nitrogen concentration in the alloys is decreasing, with increasing temperature the hardness increases in the temperature range examined. However at 750°C the hardnesses of nitrided Fe-2^a/o, 1^a/o and 0.5^a/oTi are only 750, 580 and 450 V.M.H. respectively. The increasing strength of nitrided Fe-Ti alloys with temperature between 480 and 650°C may possibly be explained in terms of a particle shear mechanism. The work required for a dislocation to cut through a particle depends on the coherency strain between the particle and the matrix and this increases with particle thickness. With particle coarsening i.e. above a critical particle size and inter-particle spacing the mechanism for dislocation movement may change from particle shearing to an Orowan looping. This might account for the large decrease in hardness between 650 and 750°C. Certainly in alloys nitrided at 650 and 750°C there is evidence of TiN precipitation and individual zones or precipitates can be resolved (see Section VII.1.).

Fig. IX. 5.

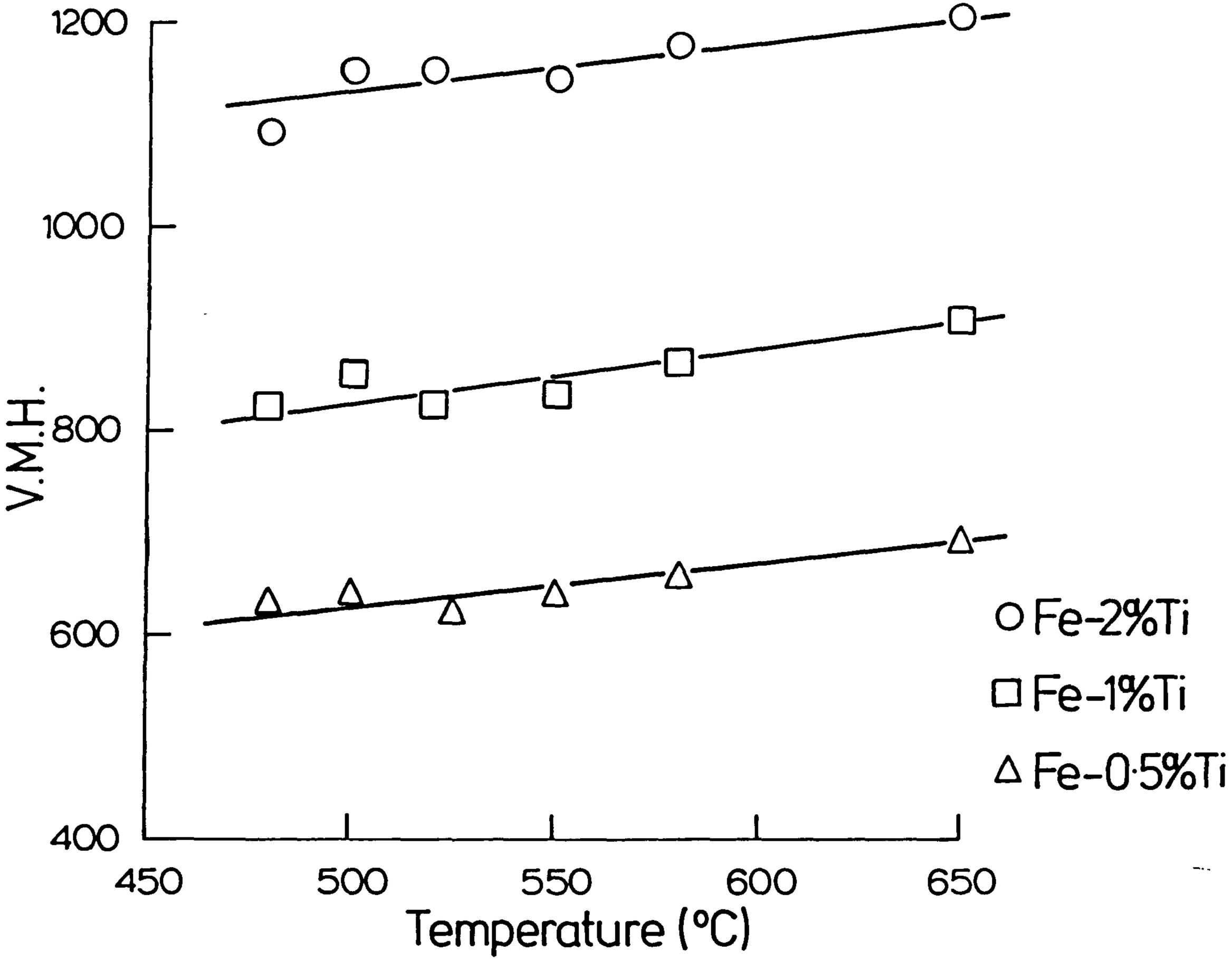

Variation of Hardness with Nitriding Temperature for Fe-Ti Alloys

IX.3. Conclusions

(i) The strengthening mechanism for Fe-Ti alloys nitrided at 450-650°C is one of particle shear and is consistent with the proposed structure consisting of a dense oriented and periodic array of very finely dispersed disc-shaped Ti-N clusters.

(ii) The zone density in Fe-Ti alloys remains constant with increasing nitriding potential at a given temperature and the strength of each zone increases only slightly because the "excess nitrogen" is weakly bonded in the zones.

(iii) The strength of Fe-Ti alloys increases with nitriding temperature between 480 and 650°C. The increase in strength is unexplained.

Chapter X

THE NITRIDING BEHAVIOUR OF Fe-Mo ALLOYS

X.1. Introduction

Much work has already been carried out on the nitriding of Fe-Mo alloys (see Chapter II) to determine the nitriding kinetics, the zone solvuses and the zone structure. Nothing has so far been reported on the variation of nitrogen content with nitriding conditions or on the X-ray diffuse scattering effects. In the present investigation such information for nitrided Fe-Ti alloys has been useful in determining the structure and morphology of the zones and it was thought that similar information for Fe-Mo alloys was essential particularly for the eventual comparison of the Fe-Ti-N and Fe-Mo-N systems with Fe-Mo-Ti-N.

X.2. The Morphology of Nitrided Fe-Mo Alloys

Figure X.1(a) shows the electron microstructure of Fe-3^{a}/oMo nitrided at 500^{o}C in 12NH_3:88H_2. It is identical with that previously observed by Driver (1973) and consists of a dense array of very thin disc-shaped clusters about 150$\mathring{A}$ in diameter. The diffraction patterns (see Figure X.1(b)) are the same as previously observed, showing well-defined sharp continuous streaking along $\langle 100 \rangle$ matrix directions.

Fig. X.1.

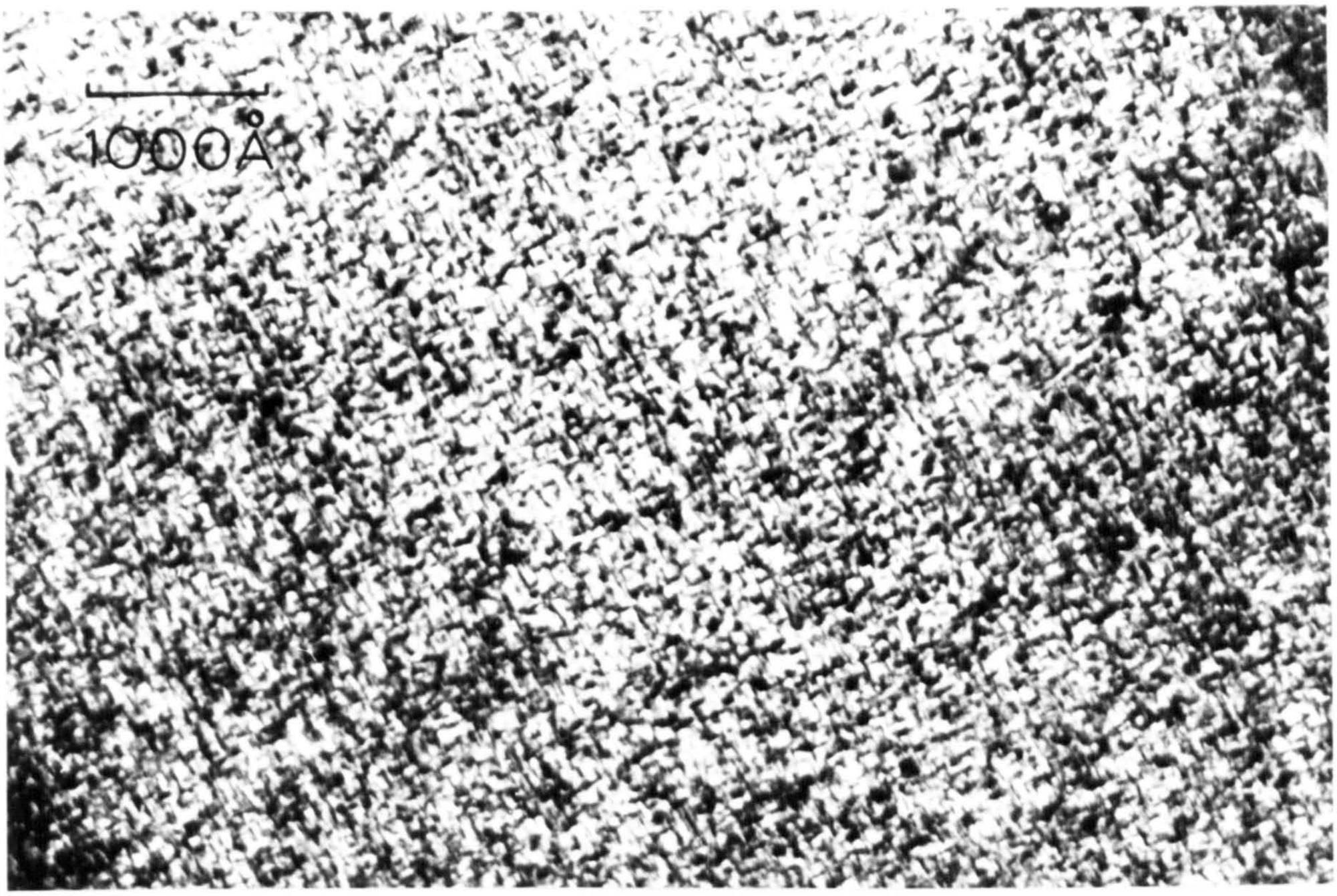

(a)

(b)

(a) Bright Field Micrograph of Fe-3% Mo Nitrided at 500°C in 12 NH_3 :88 H_2

(b) Electron Diffraction Pattern for the Area Shown in (a). <100> zone

Figure X.2 shows an X-ray powder photograph of Fe-3^{a}/oMo nitrided under the same conditions as the alloy of Figure X.1. Diffuse scattering is observed on the high-angle side of all the Bragg reflections. This appears as well-defined side bands for the $\{110\}$, $\{200\}$ and $\{220\}$ and the modulation period, $\lambda_m = 100 \pm 20$Å, is the same for all three side-bands within experimental error. Figure X.3 shows a diffractometer trace of the $\{200\}$ reflection, from which $\lambda_m = 110 \pm 20$Å. The similarity of these X-ray diffuse scattering effects with those observed for nitrided Fe-Ti alloys implies that the morphology of the two alloys is similar i.e. they both consist of domains of periodic or pseudo-periodic arrays of plate-like G.P. zones. However, the side bands for the nitrided Fe-3^{a}/oMo are more intense relative to the main Bragg peak and less diffuse than those observed for Fe-Ti alloys. This implies (De Fontaine, 1966) that the plate-like zones in the Fe-Mo alloys are thicker than in nitrided Fe-Ti; there is also a scattering factor (f) contribution (since, $f_{Mo} > f_{Fe}$). Both the electron micrographs and the diffuse X-ray scattering suggest that the structure of the nitrided Fe-Mo alloys is coarser than that of Fe-Ti.

X.3. The Variation of Nitrogen Content of Fe-Mo Alloys with Nitriding Potential at 580°C

The nitrogen concentration of Fe-Mo alloys during nitriding at 580°C as determined by weight gain measurements is shown in Figure X.4 as a function of nitriding potential. The measurements were carried out on thin foils (~0.1mm thick) nitrided for the minimum time to obtain full saturation without heterogeneous precipitation. The

Fig. X. 2.

X-ray Powder Photograph of Fe-3%Mo Nitrided at 500°C in $12NH_3:88H_2$ ($Fe K\alpha$ radiation)

Fig. X.3.

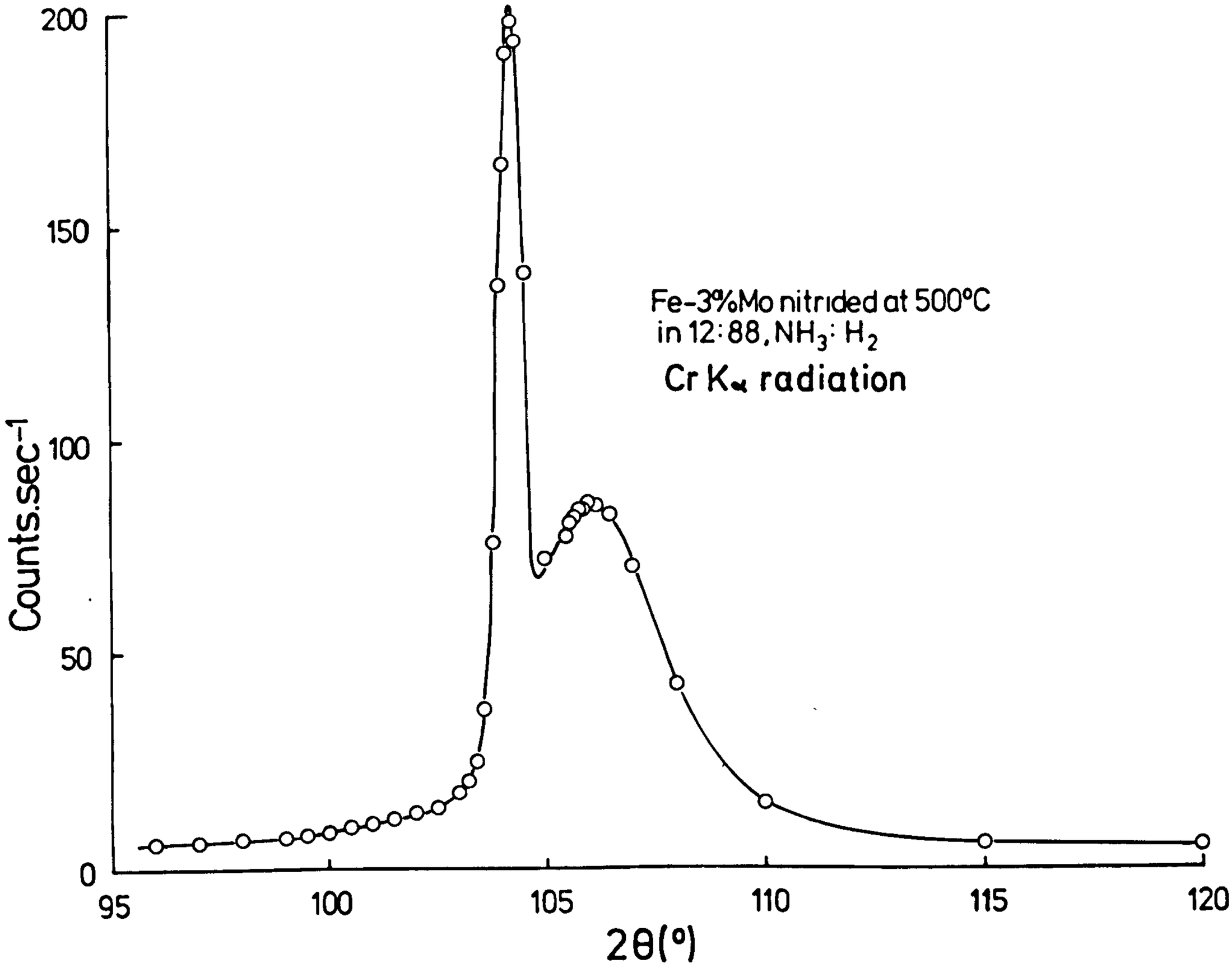

X-ray Diffraction Profile of {200} Reflection

Fig. X. 4.

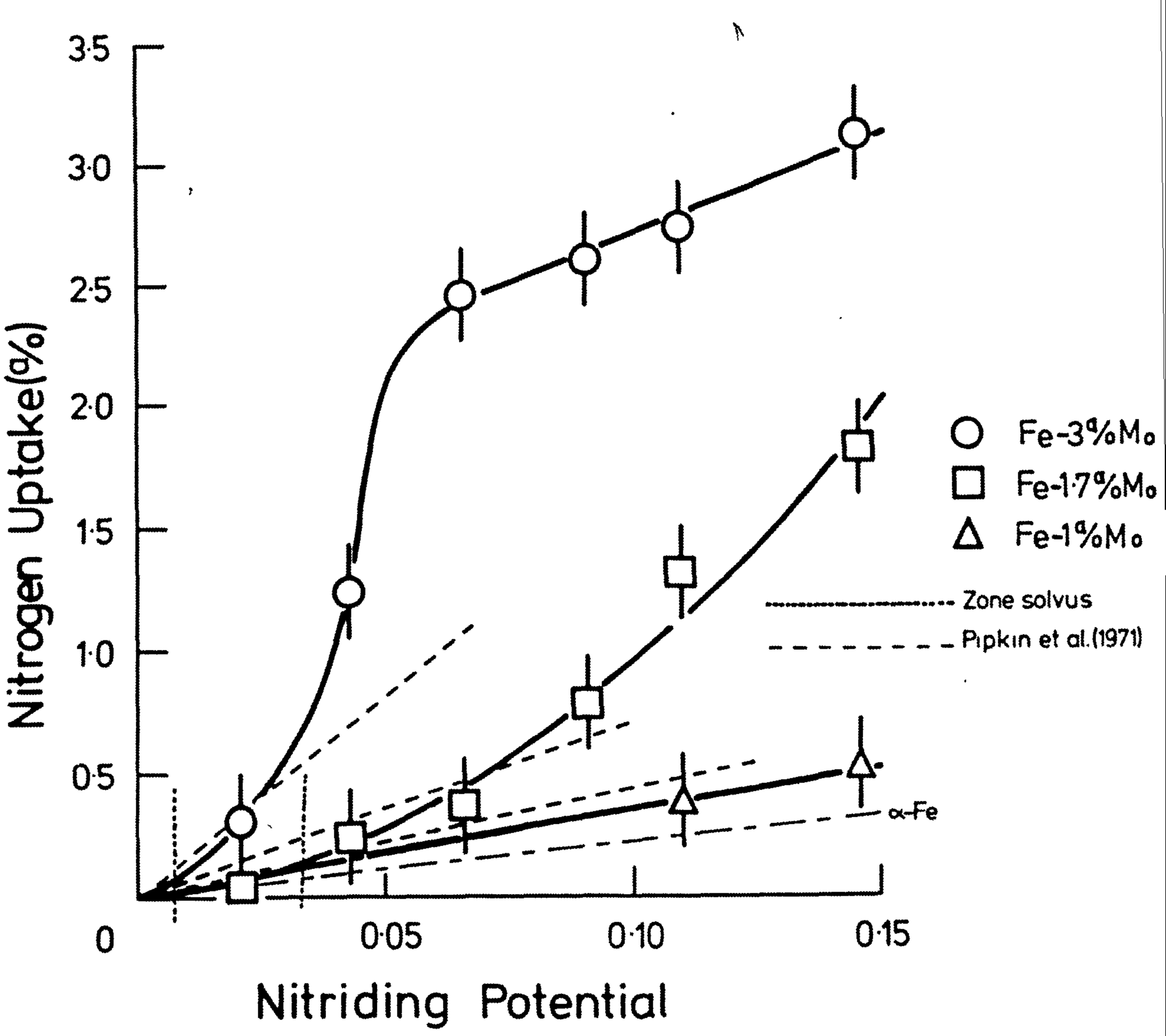
Nitrogen Uptake(%)
3·5
3·0
2·5
2·0
1·5
1·0
0·5
0
0·05
0·10
0·15
Nitriding Potential
Fe-3%Mo
Fe-1·7%Mo
Fe-1%Mo
Zone solvus
Pipkin et al.(1971)
α-Fe

nitrogen concentration predicted for pure iron under similar conditions is also shown as well as that for the same Fe-Mo alloys by extrapolation of the data of Pipkin et al (1971), (see Chapter II). Within experimental error and the errors incurred by extrapolation, the results for Fe-1^a/oMo agree with those derived from equations II.2 and II.3. Hayes (1972) also observed no zone solvus for this alloy over the range of nitriding potentials used and Driver (1973) observed no evidence of zone formation in this alloy. At low molybdenum and nitrogen levels $\log f_N^{Mo}$ is proportional to the molybdenum concentration (Pipkin et al, 1971) but at higher concentrations of both solutes the relationship might be expected to contain second order terms since Henry's Law is less likely to apply. It can be seen in Figure X.4 that the deviation from the results predicted by linear extrapolation increases with both molybdenum and nitrogen concentrations. Also, the deviations first occur close to the zone solvuses determined by Hayes (1972) and so are probably due to zone formation. Although Hayes determined the zone solvus for 1.7^a/oMo, Driver has shown that the molybdenum concentration is close to the critical limit for zone formation and that some precipitation takes place as well as zone formation but in Fe-3^a/oMo no precipitation takes place. Zones are formed in Fe-3^a/oMo even at low nitriding potentials. In Figure X.4 the graph for Fe-3^a/oMo can be split into three parts:

(i) at nitrogen concentrations below the zone solvus where solute atom clustering does not take place;

(ii) a transition region above the zone solvus where mixed substitutional-interstitial solute atom clusters are formed and where the nitrogen concentration increases rapidly with nitriding potential;

(iii) high nitrogen concentrations ($>1.6^a$/o) where the nitrogen content of the zones increases with nitriding potential.

Chapter XI

HOMOGENEOUS PRECIPITATION IN NITRIDED Fe-1.4^{a}/oMo-1.1^{a}/oTi

XI.1. The Morphology of Nitrided Fe-1.4^{a}/oMo-1.1^{a}/oTi

The electron microstructures of nitrided Fe-1.4^{a}/oMo-1.1^{a}/oTi are very similar to those observed for nitrided Fe-Ti alloys (see Figure XI.1) and show the characteristic tweed patterns. Also, the diffuse electron scattering effects have the same features as for nitrided Fe-Ti alloys. It is therefore likely that the morphology of the nitrided Fe-1.4^{a}/oMo-1.1^{a}/oTi alloy and the elastic interactions in the matrix are very similar to those of those Fe-Ti alloys where the zone density is high. That is, Fe-1.4^{a}/oMo-1.1^{a}/oTi consists of a dense, finely dispersed array of very thin plate-like zones which is ordered or partially ordered.

The X-ray diffuse scattering effects observed for nitrided Fe-1.4^{a}/oMo-1.0^{a}/oTi are also similar to those observed for nitrided Fe-Mo and Fe-Ti alloys. However, the relative intensities of side-bands and Bragg reflections for the Fe-Mo-Ti-N alloys are more like those observed for Fe-Ti-N alloys than for Fe-Mo-N alloys (see Figure XI.2). They are generally weak and diffuse. From the side-band separation when the alloy is nitrided at 500°C in $17NH_3:83H_2$, $\lambda_m = 63\pm15$Å which compares closely with the 55Å for Fe-1^{a}/oTi nitrided under the same conditions and is much smaller than that for Fe-3^{a}/oMo nitrided at

Fig. IX.1.

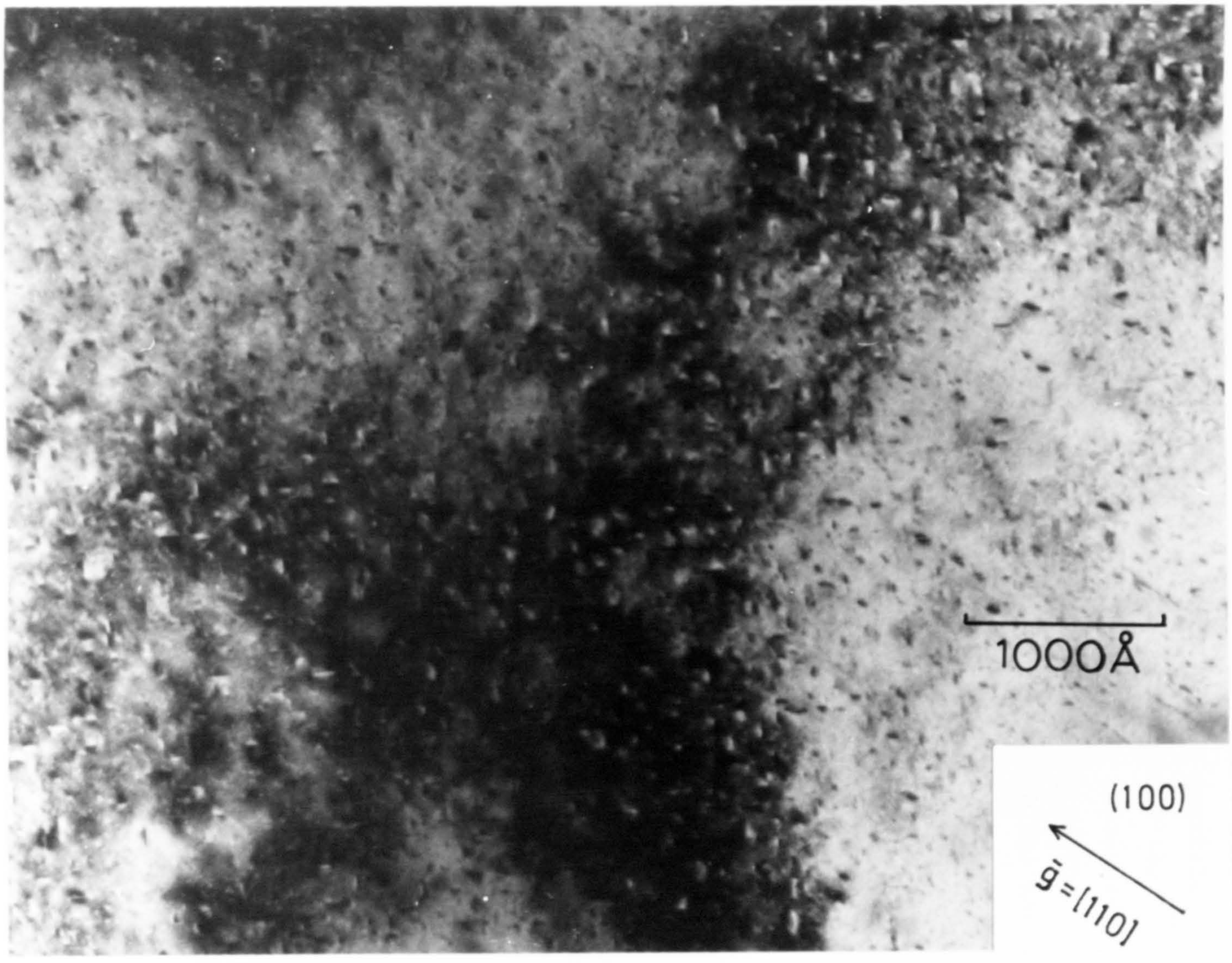

Bright Field Micrograph of Fe-0·2%Ti Nitrided at 580°C in $0{\cdot}5NH_3:99{\cdot}5H_2$

Fig. XI.1.

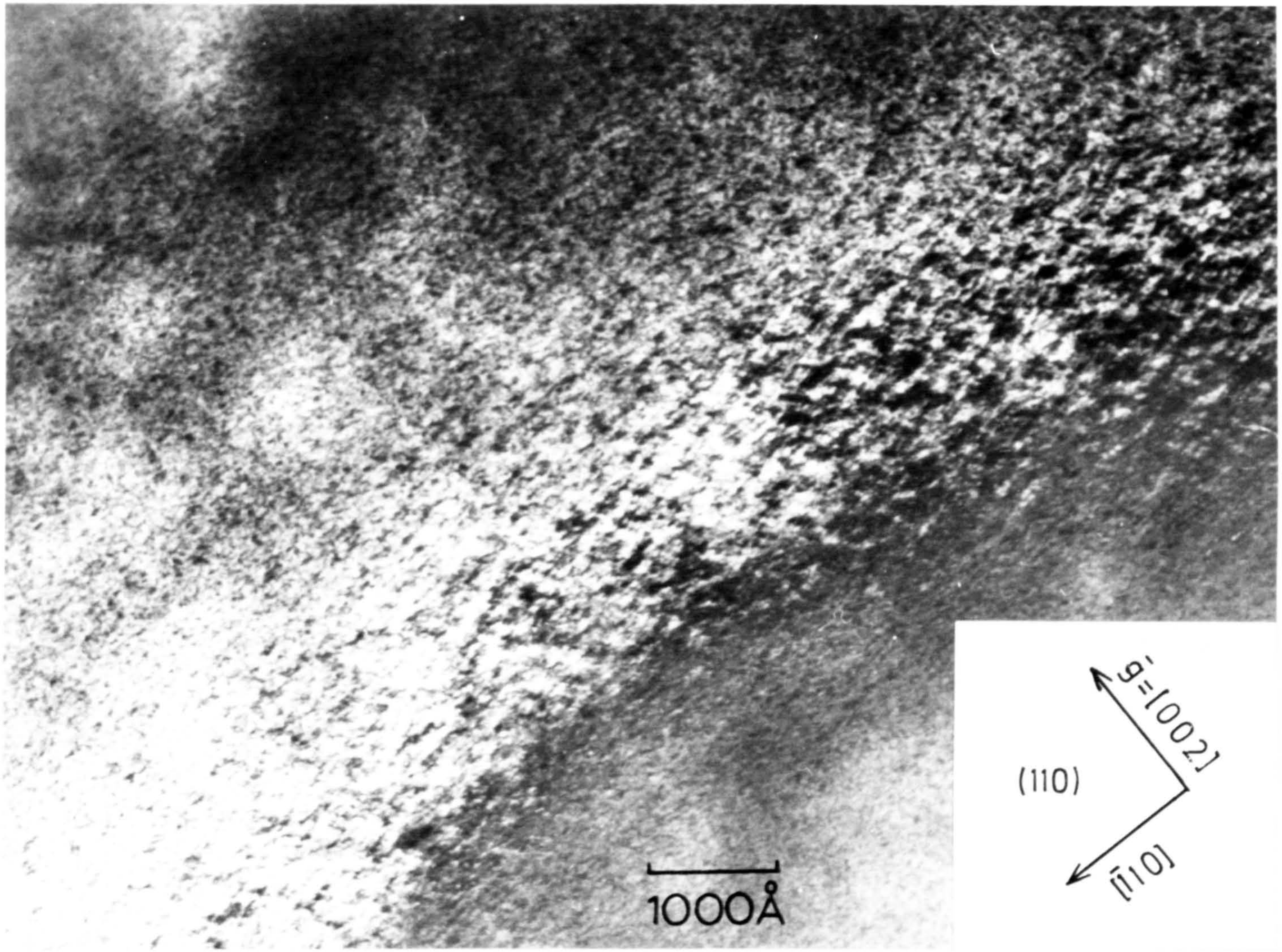

Bright Field Micrograph of Fe-1·4%Mo-1%Ti Nitrided at 580°C in $5NH_3:95H_2$

Fig. XI.2.

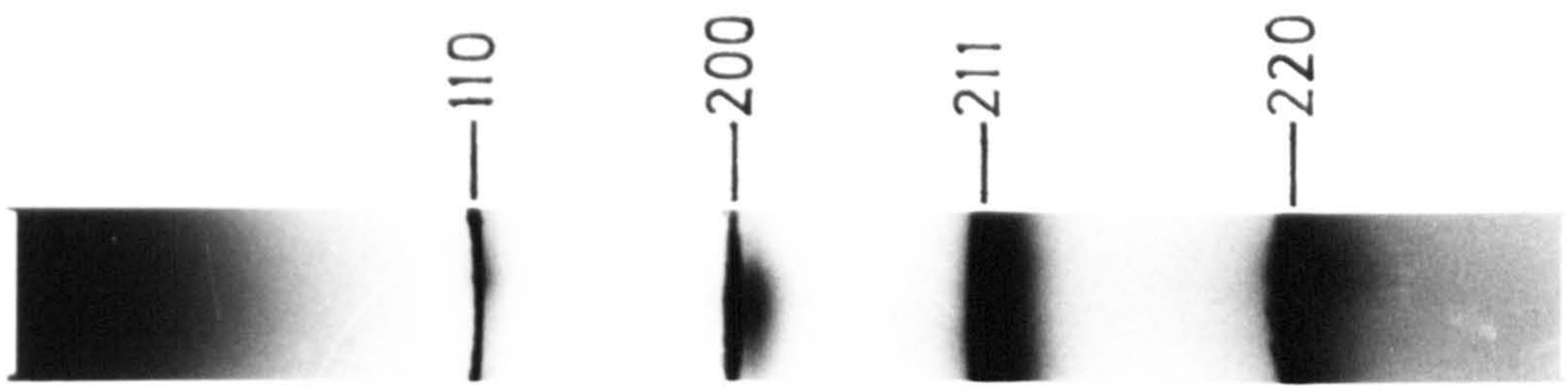

X-ray Powder Photograph of Fe-1 4%Mo-1%Ti
Nitrided at 500°C in $17NH_3:83H_2$
(FeK_α radiation)

500°C (110±20Å) even though the latter has a high total substitutional solute content. It seems that the morphology of nitrided Fe-1.4^{a}/oMo-1.1^{a}/oTi is determined primarily by the titanium present - probably a result of the much greater affinity of nitrogen for titanium than molybdenum.

The close similarity of electron microstructures and the electron and X-ray diffuse scattering effects for nitrided Fe-Ti and Fe-Mo-Ti suggests that the zones in both alloys have identical morphologies and structures in which molybdenum and titanium atoms are mutually replaceable.

XI.2. The Nitrogen Uptake of Fe-1.4^{a}/oMo-1.1^{a}/oTi

Figure XI.3 shows the variation of nitrogen concentration as a function of nitriding potential for Fe-1.4^{a}/oMo-1.1^{a}/oTi nitrided at 580°C. The uptake of nitrogen is accompanied by an increase in hardness to about 1050 V.M.H. and an increase in lattice parameter. This evidence together with the observed electron microstructures show that mixed substitutional-interstitial clusters are formed. Also shown in Figure XI.3 is the curve for the sum of the estimated nitrogen uptake for Fe-1.4^{a}/oMo and for Fe-1.03^{a}/oTi derived from the graphs shown in Figures VII.2 and X.4. This curve lies at lower nitrogen levels and is approximately parallel to the curve drawn through the experimental data. The nitrogen concentration of Fe-1.4^{a}/oMo-1.1^{a}/oTi cannot therefore be explained simply in terms of a summation of the individual effects of titanium and molybdenum in the appropriate binary alloys. Zones are not formed in

Fig. XI.3.

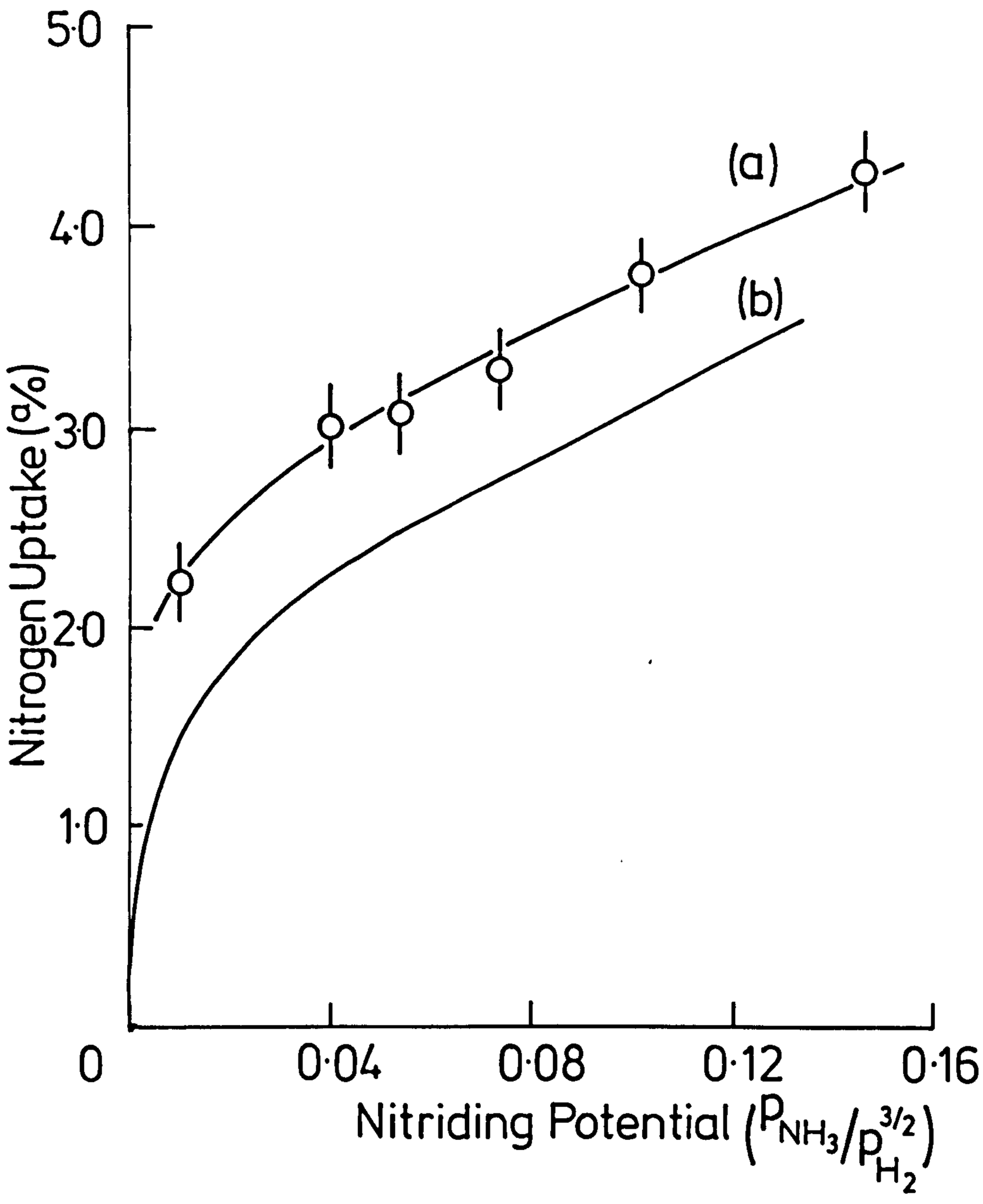

Variation of Nitrogen Uptake with Nitriding Potential for Fe-1·4%Mo-1%Ti

(a) Determined by Experiment

(b) Computed from Data for Nitrided Fe-Mo and Fe-Ti Alloys

Fe-Mo alloys with such a low molybdenum concentration (Driver, 1973). The higher nitrogen concentration must therefore be due to formation of nitride zones containing both molybdenum and titanium. Further evidence for this, is the high hardness of nitrided Fe-1.4a/oMo-1.1a/oTi (1050 V.M.H.) compared with Fe-1a/oTi (850 V.M.H.) nitrided under similar conditions.

The lattice parameters of Fe-1.4a/oMo-1.1a/oTi nitrided and then hydrogen-reduced are consistent with the nitrogen contents determined by weight measurements. For example for Fe-1.4a/oMo-1.1a/oTi nitrided in $5NH_3:95H_2$ at 580°C and then hydrogen reduced at the same temperature for 26 hours the lattice parameter is 2.884 ($\pm$0.0015)Å. This implies that all the 1.31a/oN (determined by weight gain) is in solid solution if the expansion of the ferrite unit-cell dimensions is 0.006Å/a/oN. From results obtained for Fe-Ti and Fe-Mo alloys it might be expected that prolonged hydrogen reduction would remove all "excess nitrogen" and also that associated with the molybdenum atoms, leaving only the nitrogen strongly associated with the 1.1a/o titanium i.e. leaving 1.1a/oN. The higher nitrogen content (1.31a/oN) of the hydrogen reduced alloy can only be explained if some or all of the molybdenum in the alloy is associated with titanium and nitrogen in Ti-Mo-N zones.

A possible structure for the zones in nitrided Fe-Mo-Ti alloys is shown in Figure XI.4. The structure is similar to that for Ti-N zones in nitrided Fe-Ti alloys (see Figure VI.6); it is based on a TiN monolayer as for Fe-Ti alloys but the N atoms in the monolayer may be coordinated by Mo atoms above and below the plane of the monolayer. Each Mo atom is coordinated by at least one N atom in the TiN monolayer. The exact Mo:N and Ti:N

Fig. XI.4.

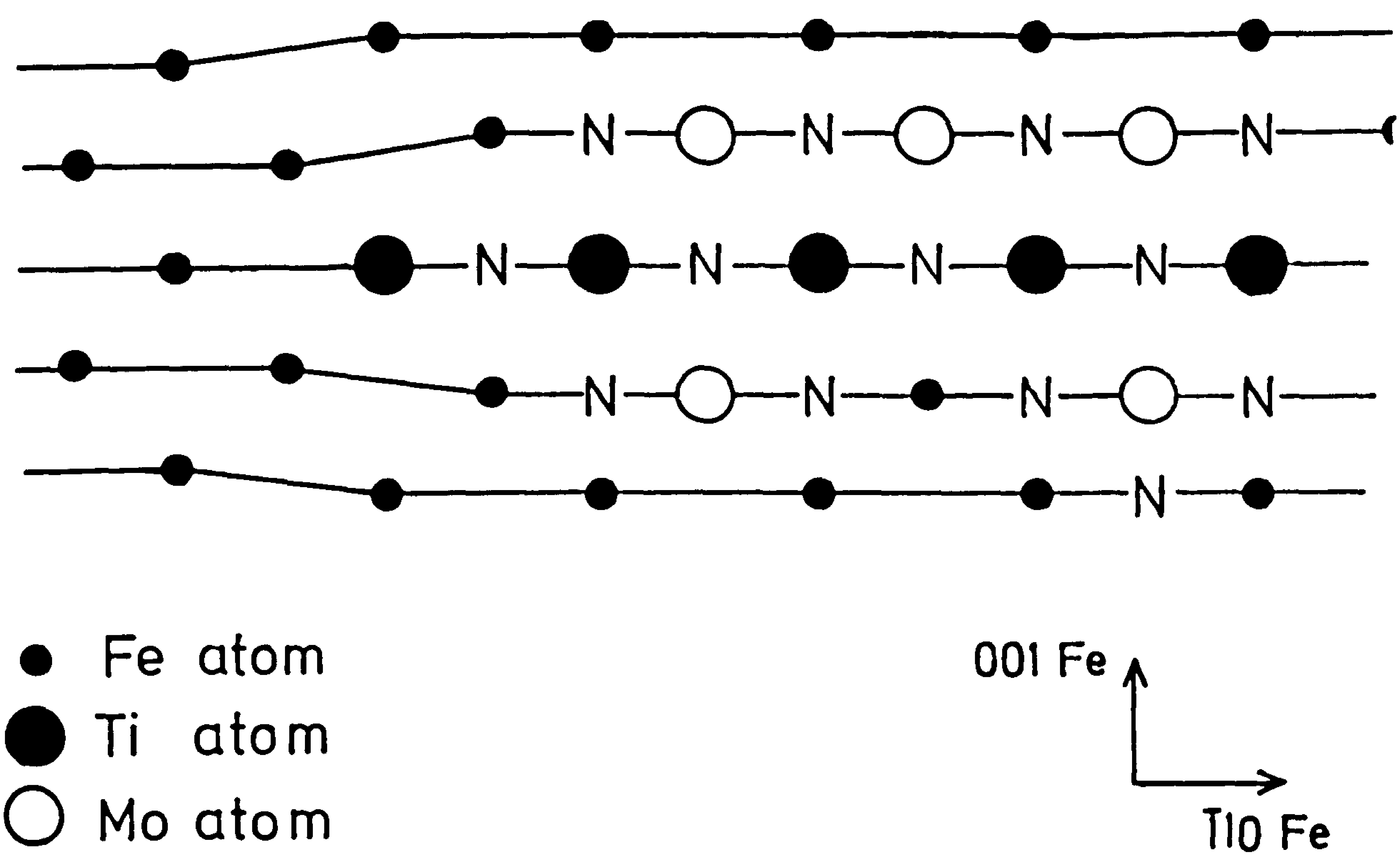

Proposed Model for the Structure of Zones in Nitrided Fe-Mo-Ti Alloys

coordination will be determined by the nitriding conditions and the relative substitutional element concentrations in the alloy.

The activity product $[Ti] \cdot [N]$ necessary for zone formation in nitrided Fe-Ti alloys is extremely small since zones are formed during nitriding at very low nitriding potentials and very low titanium concentrations ($> 0.2^a/o$). It is therefore possible that during nitriding of $Fe-1.4^a/oMo-1.1^a/oTi$ fine Ti-N zones are formed which act as nuclei for the growth of Ti-Mo-N zones. Hydrogen reduction would remove any nitrogen associated with molybdenum atoms but not nitrogen associated with titanium or possibly with titanium and some molybdenum; see Figure XI.4; this would result in the observed high nitrogen content of the hydrogen-reduced alloy.

XI.3. Nitrided and Aged $Fe-1.4^a/oMo-1.1^a/oTi$

The microstructure of $Fe-1.4^a/oMo-1.1^a/oTi$ nitrided at 580^oC in $4NH_3:96H_2$, hydrogen-reduced at the same temperature and then aged in argon at 830^oC for 20hrs is similar to that for $Fe-2^a/oTi$ treated under similar conditions (see Chapter VIII). The microstructure (Figure XI.5) consists of plate-like precipitates about $200\mathring{A}$ diameter lying on $\{100\}$ matrix planes and gives rise to precipitate reflections on electron diffraction patterns occurring in the same position as TiN reflections. The electron diffraction patterns of the aged Fe-Ti-N and Fe-Mo-Ti-N alloys are indistinguishable from each other and suggests that some of the molybdenum of the Ti-Mo-N zones formed transform to a f.c.c. (Ti,Mo)N precipitate on overageing.

Fig. XI. 5.

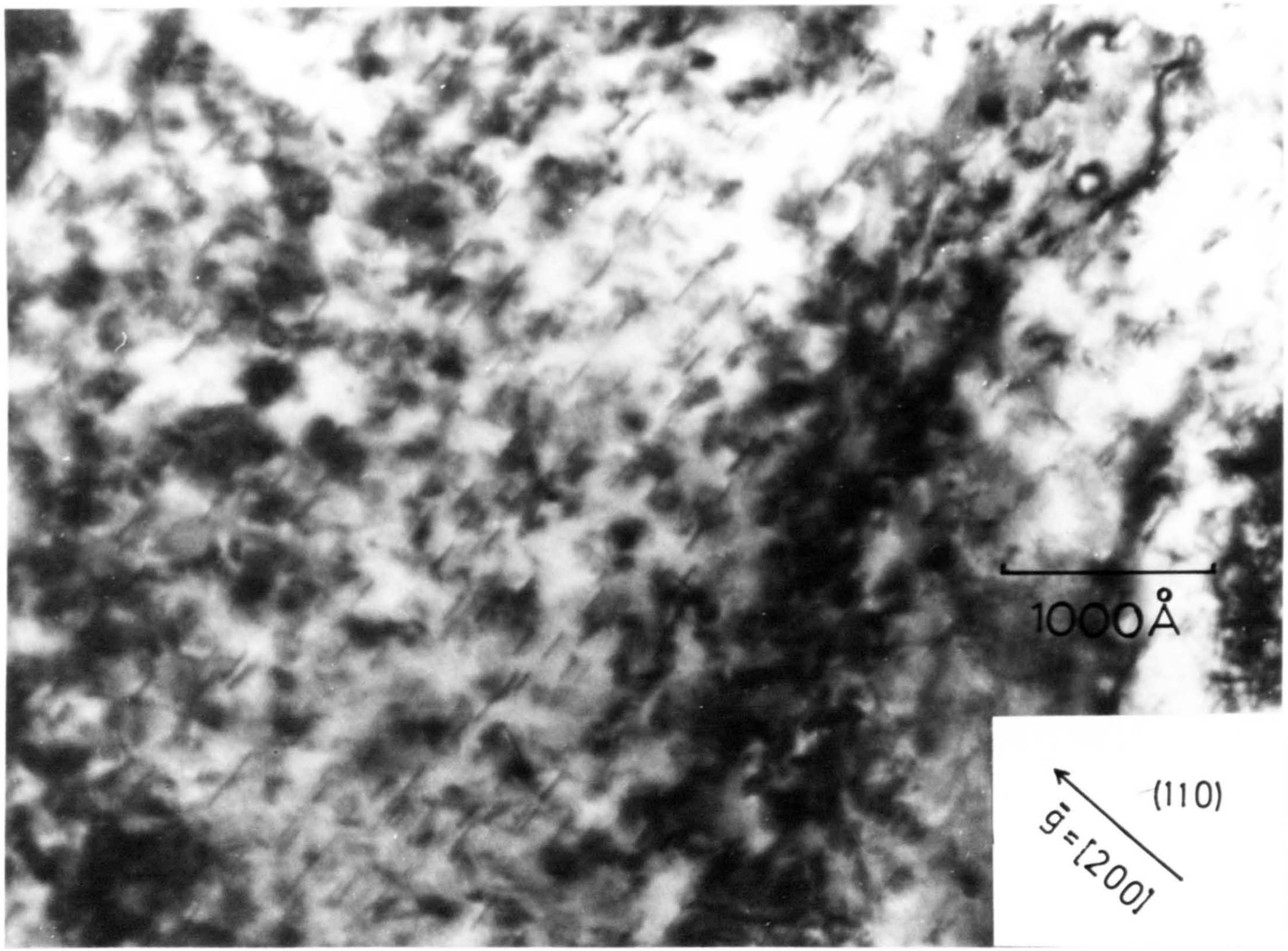

Bright Field Micrograph of Fe-1·4^{a}/$_{o}$Mo-1^{a}/$_{o}$Ti Nitrided at 580°C, Hydrogen Reduced at 580°C and Aged in Argon at 830°C for 20hr..

Chapter XII

THE NITRIDING KINETICS OF Fe-1.4^a/oMo-1.1^a/oTi

XII.1. Results

Figure XII.1 shows the hardness profiles of Fe-1.4^a/oMo-1.1^a/oTi nitrided at 580^{o}C in $4NH_3$:$96H_2$ for various times. Similar profiles were observed for specimens nitrided at 450^o and 500^{o}C. The characteristic features are:

(i) the boundary between the nitrided case and the core is not sharp;

(ii) the hardness of the nitrided subscale increases with nitriding time until it reaches a maximum value;

(iii) the hardness of the core is the same as that of the unnitrided alloy;

(iv) the increase in hardness of the subscale after very short nitriding times is very close to that observed for Fe-1^a/oTi nitrided under similar conditions.

Figure XII.2 shows the change in subscale depth (X) with nitriding time for specimens nitrided at 450^o, 500^o and 580^{o}C; the position of the subscale boundary is defined as that position where the hardness of the alloy is the same as the maximum hardness observed after very short nitriding times e.g. for the alloy nitrided at 580^{o}C this hardness was about 800 V.M.H. Variations of this value did not affect the form of the graphs shown in Figure XII.2. After relatively short nitriding times

Fig. XII.1.

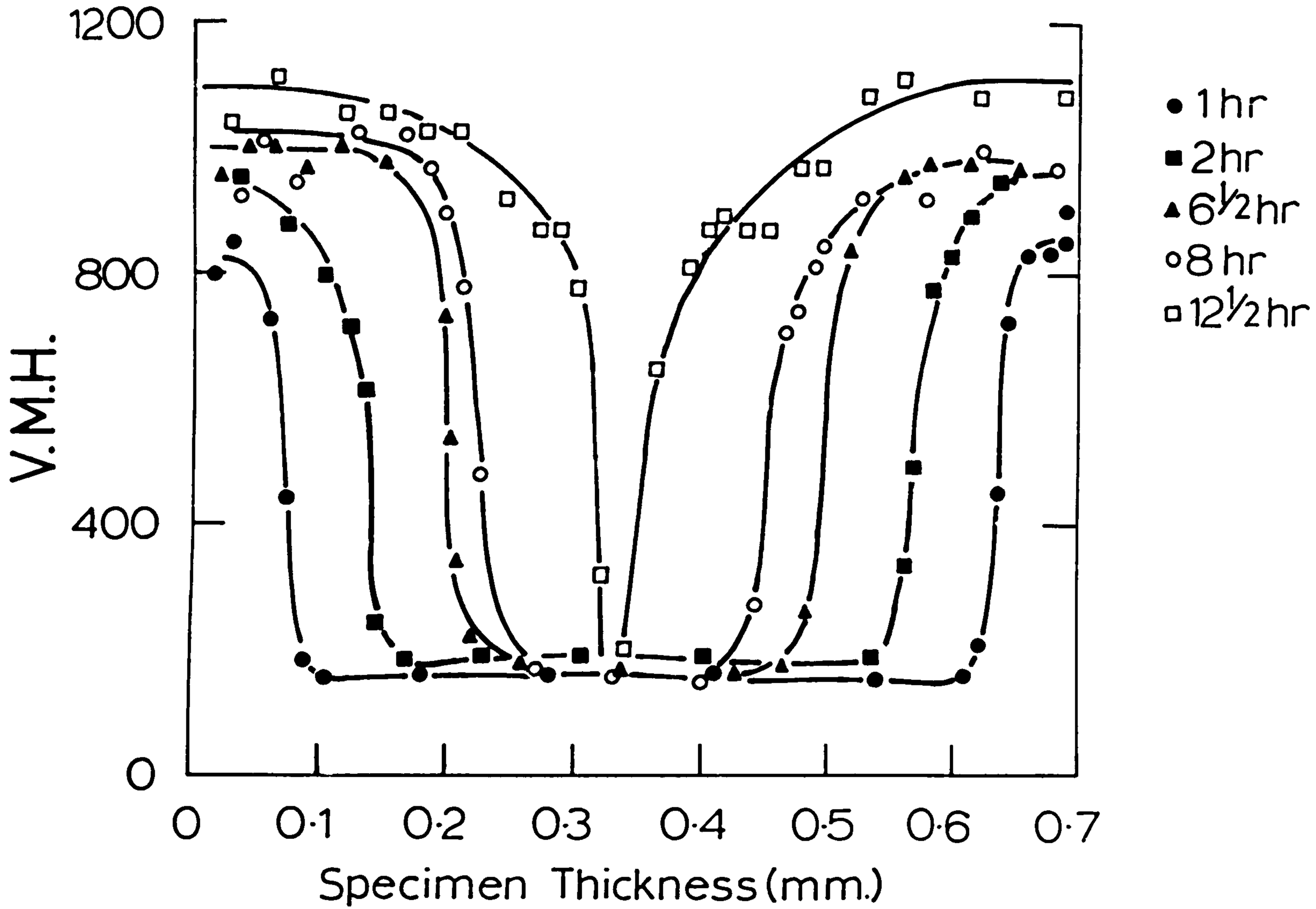

Hardness Profiles of Fe–1·4%Mo–1%Ti Nitrided at 580°C in $4NH_3:96H_2$

Fig. XII.2.

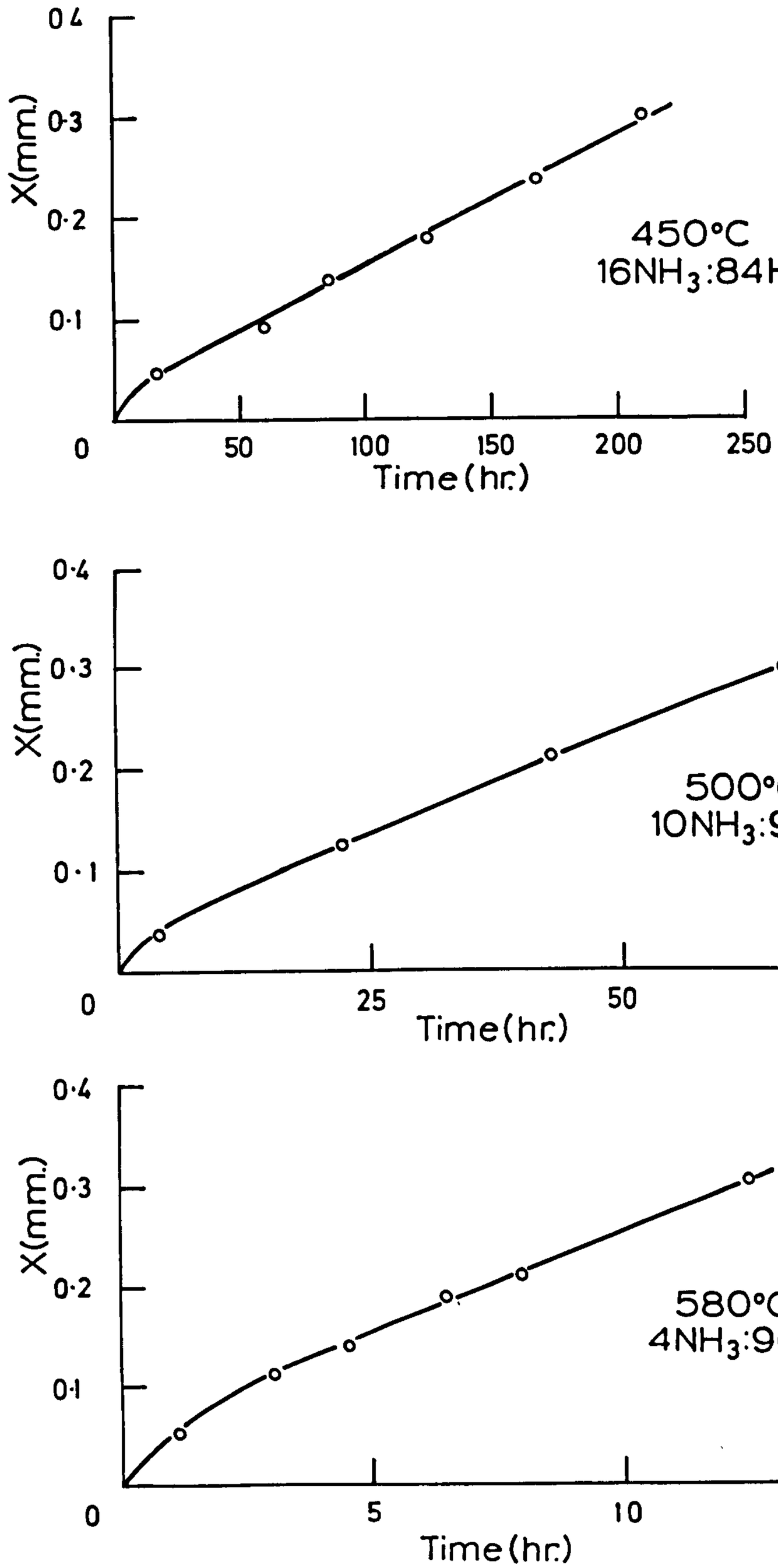

Variation of Subscale Depth (X) with Nitriding Time for Fe-1·4% Mo-1% Ti

the subscale depth (X) varies linearly with nitriding time at all three temperatures. However the shapes of the graphs drawn suggest that the initial rate of subscale advance may be parabolic with time although this cannot be confirmed owing to the limitations of the experimental methods used to determine subscale thickness.

XII.2. Discussion

For most Fe-X-N alloys (including Fe-Ti-N) nitriding occurs by the advance of a sharply-defined hard subscale; the rate of subscale advance is parabolic with time (see Chapter II). However, in Fe-Mo-N alloys nitriding occurs by a gradual build up in hardness across the whole specimen until peak hardness is reached. The hardness profiles in partially nitrided Fe-Mo specimens are dish-shaped.

In Fe-1.4^{a}/oMo-1.1^{a}/oTi at short nitriding times the initial hardness increases and the hardness profiles (see Figure XII.1) are very similar to those observed for Fe-1^{a}/oTi nitrided under similar conditions. It might be inferred therefore that during the initial nitriding period, Ti-N zones are formed in the alloy and that initially molybdenum plays very little part in the solute interactions; it is known that Ti-N zones are formed in ferrite with very low titanium and nitrogen activities (see Chapters VI and IX) whereas relatively high molybdenum and nitrogen activities are required for Mo-N zone formation (see Chapters II and X). Also, Mo-N clustering can not take place independently in alloys with such a low molybdenum concentration ($<1.7^{a}$/o). The increasing hardness of the subscale at longer nitriding

times implies that molybdenum takes part in Mo-Ti-N zone formation at a later stage, increasing the strength of the zones i.e. the Ti-N clusters act as nuclei for growth of Ti-Mo-N zones. These observations are consistent with the model for zones in nitrided Fe-Mo-Ti alloys proposed in Chapter XI where the zone structure is based on a TiN monolayer (see Figure XI.4).

For Fe-Ti alloys nitrided at 580°C Jack et al, (1971) observed a short incubation period (about 3 hours) before subscale advance began at a parabolic rate with time. No incubation period is observed for Fe-Mo-Ti alloys; the initial rate of subscale advance is high and then levels off to a linear rate. After allowing for the incubation period and different nitriding potentials the data for Fe-1^{a}/oTi (Jack et al, 1971) is almost coincident with the data for Fe-Mo-Ti for nitriding times up to about 12 hours. Because of this, it might be implied that the rate of subscale advance in Fe-Mo-Ti alloys is also parabolic with time. However there is insufficient data for long nitriding times to confirm this suggestion, owing to the thickness of material available for testing (<1mm thick).

Chapter XIII

GENERAL DISCUSSION

As in other Fe-X-N systems, streaking on electron diffraction patterns shows that the zones in Fe-Ti-N alloys are very thin plates. Nitriding and hydrogen reduction experiments show that the N:Ti atom ratio in the zones can vary between 1 and 3. The most probable structure for the zones is shown in Figure VI.6. The composition of the zones varies between Fe_2TiN and Fe_4TiN_3 depending on the nitriding conditions. The titanium and nitrogen atoms occupy the same types of site as in the equivalent random solid solution and the zones fit into the ferrite matrix on $\{100\}$ planes without causing any structural discontinuity.

The formation of metastable zones in Fe-Ti-N alloys is only part of the precipitation sequence of f.c.c. TiN from the supersaturated solution. Only when Fe-Ti alloys are nitrided at high temperatures ($>650^{o}C$) do diffuse TiN precipitate spots begin to appear on electron diffraction patterns. Results of ageing experiments (Chapter VIII) show that although well-defined precipitate spots are observed on electron diffraction patterns of a nitrided and aged alloy, the lattice parameter of the matrix determined by X-rays is still much higher than that of ferrite and so the distinction between precipitates and clusters can not be as unequivocal - at least in this limited region of the transformation process - as suggested by Krawitz and Sinclair (1975). It may be implied that

the matrix and precipitates diffract electrons separately but diffract X-rays coherently. This difference in behaviour might be due to the fact that the wavelength of electrons is smaller than the wavelength of X-rays - about 0.04Å for electrons compared to about 1.4Å for X-rays.

When Ti-N clusters form in nitrided Fe-Ti alloys strain energy is minimised if they occur as plates and grow in the plane of the plates. There is however tetragonal distortion of the matrix and maximum strain is perpendicular to the plates. Because of this strain and the high density of zones, neighbouring zones might be expected to be aligned edge to face in the same way that precipitates in CoPt arrange themselves in a pseudo-periodic array to maximise the number of edge-face configurations (Eurin et al, 1973). The pseudo-periodic arrays in Fe-Ti-N alloys give rise to strain modulations throughout the material. These strain modulations and the pseudo-periodic array of zones give rise to the "tweed" morphologies observed in electron micrographs and the diffuse scattering effects on X-ray and electron diffraction patterns. The very strong interaction between titanium and nitrogen atoms accounts for the structure of the zones and their characteristic morphology. It follows, therefore, that the high mutual affinity of titanium and nitrogen also accounts for the stability of this morphology and its resistance to overageing at high temperatures.

The morphology of nitrided Fe-1.4$^{a}/_{o}$Mo-1.1$^{a}/_{o}$Ti is determined chiefly by the titanium in the alloy and is very similar to that of nitrided Fe-1$^{a}/_{o}$Ti. This reflects the much stronger interaction of titanium and nitrogen compared with molybdenum and nitrogen. However the molybdenum is incorporated as Ti-Mo-N clusters and contributes to the strengthening.

REFERENCES

Abrahamson, E.P. & Lopata, S.L., 1966, Trans. A.I.M.E., 236, 76.

Austin, J.B. & Ricketts, R.L., 1939, Trans. A.I.M.E., 135, 396.

Baen, S.R. & Duwez, P., 1951, Trans. A.I.M.E., 191, 331.

Balli, D. & Zakharova, M., 1954, Doklady Akad. Nauk. S.S.S.R., 96, 453, 737.

Biedermann, E., 1960, Acta Cryst., 13, 650.

Booker, G.R., Norbury, J. & Sutton, A.L., 1957, J.I.S.I., 187, 205.

Bowman, F.E., Parke, R.M. & Herzig, A.J., 1943, Trans. Am. Soc. Metals, 31, 487.

Brenner, S.S. & Goodman, S.R., 1971, Scripta Met., 5, 865.

Brown, L.M. & Ham, R.K., 1971, "Strengthening Methods in Crystals" (edited by Kelly, A. & Nicholson, R.B.), Amsterdam; Elsevier, p. 9.

Brown, L.M., Cook, R.H., Ham, R.K. & Purdy, G.R., 1973, Scripta Met., 7, 815.

Chen, F.P.H., 1965, Ph.D. Thesis, Rensselaer Polytechnic Institute, Troy, New York.

Corney, N.G. & Turkdogan, E.T., 1955, J.I.S.I., 180, 344.

Daniel, V. & Lipson, H., 1943, Proc. Roy. Soc., A.181, 368.

Darken, L.S. & Gurry, R.W., 1945, J. Am. Chem. Soc. 67, 1398.

De Fontaine, D., 1966, "Local Atom Arrangements Studied by X-ray Diffraction" (edited by Cohen, J.B. & Hilliard, J.E.). New York: Gordon & Breach, Science Publishers, pp. 51-88.

Dijkstra, L.J., 1949, Trans. A.I.M.E., 185, 252.

Driver, J.H., 1972, unpublished work, Dept. of Metallurgy, University of Newcastle upon Tyne.

Driver, J.H., 1973, unpublished work, Dept. of Metallurgy, University of Newcastle upon Tyne.

Driver, J.H. & Papazian, J.M., 1973, Acta Met., 2, 1139.

Driver, J.H., Handley, J.R. & Jack, K.H., 1972, Scand. J. Met., 1, 211.

Driver, J.H., Unthank, D.C. & Jack, K.H., 1972, Phil. Mag., 26, no. 5, 1227.

Emmett, P.H., Hendricks, S.B. & Brunhauer, S., 1930, J. Am. Chem. Soc., 52, 1456.

Ericsson, T. & Cohen, J.B., 1971, Acta Cryst., A.27, 97.

Ericsson, T., Mourikis, S., & Cohen, J.B., 1970, J. Mat. Sci., 5, 901.

Eurin, P.H., Penisson, J.M. & Bourret, A., 1973, Acta Met., 21, 559.

Fillingham, P.J., Leamy, H.J. & Tanner, L.E., 1972, "Electron Microscopy and Structure of Materials" (edited by Thomas, G.). Berkeley: Univ. of Cal. Press, p. 163.

Guinier, A., 1955, Acta Met., 3, 510.

Guljaev, A.P. & Trusova, E.F., 1950, Zh. Tekhn. Fix., 20, 66.

Handley, J., 1974, Ph.D. Thesis, University of Newcastle upon Tyne.

Hansen, M., 1958, "Constitution of Binary Alloys". New York: McGraw-Hill.

Hargreaves, M.E., 1951, Acta Cryst., 4, 301.

Hayes, P.C., 1972, M.Sc. Thesis, University of Newcastle upon Tyne.

Hayes, P.C., 1973, Ph.D. Thesis, University of Strathclyde.

Hendry, A., 1974, unpublished work, Dept. of Metallurgy, University of Newcastle upon Tyne.

Hepworth, M.T., Smith, R.P. & Turkdogan, E.T., 1966, Trans. A.I.M.E., 236, 1278.

Hillert, M., Cohen, M. & Averbach, B.L., 1961, Acta Met., 2, 536.

Higgins, J. & Wilkes, P., 1972, Phil. Mag., 25, 599.

Hirsch, P.B., Howie, A., Nicholson, R.B., Pashley, D.W. & Whelan, M.J., 1970, "Electron Microscopy of Thin Crystals". London: Butterworths.

Hornbogen, E., 1961, J. Appl. Phys., 32, 135.

Jack, D.H., 1971, unpublished work, Dept. of Metallurgy, University of Newcastle upon Tyne.

Jack, D.H., 1976, Acta Met., 24, 137.

Jack, D.H., Lidster, P.C., Grieveson, P. & Jack, K.H., 1973, "Chemical Metallurgy of Iron and Steel". London: I.S.I., pp. 374-376.

Jack, K.H., 1951a, Proc. Roy. Soc., A,208, 216.

Jack, K.H., 1951b, ibid., p. 200.

Jack, K.H., 1972, Scand. J. Met., 1, 195.

Jack, K.H., 1974, Met. Science, 8, 271.

Jack, K.H., 1975, "Heat Treatment '73". London: The Metals Society, pp. 39-50.

Kirkwood, D.H., Atasoy, O.E. & Keown, S.R., 1974, Met. Science, 8, 49.

Krawitz, A. & Sinclair, R., 1975, Phil. Mag., 31, 697.

Lehrer, E., 1930, A. Electrochem., 36, 383.

Mehl, R.F., Barrett, C.S. & Jerabek, H.S., 1934, Trans. A.I.M.E., 113, 211.

Mortimer, B., 1971, Ph.D. Thesis, University of Newcastle upon Tyne.

Mortimer, B., Grieveson, P. & Jack, K.H., 1972, Scand. J. Met., 1, 203.

Phillips, V.A. & Tanner, L.E., 1973, Acta Met., 21, 441.

Pipkin, N.J., 1968, Ph.D. Thesis, University of Newcastle upon Tyne.

Pipkin, N.J., Roberts, W., Speirs, D.L., Grieveson, P. & Jack, K.H., 1973, "Chemical Metallurgy of Iron and Steel". London: I.S.I., pp. 351-352.

Pope, M., 1972, Ph.D. Thesis, University of Newcastle upon Tyne.

Pope, M., Jones, D.M., & Jack, K.H., 1975, "Proc. of Fifth Int. Conf. on Internal Friction and Ultrasonic Attenuation in Crystalline Solids", Aachen, 1973, edited by Lenz & Lücke. Berlin-Heidelberg: Springer-Verlag, pp. 266-275.

Roberts, W., 1970, Ph.D. Thesis, University of Newcastle upon Tyne.

Schwerdtfeger, K. & Turkdogan, E.T., 1970, "Techniques for Metals Research", vol. 4, part 1., New York: Interscience.

Speirs, D.L., 1969, Ph.D. Thesis, University of Newcastle upon Tyne.

Speirs, D.L., Roberts, W., Grieveson, P. & Jack, K.H., 1970, "Proc. of the 2nd Int. Conf. on the Strengthening of Metals and Alloys", Asilomar, 1970. American Society for Metals, pp. 601-605.

Stephenson, A., 1973, Ph.D. Thesis, University of Newcastle upon Tyne.

Sutton, A.L. & Hume-Rothery, W., 1955, Phil. Mag., 46, 1295.

Szabo-Miszenti, G., 1970, Acta Met., 18, 477.

Tanner, L.E., 1966, Phil. Mag., 14, 111.

Tiedman, T.J., Bouman, J. & Burgers, W.G., 1957, Acta Met., 5, 310.

Tillman, C., 1974, unpublished work, Dept. of Metallurgy, University of Newcastle upon Tyne.

Unthank, D.C., Driver, J.H., & Jack, K.H., 1972, Nature Phys. Sci., 238, 136.

Wriedt, H.A. & Zwell, L., 1962, Trans. A.I.M.E., 185, 252.

Zwell, L. & Wriedt, H.A., 1966, Trans. A.I.M.E., 236, 1387.